

# Technical Memo

# 864

## The NWP impact of Aeolus Level-2B winds at ECMWF

Michael P. Rennie and Lars Isaksen  
(Research Department)

June 2020

Series: ECMWF Technical Memoranda

A full list of ECMWF Publications can be found on our website under:

<http://www.ecmwf.int/en/publications>

Contact: [library@ecmwf.int](mailto:library@ecmwf.int)

© Copyright 2020

European Centre for Medium-Range Weather Forecasts, Shinfield Park, Reading, RG2 9AX, UK

Literary and scientific copyrights belong to ECMWF and are reserved in all countries. This publication is not to be reprinted or translated in whole or in part without the written permission of the Director-General. Appropriate non-commercial use will normally be granted under the condition that reference is made to ECMWF.

The information within this publication is given in good faith and considered to be true, but ECMWF accepts no liability for error or omission or for loss or damage arising from its use.

## Abstract

The European Space Agency's Aeolus mission has been demonstrated to be a success as the first space-based Doppler Wind Lidar mission, by providing wind observations of good enough quality to improve weather forecasting. This conclusion was reached by comparing the Level-2B (L2B) horizontal line-of-sight (HLOS) wind observations to the ECMWF NWP model equivalents and by the positive impact of Aeolus in Observing System Experiments (OSEs).

The L2B Rayleigh-clear HLOS wind (one-sigma) random errors were estimated to be typically 4-5 m/s and 3 m/s for Mie-cloudy HLOS winds, but with high variability depending on the signal levels which vary with meteorological conditions. The magnitude of the Mie HLOS wind noise is close to meeting the mission requirements in the free troposphere; however, the Rayleigh noise is larger than the pre-launch mission requirements. The systematic errors (biases) are complex and vary with time. It was necessary to use a bias correction scheme with the ECMWF model as a reference in OSEs to provide a significant positive impact from Aeolus. An understanding of the dominant sources of bias was found via relating O-B departures to the satellite's housekeeping datasets — particularly for the Rayleigh biases which were found to depend strongly on the temperature of the instrument's main telescope. A bias correction scheme using the instrument temperatures as predictors was developed as part of the L2B processing, removing the need to bias correct Aeolus winds in ECMWF's data assimilation system.

OSEs were done using the ECMWF data assimilation system for three periods of the mission. The impact of the assimilation of Aeolus L2B HLOS winds on short range forecasts is demonstrated to be positive, via statistically significant improvements in the forecast fit to other observation types sensitive to temperature, wind and humidity (such as radiosonde observations, GNSS radio occultations, aircraft observations and humidity sensitive microwave radiance observations). The largest short-range impact is found in the tropical upper troposphere (at ~150 hPa); however positive impact can be seen from surface to ~35 km altitude. The forecast impact is positive in the tropical upper troposphere and lower stratosphere and in polar regions; particularly at 2-3 day forecast range; reaching ~2% improvement in RMS error for wind and temperature. Most of the tropical impact comes from the Rayleigh winds, but the Mie provides more of the impact near the poles. It has been shown that the impact of Mie winds can be improved by accounting for representativeness error.

Aeolus' impact on forecast skill is very good given the higher than pre-launch expected noise levels, complex biases and despite the relatively small size of the assimilated Aeolus dataset compared to most other components of the observing system. The forecast sensitivity observation impact (FSOI) metric, that is available since Aeolus went operational at ECMWF on 9 January 2020, also confirms that Aeolus provides a useful contribution to the global observing system.

## 1 Introduction

This Technical Memorandum (TM) documents ECMWF's assessment of Aeolus Level-2B HLOS (horizontal line-of-sight) wind data quality. This is done via monitoring using the short-range forecasts of the ECMWF NWP (Numerical Weather Prediction) system and by the assessment of Aeolus' NWP impact via data assimilation experiments. It also provides early guidance to other NWP centres and the scientific community on the usage of the Aeolus wind observations. It should be kept in mind that Aeolus is a research mission and that the data is being constantly improved via the efforts of the Aeolus DISC (Data Innovation Science Cluster) and CAL/VAL teams, and this TM only represents the data at the time of writing. A list of acronyms used can be found in the Appendix.

Wind profiles were listed as the highest priority critical atmospheric variable that is not adequately measured by current or planned observing systems according to the World Meteorological Organisation (WMO) Rolling Review of Requirements (WMO, 2018). Many studies have suggested the potential benefits of more wind profile observations for NWP; such as: Stoffelen et al. (2006), Marseille et al. (2008), Baker et al. (2014), Horányi (2015a), Tan et al. (2007), Weissman and Cardinali (2007), Illingworth et al. (2018).

The European Space Agency's Aeolus satellite was launched on 22 August 2018 with the payload of the first Doppler Wind Lidar (DWL) in space and the first European lidar in space. Aeolus partially fills the wind data gap in the global observing system and hence it is of great interest for demonstrating the value of satellite wind profiles for NWP.

Aeolus is an Earth Explorer (EE) mission which is part of the ESA's Living Planet Programme (ESA, 2019). The mission's main objective is to provide profiles of high-quality wind component observations from the surface up to the lower stratosphere, using a DWL instrument (called Atmospheric LAsER Doppler Instrument (ALADIN)) in a polar sun-synchronous, 320 km altitude, dawn-dusk orbit with a 18:00 local time equator crossing for the ascending node. The observation consists of slant path profiles of the horizontal line-of-sight (HLOS) wind component, pointing in the direction perpendicular to the satellite-earth surface velocity vector. The mission lifetime is defined to be at least three years. A detailed description of the mission and the ALADIN instrument can be found in ESA's ADM-Aeolus Science Report (ESA, 2008).

The ALADIN instrument is a powerful and highly frequency-stabilised pulsed ultraviolet (UV, 355 nm) DWL. The instrument laser emits pulses of around 60 mJ at a frequency of 50.5 Hz through its 1.5 m diameter Cassegrain telescope into the atmosphere. The light is scattered by air molecules (Rayleigh scattering), particles and hydrometeors (Mie scattering), and a very small fraction of the scattered light makes its way back to the instrument where it is received via the instrument's telescope. The backscattered signal is sampled in two channels; one for the backscatter from the clear-air molecules (a Double Fabry-Pérot spectrometer called the Rayleigh Channel) and one for the particulate backscatter (a Fizeau spectrometer called the Mie channel). The received signal is Doppler shifted (frequency shifted) due to the motion of the atmospheric scatterers along the instrument's field of view, which is determined by comparing the backscatter frequency to the instrument emit frequency.

We focus in this report on the data available during the first year and a half of Aeolus HLOS winds, which covers the period from September 2018 until April 2020. During this whole period, the Level-2B (L2B) processing team (ECMWF and KNMI) collaborated closely with ESA and the Level-1 processing teams (DLR, DoRIT, Météo-France) as part of the Aeolus DISC project to characterize, calibrate and validate the ALADIN instrument and the Aeolus data products.

Short-range NWP forecasts have been used for decades to detect issues with observations e.g., Hollingsworth et al. (1986), Stoffelen (1999) and Lu et al. (2011). Via comparisons of Aeolus to the short-range forecast, anomalies were detected and reported. This has subsequently led the Aeolus DISC to improvements in the data quality as the ground processing chain evolves.

In Section 2 we describe the methods that we used to obtain the monitoring and assimilation results: such as information on which L2B datasets were investigated, how comparisons of Aeolus L2B HLOS winds to the ECMWF model was done and the settings and quality control decisions for Observing System Experiments (OSE) for assessing Aeolus' NWP impact. In Section 3, the quality of the L2B HLOS wind observations is assessed using the ECMWF global model as a reference. In Section

4, the results of the NWP impact assessment are provided. This is followed by the discussion and conclusions.

## 2 Methods

### 2.1 Aeolus Level-2B wind data

Aeolus wind products are the output of a multiple stage ground processing chain. The different processing levels are described in detail in the ADM-Aeolus Science Report ESA (2008) and are also provided in the Algorithm Theoretical Basis Documents (ATBDs) for the various product levels (Level-1B and Level-2B (Rennie et al., 2019)). The Aeolus Level-2B (L2B) HLOS wind product contains observations suitable for use in NWP and scientific research, due to several important corrections which are applied relative to the Level-1B (L1B) HLOS wind products. The Aeolus ground segment processing chain has been developed since the early 2000's by various groups: ESA, Airbus DS, DLR, MDA, DoRIT, KNMI, Météo-France and ECMWF. Tan et al. (2008) explains the concepts of the L2B processor, however this reference is partially obsolete due to several significant algorithm updates since then (the L2B processor ATBD is the most up-to-date description).

Different periods of L2B data have been assessed for NWP impact. This is because Aeolus is a novel Earth Explorer, hence processing algorithms, instrument performance and data availability was constantly evolving, some of which led to natural boundaries for periods of assessment. A complete reprocessing of the dataset with today's improved processing algorithms is required to avoid such boundaries — but such a complete reprocessed dataset is not yet available.

For the mission's Commissioning Phase (CP, which is from launch until end of January 2019), the L2B dataset used in this study is a combination of reprocessed and operational near real-time (NRT) produced data (both created by ESA's Payload Data Ground Segment (PDGS)). This data was produced with the L1B processor version 7.04 and L2B processor version 3.01 (the Payload Data Ground Segment baseline of 2B02). The period from 3 September to 19 November 2018 used reprocessed data for which the L2B Earth Explorer (EE) product was generated by the PDGS. The reprocessed L2B EE products were converted to BUFR products by the L2B processing algorithm team. In operations, ECMWF's L2/Met PF (Level-2 Meteorological Processing Facility), which is part of the PDGS, provided the L2B EE and corresponding BUFR data. The L2B BUFR data are used by NWP centres as the nominal method of getting the data into their data assimilation systems.

The L2B processor settings determine many characteristics of the L2B wind observations. One such important setting is the maximum horizontal averaging length-scale, which was set during the CP to be one Basic Repeat Cycle (BRC) for both the Rayleigh and the Mie observations, meaning the HLOS winds are produced from up to 30 smaller horizontal-scale (~2.9 km) measurements, resulting in observations of up to approximately 87 km horizontal extent. The vertical resolution is defined by the vertical range-bin settings (RBS) commanded on-board the satellite and the ground processing chain does not modify this. The thickness of the 24-available range-bins can vary with height and can be set from 250 m to 2 km in 250 m increments, nominally becoming thicker with height to compensate for the decrease in signal levels with altitude (Rayleigh scattering is a function of density). The Mie and Rayleigh channels typically have different range-bin settings according to their strengths and weaknesses. The range-bin settings were kept fixed during nearly all the CP, with a high sampling of range-bins near the ground to ensure decent ground returns. Ground returns provide a zero-wind

reference, which is an important source of wind calibration, so it was very important to ensure this worked during the CP, as it is critical for the rest of the mission.

For the April to June 2019 FM-A (Flight Model A laser) OSEs, the L2B dataset was produced via ECMWF’s own offline reprocessing mechanism with specially defined QC (quality control) settings in the L2B processor settings file (AUX\_PAR\_2B) to try to minimise the effect of data problems that existed at the time such as the wind biases affecting specific range-bins.

The FM-B (Flight Model B laser) L2B dataset was obtained from the PDGS’s NRT processing chain, but for data assimilation purposes we used data from 2 August 2019 onwards due to inappropriate calibration files (FM-A files) being implemented in the FM-B data before that date (FM-B started producing winds on 28 June 2019).

There have been many changes in the operational processing chain since launch that affect the quality of the L2B winds, some of the main ones a listed in Figure 1 (up to end of April 2020) for reference.

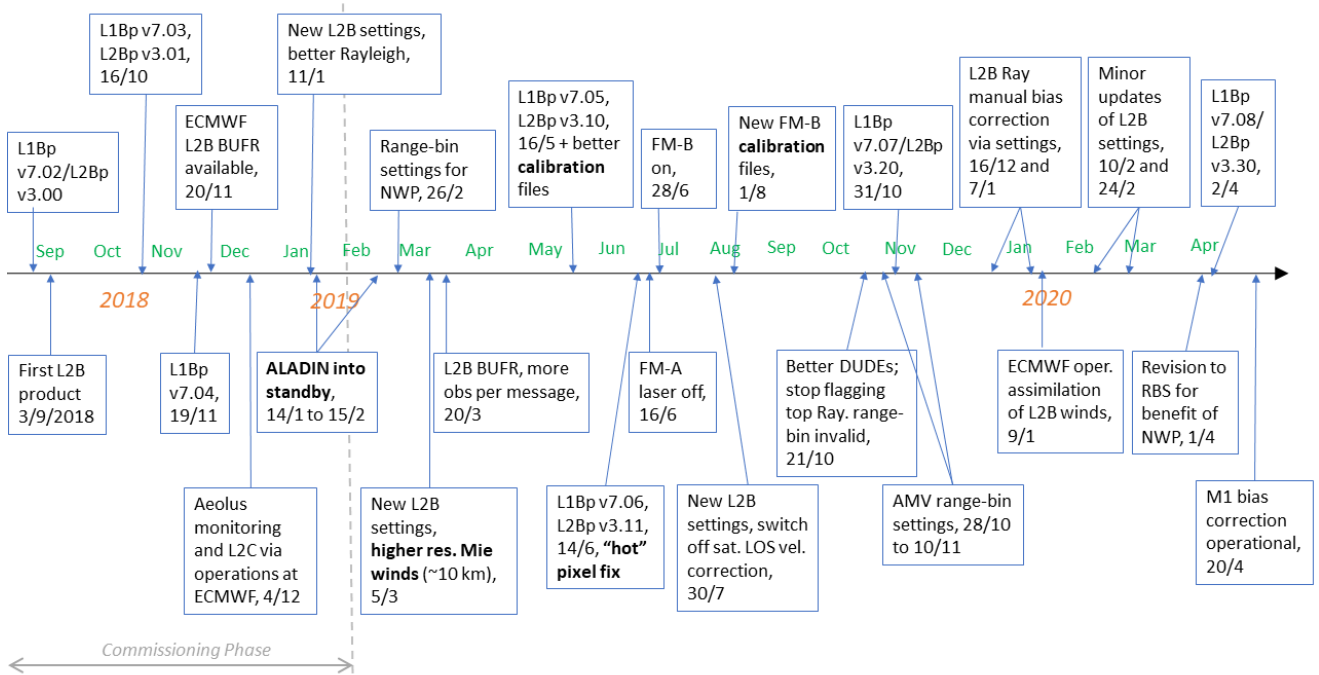


Figure 1. A timeline to illustrate the main changes in the Aeolus Level-2B dataset for NRT operational processing during the mission up to April 2020.

At the time of writing there are four available L2B wind observation types (Rayleigh-clear, Rayleigh-cloudy, Mie-clear, Mie-cloudy). We focus on the Rayleigh-clear and Mie-cloudy winds, as they are better quality than the other two types. If the L2B processor classification is perfect, then there should not be any Mie-clear wind data. In practice there are a few due to the noise at measurement-bin level classification (e.g. in L1B scattering ratios values to distinguish clear and cloudy conditions). The Rayleigh-cloudy winds sample the same locations in the atmosphere as the Mie-cloudy winds. It has always been the expectation that Rayleigh-cloudy winds would be of little value due to the presence of decent quality Mie-cloudy winds at the same locations. However, this should be investigated more

thoroughly in the future, to see if we can benefit from these extra winds (measured via different spectrometers i.e. independent observations and associated errors).

An early example of Aeolus L2B HLOS wind observations (both L2B Rayleigh-clear and Mie-cloudy) during the CP from one orbit on 15 September 2018 is shown in Figure 2. With one BRC averaging used for both Mie and Rayleigh, there were around 5.5 times more Rayleigh-clear than Mie-cloudy winds. ALADIN's line-of-sight points perpendicular to the satellite orbit and is approximately 10 degrees off the zonal direction for most of the orbit. Therefore, the HLOS winds generally provide more information on the zonal ( $u$ ) wind component than on the meridional ( $v$ ) wind component. However, near the Poles ALADIN has increased sensitivity to the meridional ( $v$ ) wind component, as is evident from the typical one-day coverage in Figure 3 for northern latitudes. Outside polar regions, for ascending orbit phases Aeolus measures the predominantly westerly jet streams as positive HLOS winds, and for descending orbit phases the westerly jet streams are measured as negative HLOS winds. To help interpret the data, the strongest winds (jet streams) are annotated in Figure 2. Being an active space-borne optical instrument, ALADIN is totally attenuated by optically thick clouds or aerosols, hence there are areas (coloured black) with no observations.

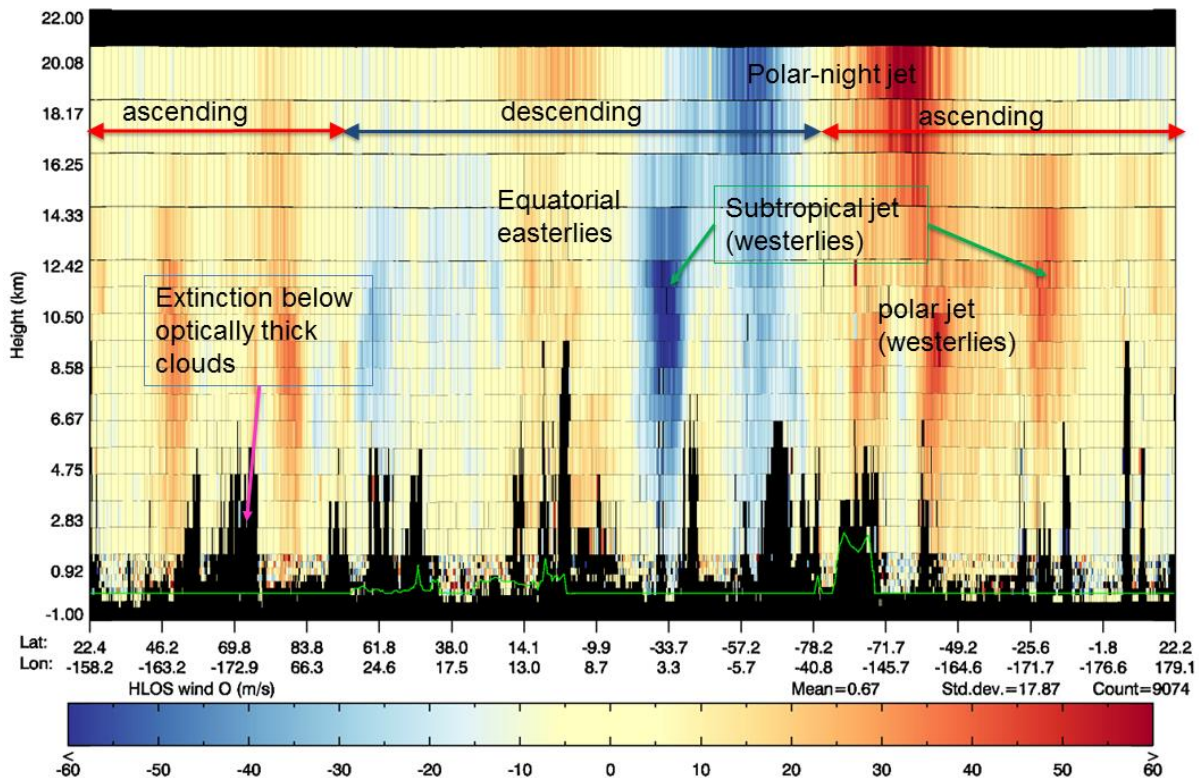


Figure 2. L2B Rayleigh-clear and Mie-cloudy HLOS wind observations for one orbit from 15 September 2018. The vertical axis is the geometric height relative to EGM96 (Earth Gravity Model from 1996; <https://cddis.nasa.gov/926/egm96/nasatm.html>) geoid and the horizontal axis is the time along the orbit (but labelled with latitude/longitude geolocations along the orbit). The colour scale indicates the HLOS wind speed. Winds blowing away from the satellite produce positive HLOS winds and winds blowing towards the satellite produce negative HLOS winds. To more clearly show lower wind speeds, the scale saturates at  $\pm 60$  m/s, despite the speed in some of the jet streams

reaching larger values. Black areas indicate an absence of observations. Each observation is plotted as a coloured rectangle with boundaries indicating the spatial limits of the observation, hence the vertical sampling (range-bin thicknesses) are evident (the horizontal extent of an observation is not easily seen for this whole orbit plot). The Digital Elevation Model i.e. Earth's surface is shown in green (Antarctica is clearly visible as higher ground at the lowest latitudes)

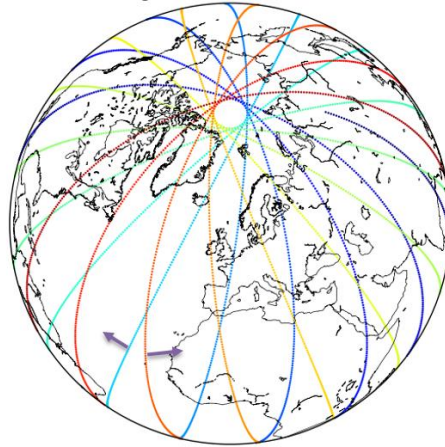


Figure 3. An example of Aeolus' near surface geolocations in one day. The line-of-sight pointing direction of ALADIN is indicated by the purple arrows for an ascending (eastwards pointing) and descending (westwards pointing) orbit phase. The greater spatial sampling near the North Pole is evident.

### 2.1.1 Commissioning Phase L2B dataset

The vertical range-bin settings applied during the CP are shown in the example data of Figure 2 (vertical range-bin sampling intended to be more suitable for NWP exploitation has been applied since 26 February 2019). This meant reducing the range-bin resolution near the ground for ground returns. The RBS varied from 250 m for several range-bins near the surface to 2 km thickness in the lower stratosphere, and reached a maximum altitude of around 20 km. This RBS was in place from the start of the mission until 25 February 2019, during the phase where instrument calibration had priority over NWP impact. The near-surface 250 m range-bins are too thin to provide enough signal for good quality Rayleigh winds, but the Mie winds are good, due to relatively large backscatter from cloud tops.

To retrieve HLOS wind observations, calibration information on how the Rayleigh and Mie spectrometer instrument responses change with frequency is required (ESA, 2008). To characterize and quantify the different contributors to the Aeolus instrument drift, to verify the satellite Attitude and Orbital Control Systems (AOCS) and the calculations of the satellite attitude, the CP dataset was generated from a fixed set of instrument response calibration files. However, weekly calibration procedures were performed during the CP and are planned to continue throughout the mission lifetime. Another source of calibration is ground return winds which can be used to correct for possible satellite miss-pointing, thermal and range dependencies, which can lead to height dependent and short (within an orbit) or long (seasonal effects) term biases. An appropriate calibration strategy for Aeolus is still being investigated and developed at the time of writing and will be continuously reassessed and improved by scientists working on the processing chain.

The calibration for the L2B processor Rayleigh winds is provided via the Rayleigh-Brillouin Correction look-up table (AUX\_RBC\_L2 file) which is produced by the Calibration Suite software. For

the CP dataset the AUX\_RBC\_L2 was derived from an Instrument Spectral Response (ISR) (ESA, 2008) measured on 19 September 2018; an Instrument Response Calibration (IRC) was not directly used (via the so-called update Corrected Spectral Registration (CSR) procedure, which is part of the Aeolus Calibration Suite data processing software). This was because testing using the IRC led to significantly biased winds (e.g. -7 m/s) when applying it to the update CSR software (version available at the time).

To account for an observed frequency offset between the internal reference and atmospheric path response curves as seen in the Rayleigh Response Calibration (RRC) after the instrument was launched, the atmospheric response curves had to be shifted by approximately 160 MHz in the AUX\_RBC\_L2 file produced by the Aeolus Calibration Suite. The resulting updated AUX\_RBC\_L2 file was used in the L2B wind processing, but this led to an almost constant global bias of several m/s with respect to ECMWF model equivalent HLOS winds during the September 2018 period. Hence, it was decided, as a preliminary measure, to adjust the frequency shift such that the L2B Rayleigh-clear global mean departures with respect to ECMWF's short-range forecast became close to zero in that period, which was achieved by changing the shift to 155.4 MHz. This tuning, using global ECMWF statistics, was not ideal but was deemed to be necessary in this very early phase of the mission to get an early dataset suitable for impact studies. It should be noted that evaluations showed that the ECMWF short-range forecast has small global and regionally averaged wind bias when compared to high quality observations such as radiosondes (e.g. less than 0.3 m/s for zonal wind component). More recently (in February/March 2019), several improvements in the Rayleigh calibration processing were made, so tuning to the ECMWF model was not required. Improvements in the RBC file generation are still being pursued. For example, Météo-France are investigating a method to obtain the appropriate frequency shift from the difference between internal reference and ground return Rayleigh response.

The applied L2B processor Mie wind calibration information (the Mie Response Calibration (MRC)) is the same as that used by the L1B product Mie wind observations. It was chosen by the Level-1 experts based on assessments of the quality of the weekly MRCs (based on ground returns over polar regions in nadir pointing mode). An MRC valid on 15 October 2018 was chosen and applied in the processing/re-processing of the whole CP dataset. Nominally the L2Bp obtains the MRC information from the L1B wind mode product, but in an offline testing mode it is possible to read the MRC information directly (from AUX\_MRC\_1B file). Testing showed that it is possible to tune the MRC parameters to minimise the Mie wind bias with respect to the ECMWF model, however because the Mie bias was relatively small, it was not done to avoid a possible risk of introduction NWP model biases into the satellite observation dataset.

### 2.1.2 Late FM-A L2B dataset

This period covered from 2 April 2019 to 14 June 2019. Note that data was available from mid-February 2020 (Figure 1) after FM-A was switched back on (following a temporary outage); the period tested for NWP impact was chosen based given the possibility to run OSEs with our own modified L2B data at the time. The L2B data for testing in this period was produced via L1Bp v7.04 and L2Bp v3.01 patch 1. The L2B processing was done at ECMWF from a non-operational set-up (L2/Met PF back-up server) and specific AUX\_PAR\_2B settings were manually chosen to avoid biased HLOS wind on specific range-bins. These range-bin specific biases were due to hot pixels, which are increased dark current rates for specific ALADIN ACCD detector pixels, which can cause large biases in HLOS winds if not corrected for. This QC was necessary because a correction for hot pixels was not implemented in

operations until 14 June 2019 (see Figure 1). The correction is via the application of so-called DUDE (Down Under Dark Experiment) calibration data four times per day in combination with L1B processor v7.06. This led to a dramatic improvement in the quality of the L2B winds.

The choice of AUX\_RBC\_L2 and AUX\_MRC\_1B resulted in small global average biases. This experimental period ended when the ALADIN laser switched from FM-A to FM-B.

Some of the features of the L2B wind quality for this period include:

- FM-A laser energy at its lowest reported values for the mission so far (~40-45 mJ reported by the instrument).
- Hot pixels were increasing in number causing more biased range-bins. However, our specially processed dataset had the affected range-bins properly rejected via manually updates of the AUX\_PAR\_2B file. Hot pixel range-bins are flagged invalid for whole period, meaning that ~20-25% winds are rejected. The range-bins rejected for the Mie channel were number (counting 1 as the top altitude range-bin); 24, 16, 13, 5 and 2. For the Rayleigh channel there were: 20,15, 11, 5 and 1.
- Using more appropriate instrument response calibrations via choice of AUX\_RBC\_L2 and AUX\_MRC\_1B.
- More appropriate range-bin altitude settings for NWP impact. In particular thinner range-bins in the upper troposphere and lower stratosphere and fewer 250 m range-bins near the surface.
- Higher horizontal resolution (and hence more) Mie winds due to the L2Bp grouping algorithm settings chosen. The Mie-cloudy winds were produced with horizontal averaging maximum size of 10 km during this period, compared with up to 1 BRC (80-90 km) in the CP. The change in Mie horizontal averaging occurred on 5 March 2019, see Figure 1.

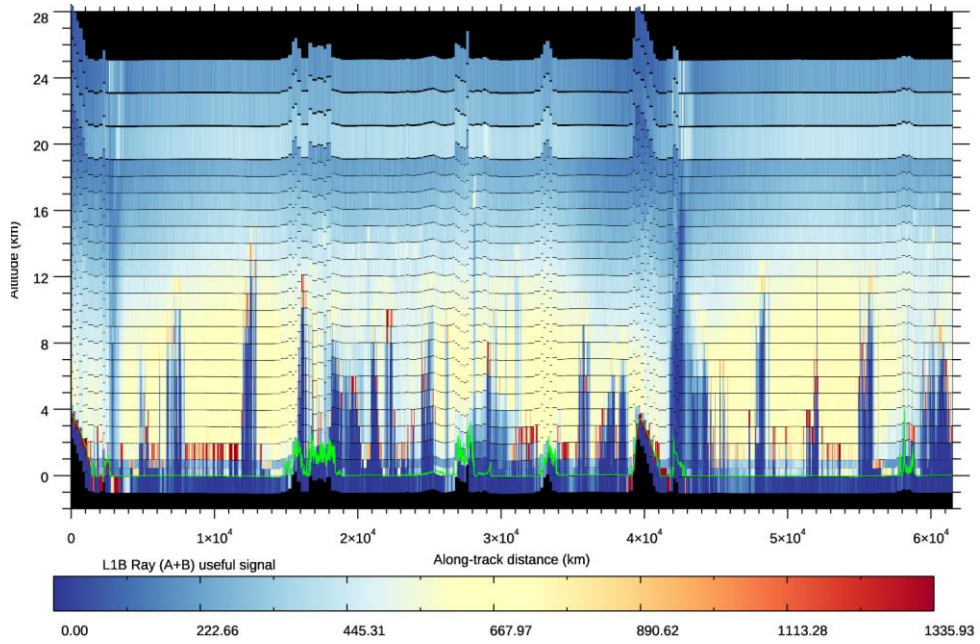
### 2.1.3 Early FM-B L2B dataset

This period covered from early August 2019 to the end of December 2019. The dataset for this period is the operationally produced L2B products from the NRT PDGS processing. The L2B dataset is from the operationally produced L2B BUFR data using L2BP v3.11 and L1Bp v7.06 followed by L1Bp v7.07 and L2Bp v3.20 since 31 October 2019. The data used in OSEs started on 2 August 2019 which is when reasonable FM-B calibration files were used operationally and hence the global average bias became reasonable. The calibration files remained constant because reasonably small global average bias was seen in August 2019; however, we shall see in the Section 3.2 that the bias later drifted with time.

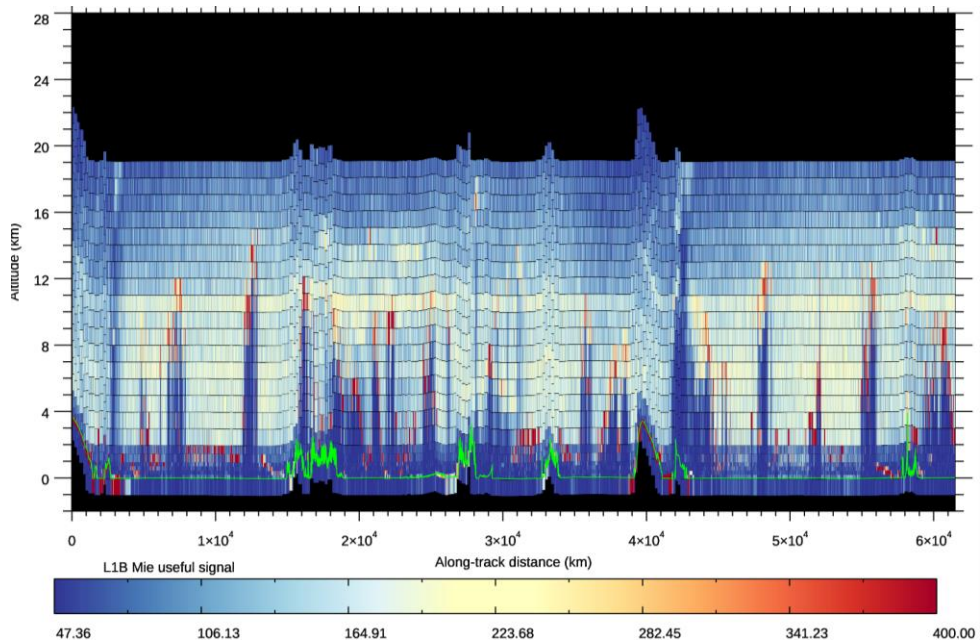
The vertical range-bin settings were changed on several occasions during this period. For example, the range-bin settings (although more suitable than the CP settings for NWP) did not change with latitude until 21 October 2019; see Figure 4 for the settings applied in August 2019. By January 2020, the RBS's had considerable variation with latitude bands to try to maximise NWP impact, see Figure 5. RBS for maximising co-locations with Atmospheric Motion Vector (AMV) winds (for a CAL/VAL study) were implemented between 28 October 2019 and 10 November 2019, which increased the resolution of the bins considerably and consequently reduced the maximum altitude (which may have had a strong effect on NWP impact). RBS for the Strateole-2 (high altitude super-pressure balloons) campaign with top range higher than 20 km in the tropics from 10 November 2019 onwards was also implemented (these are shown in the tropics in Figure 5).

Some miscellaneous things to note on the L2B data:

- Until 21 October 2019 all Rayleigh range-bin 1 (top altitude range-bin) HLOS winds were flagged as invalid, due to a limitation in the DUDE calibrations for this range-bin. After this date they are valid again.
- The AUX\_PAR\_2B (L2B processor settings file) was set (with FM-B) to not use the AOCS LOS velocity correction as this was shown to degrade rather than improve biases
- There is a reduction in Mie wind observation counts with the update of the processing chain on 31/10/2019 (to be resolved in a future processor version). Also, the Mie horizontal maximum accumulation length increased to 12 km and the Rayleigh was changed to exactly 1 BRC (approximately 86 km).
- On 16/12/2019 the AUX\_PAR\_2B was updated to perform a manual bias correction of the Rayleigh winds to compensate for a global average bias drift. The manual bias correction was +4 m/s.
- There was a bug which affected all L2B data since launch that was fixed in the operational L1B processing on 2 April 2020. It caused the Rayleigh estimated instrument error to be overestimated in the summer Poles by ~20-30%, particularly at high altitudes. This is due to the term for solar background noise being too large in the Rayleigh SNR (signal to noise ratio) calculation.

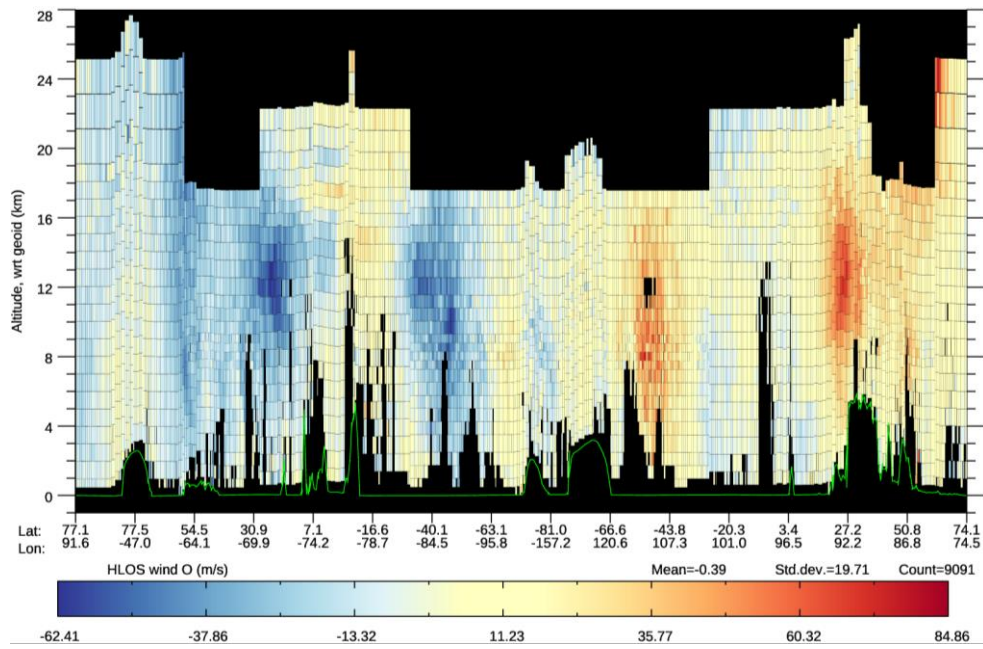


a)

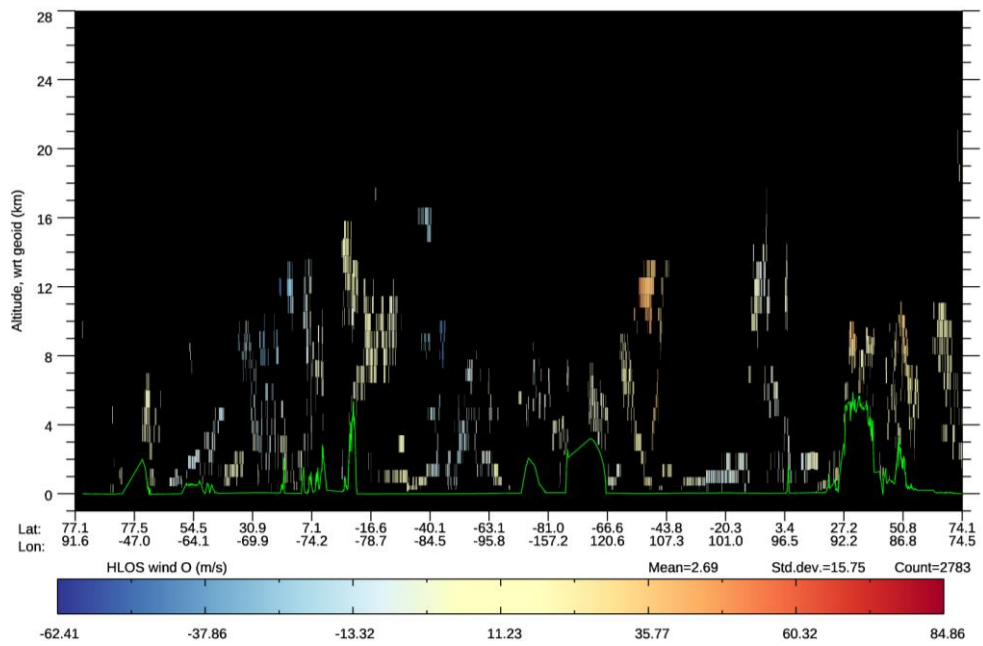


b)

Figure 4. Examples of the range-bin settings applied for a) the Rayleigh channel and b) the Mie channel for an orbit in August 2019 during the early FM-B period, as shown via plots of the useful signal levels at measurement level for one L1B file.



a)



b)

Figure 5. Example of the range-bin settings applied for a) L2B Rayleigh-clear and b) L2B Mie-cloudy on 22 January 2020 for the FM-B period, as shown via plots of the L2B HLOS winds for one L2B file.

## 2.2 Aeolus observation operator at ECMWF

The Aeolus HLOS (horizontal line-of-sight) wind observation operator applied at ECMWF is:

$$v_{HLOS} = -u \sin \theta - v \cos \theta \quad (1)$$

HLOS wind is a linear function of the NWP model zonal wind component ( $u$ ) and meridional wind component ( $v$ ) which are interpolated to the observation geolocation.  $\theta$  is the azimuth angle, describing the line-of-sight pointing of the laser projected onto the horizontal plane, provided as part of the observation geolocation information. The horizontal interpolation of model fields to the observation is a combination of bi-cubic twelve-point interpolation for full resolution outer loop trajectories and bi-linear four point interpolation for lower resolution 4D-Var minimisation trajectories — Aeolus is just using the default interpolation method. For the computation of model equivalents, we have an effective time resolution of  $\pm 15$  minutes, because the observations are grouped into 30 minute time slots in the 4D-Var assimilation window. The  $u$  and  $v$  wind components used in the HLOS formula are interpolated to the observation's centre-of-gravity geolocation point.

The vertical wind component,  $w$ , is assumed to be negligible in the HLOS wind formula. This can be a poor assumption in certain conditions e.g. in convective areas or in strong gravity waves. However, most of the vertical motion associated with strongly convective cloud systems and large-scale frontal ascent occurs below cloud tops, where the Aeolus signal is strongly attenuated, and so does not provide observations. The impact of vertical motion on the Aeolus HLOS winds should be investigated in the future. Vertical wind component is not used by any observation operators at ECMWF at the time of writing, partly because  $w$  generally is small and more uncertain in the model.

The point observation operator is thought to be a reasonable approximation in the horizontal dimension given that the effective resolution of ECMWF's global model is in reasonable agreement with the horizontal resolution of Rayleigh-clear winds (on the order of 4-8 times the grid spacing, see Abdalla (2013), where the grid spacing now is around 9 km). The Mie winds have higher horizontal resolution than the ECMWF model. However, vertically it is a poorer assumption to treat Aeolus winds as point winds, given that the model's winds often vary significantly over Aeolus' thickest (1-2 km) range-bins. In the tropical upper troposphere and along tropospheric frontal zones the HLOS wind vertical shear in the ECMWF model is often more than 20 m/s per km, as shown in Figure 6. The vertical spacing of the operational ECMWF model's 137 levels is shown using crosses in Figure 7; it describes the relationship between pressure and altitude. In the 137-level configuration, the vertical level spacing is stretched with altitude; the vertical resolution is 300 m in the upper troposphere, 400 m at 50 hPa, 1 km at 5 hPa and 3 km near the model top.

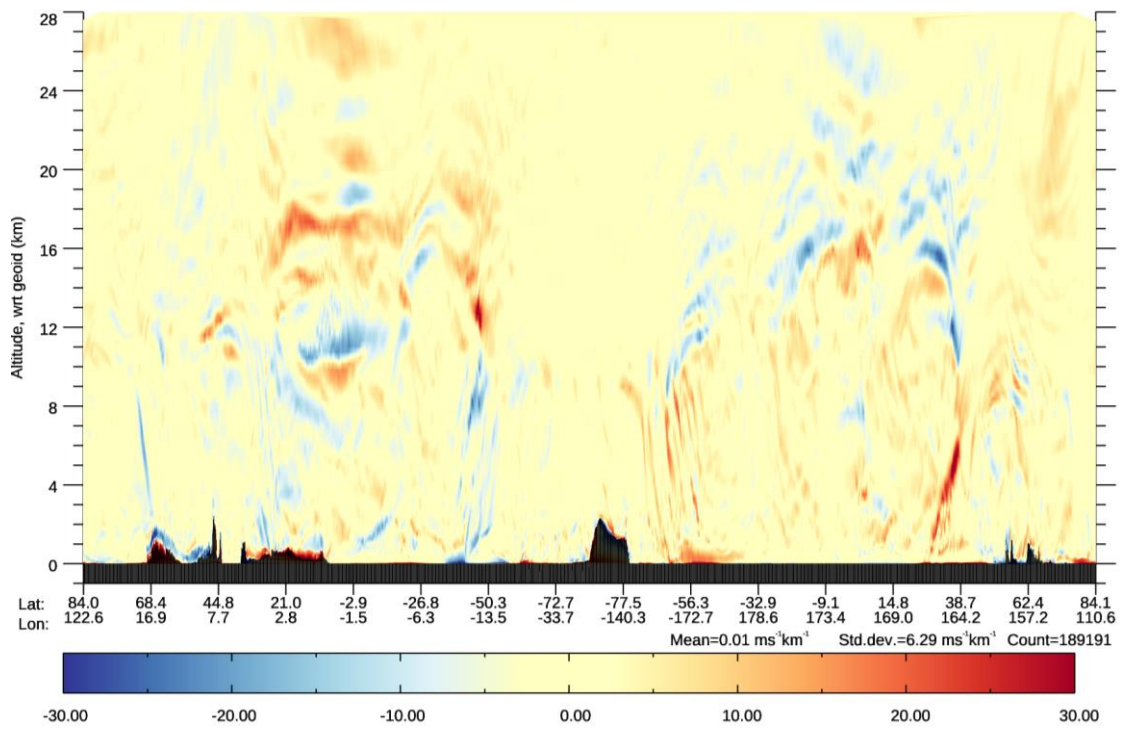
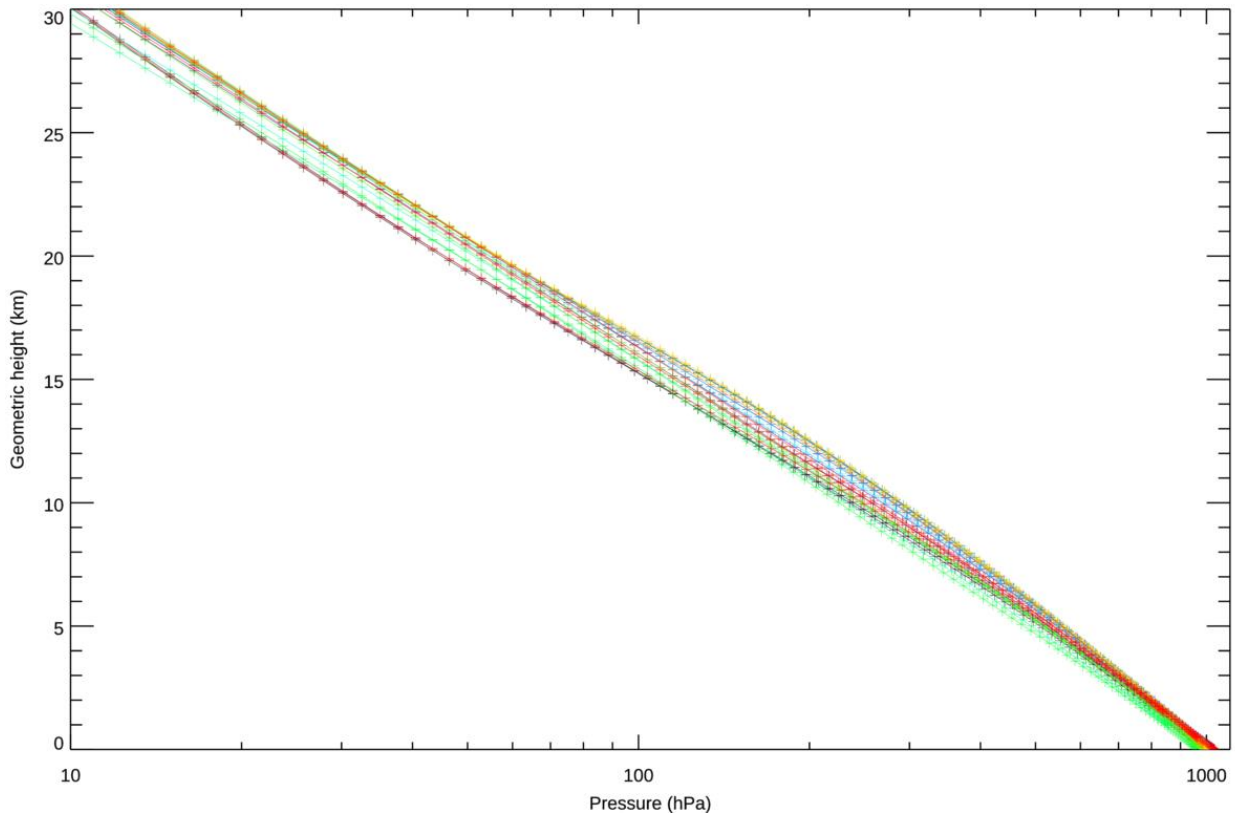


Figure 6. Vertical shear of ECMWF model simulated HLOS wind ( $dHLOS/dz$ ) along one Aeolus orbit as derived from AUX\_MET data. The HLOS wind vertical shear has units of  $ms^{-1}km^{-1}$ .



*Figure 7. The dependence of geometric height (altitude) on pressure from the ECMWF global model (which has 137 vertical levels) for a range of atmospheric conditions across the globe along a simulated Aeolus orbit (different coloured lines). This can be referred to throughout the document to relate altitude to pressure.*

A more accurate observation operator that accounts for the averaging kernel defined by the lidar equation may be pursued in the future. Such an operator for the Rayleigh channel could account for the molecular attenuated backscatter variation throughout the range-bin. A solution for the Mie is less obvious since we do not know the location of the backscatters within the bin. Of course, assigning thinner range-bin settings can alleviate this issue, but at the cost of reduced vertical coverage given the limitation of 24 range-bins. The theoretically most optimal extraction of Aeolus information would involve assimilating L1B useful signal levels via a full lidar equation observation operator; using both the frequency shift and amplitude information of Aeolus. But this can become very complicated e.g. forward modelling cloud backscatter, more non-linear aspects to consider in 4D-Var, and instrument calibration dependencies. So, it is of low priority to investigate this.

Preparatory steps for the Aeolus observation operator are done using some standard ECMWF data assimilation routines (that it is outside the scope of this report to describe). The L2B vertical centre-of-gravity geometric heights (with respect to EGM96 geoid) are converted to an equivalent atmospheric pressure, using the background forecast (short-range forecast from the previous analysis). Firstly, the geometric heights are converted to geopotential using a normal gravity formula (Somigliana's equation), then the geopotential is converted to pressure (using standard ECMWF data assimilation conversions, see ECMWF, 2018). Figure 7 shows the typical relationship between ECMWF model pressure and the derived geometric height; this will aid in the interpretation of the NWP impact results which are shown in pressure space. It would be more accurate to forward model the geometric heights on model levels

and then to interpolate the model winds to Aeolus as a function of geometric height, however the forward modelling improvement from this is expected to be small. An advantage of having pressure as the vertical coordinate is that other wind observations at ECMWF (e.g. radiosondes, aircraft, Atmospheric Motion Vectors) are also assimilated as a function of pressure, which makes comparisons of monitoring statistics easier.

Next, vertical profiles of model wind components are horizontally interpolated to the geolocation of the L2B observation (centre-of-gravity latitude and longitude) using the default methods of interpolation at ECMWF. The model  $u$  and  $v$  components are vertically interpolated (linear in the logarithm of pressure) to the assigned pressure and the HLOS wind formula is applied as if the observation is a point-like wind.

### 2.3 Observation-minus-background departure statistics

As discussed in the introduction, the assessment of the quality of the L2B HLOS wind observations with a state-of-the-art data assimilation system and forecast model is a very powerful method. We have used the ECMWF short-range forecast model equivalent HLOS winds to compute observation-minus-background (O-B) departure statistics. The ECMWF background forecasts are of course not the truth, but over large spatial scales or large time averages they have a very high level of accuracy thanks to the assimilated global observing system and the accuracy of the coupled ECMWF atmosphere-land-wave-ocean-sea-ice Earth System. To confirm this, we have reasonable estimates of the magnitude of the forecast wind errors via O-B statistics for high quality measurements (such as radiosonde winds), and of their spatial distribution and correlations via ECMWF's Ensemble of Data Assimilations (EDA, Isaksen et al., 2011) spread.

The precision and accuracy of the L2B HLOS winds depends on many factors such as: atmospheric signal levels; the accuracy of calibration inputs; L1B and L2B processor algorithms and quality control decisions. It is outside the scope of this report to investigate thoroughly the instrumental (ALADIN) reasons for the levels of precision and accuracy found for Aeolus data.

Two methods were used to calculate O-B statistics for this study. The first is an unorthodox method, using the Aeolus auxiliary meteorological file (AUX\_MET\_12 file, shortened to AUX\_MET in the rest of the report). The AUX\_MET contains vertical profiles of ECMWF operational model fields along Aeolus' predicted ground-track geolocations (T<sub>CO</sub> 1279 (see Malardel et al., 2016) model trajectory, which corresponds to a grid spacing of around 9 km, sampled every 3 seconds (~22 km) along predicted orbit). The AUX\_MET is a necessary input for the L2B processor to perform the Rayleigh-Brillouin Correction (Dabas, 2008), using a priori model temperature and pressure. The AUX\_MET also provides wind  $u$  and  $v$  wind components (for diagnostic purposes and not for use in the L2Bp wind retrieval) as a function of geometric altitude, which can be converted to HLOS wind. Therefore, the AUX\_MET provides a convenient and co-located wind reference to calculate O-B statistics. Since the AUX\_MET data is already interpolated to the predicted ground-track of Aeolus, the nearest-neighbour winds from the AUX\_MET data is used for the departure statistics. The AUX\_MET data provides up to 30-hour forecasts, however the O-B statistics are typically restricted to use the 0-12 hour forecast range (by carefully choosing the first orbit to start just after the validity start of the AUX\_MET file). This is favourable because shorter range forecasts are more accurate.

The AUX\_MET O-B statistics are calculated and plotted via bespoke Aeolus monitoring tools developed over several years pre-launch, using Aeolus simulations (Rennie, 2016). The monitoring tool is best suited for small datasets, due to the size of the data files. To avoid outliers strongly affecting the non-robust metrics e.g. mean and standard deviation, some quality control (QC) is needed. The QC is predominantly based on the L2Bp estimated HLOS wind error, which is derived via error propagation from signal levels to HLOS wind using Poisson noise assumptions. No NWP model dependent QC, i.e. O-B related background check, is required for this method. Thresholds of estimated errors are chosen subjectively, based on the compromise between the number of observations that pass QC and the overall quality of the dataset. Thresholds for estimated observation errors of around 8-12 m/s were found to be appropriate for the Rayleigh-clear HLOS winds and 4-5 m/s for the Mie-cloudy. The QC is particularly important for the Mie winds which have many gross errors, whereas the Rayleigh observations have few.

The second, and more traditional method of deriving O-B statistics has also been extensively used, in which the Aeolus L2B BUFR data is ingested into a data assimilation analysis procedure and the O-B and O-A (observation-minus-analysis) departure statistics are calculated. At ECMWF the data assimilation analysis can be a research department experiment or the operational analysis. Aeolus was switched “on” but blacklisted (given no weight) in the operational analysis since early December 2018, meaning the data have no influence on the analysis state, but can still be compared to the background and analysis model state for monitoring purposes. Since 9 January 2020 Aeolus L2B winds have been operationally assimilated at ECMWF, which means the O-B, and especially O-A, statistics become less independent of Aeolus data itself.

In research department experiment analyses, the non-linear forecast model is typically run at a lower than operational horizontal resolution (e.g. TCO399 (~29 km), rather than TCO1279 (~9 km)), to save computational costs and running time. One advantage of using this standard method is that ECMWF’s generic observation monitoring software can be used to calculate the O-B statistics. It can handle very large datasets e.g. several months of data for generating time-series plots. It also makes it easier to do more selective diagnostics.

The QC applied to the RD (ECMWF’s Research Department) experiment or operational analysis monitoring can optionally use a model background check and the threshold checks on the L2Bp HLOS wind standard error estimate. The QC decisions applied in the time-series plots of Section 3 are to reject data which fail the background check, have overall L2B validity flag set to false and have estimated errors (before scaling) > 12 m/s for the Rayleigh and > 6 m/s for the Mie. The model background check rejects observations for which the O-B departure is greater than five times the expectation and is aimed at removing outliers (see Järvinen and Andersson, 1999).

Further validation of the Aeolus data quality through comparisons with collocated observations from ground-based and airborne (remote sensing) instrumentation is performed by the Aeolus Calibration and Validation teams (CAL/VAL teams). The CAL/VAL teams also contain members comparing Aeolus observations directly to other wind observations available in the WMO Global Observing System (GOS), such as radiosondes and wind profilers, and to other NWP models from Meteorological Centres world-wide. In this way, the Aeolus observation quality can be well characterized through many sources, and it allows also NWP model errors (including biases) to be assessed. Other CAL/VAL teams also perform NWP impact assessments of Aeolus data using their weather models. The results of the CAL/VAL validations are not further discussed here.

## 2.4 Observing System Experiments

The standard technique to evaluate the impact of a new observing system is to perform an Observing System Experiment (OSE). In such an experiment the data assimilation system is run twice, first including the observing system under investigation and the second excluding the data. The two sets of analyses and subsequent forecasts are then compared to investigate the impact of the observing system being studied (Andersson et al. 1991). OSEs are the most reliable method to assess the forecast impact of a change to the data assimilation system, such as adding Aeolus L2B HLOS winds. Many OSEs have been performed, as part of this study, to assess the NWP impact of Aeolus L2B HLOS winds. We first tested the impact of Aeolus relative to the reference assimilation system that is using the full operationally used observing system at the time of testing. Often when evaluating new observing systems, experiments are also done using reduced observing systems to more clearly see the impact from the new observations. So far, we have not tried this, however it might be useful to learn how well Aeolus can improve impact on top of a degraded observing system. Three periods have been assessed so far: CP, late FM-A and early FM-B. It should be noted that the OSEs were done very soon after the sensing periods, as part of the reason for this activity was to provide a quick assess Aeolus quality and impact.

OSE verification compares the skill of forecasts with a changed system to that without the change. The skill is assessed by treating a chosen reference analysis as “the truth” and therefore by considering differences between forecasts and the reference analysis at the validity time of the forecast to represent the forecast error. When a significant amount of new observations is added to the assimilation system, the choice of reference analysis can be critical to how the impact is perceived. For example, with the “own analysis” method the analyses of the experiment are used to calculate the experiment forecast errors and the analyses of the control are used to calculate the control forecast errors. Adding observations can increase the variability in the forecasts which can look bad compared to the control which did not use the observations. This apparent negative impact tends to become negligible after two days in the extratropics, where errors grow exponentially and fast with time for over a week, but can persist for longer in the tropics, where error growth rate gets smaller after the first day compared to the extratropics. The reference analysis can be an independent analysis such as the “operational analysis” i.e. that taken from the archive of operational data assimilation at ECMWF. This operational analysis has the advantage of often being higher resolution (and more accurate) than the OSE and is using the operation-ally applied observing system. This is a reasonable choice if the observation in question is not being operationally assimilated, which is the case for Aeolus until 9 January 2020; hence for late FM-A and early FM-B experiments we used operational analysis as the reference to try to better understand impact at the very short range. After Aeolus is operationally assimilated it will still be valid to use operational analysis as a reference in the extratropics beyond day 2-3 forecasts, since the error growth is sufficiently large such that the choice of reference analysis does not matter, but in the tropics the effects of observations can persist into medium range forecasts, hence it is unclear if operational analysis is appropriate; verification against independent observations (if available) would be a better choice.

Another issue with choice of verifying analysis is that forecast errors in the short range can be correlated with the analysis e.g. if one observation type causes a consistent analysis error structure, then the short-range forecasts may also have this error structure. Depending on whether the experiment with the change pulls to or away from this erroneous analysis has influence on the apparent impact.

## 2.4.1 Commissioning Phase OSEs

### 2.4.1.1 Experimental set-up

The control run of the CP OSE used the ECMWF model at cycle 45R1 (operational at ECMWF from 5 June 2018 until 10 June 2019), with 4D-Var outer loop horizontal resolution of T<sub>Co511</sub> (~23 km grid spacing), inner loops of T<sub>L255/319/399</sub> with 137 vertical levels up to ~80 km (see Figure 7, these model vertical levels are applied in all OSEs). The nominal ECMWF operational set of satellite and conventional observations was assimilated. The period for the OSE is from 12 September 2018 until 16 October 2018, which was chosen because it was a period during which systematic errors in the L2B dataset were relatively stable with time and the instrument health was good (see Section 3.1 for the O-B time series monitoring results). However, the OSE was also extended to the whole of the CP to see the impact. The period covers part of autumn in the Northern Hemisphere and part of spring in the Southern Hemisphere.

The experiments are the same as the control, except that they additionally assimilate the Aeolus L2B HLOS wind observations. Two experiments were performed; one assimilating both the Rayleigh-clear and the Mie-cloudy observations and one assimilating only the Mie-cloudy observations, to determine their relative importance.

The assigned Aeolus observation errors in data assimilation are based on the L2Bp estimated observation errors. The L2Bp estimated errors are accurate; they have a high correlation with the O-B standard deviation (as demonstrated in Sections 3.1.1 and 3.1.2), but they appear to be underestimated for data assimilation assigned observation errors, since they are only an instrument precision estimate using shot-noise; they do not include model representativeness error (which of course varies with the NWP model). Also, there may be terms missing in the instrument noise estimate. It was decided to scale the L2Bp estimated errors by 1.5 for the Mie-cloudy and 1.1 for the Rayleigh-clear (based at the time on experience from pre-launch simulation studies). More recent FM-B testing suggests 1.4 to be more optimal for the Rayleigh winds and 1.75 for the Mie-cloudy winds (however this was based on new smaller scale horizontal averaging of the Mie winds). It should be noted that investigations have shown that the L2B Rayleigh-clear estimated errors are too large in the polar summer by 20-30% due a bug in the L1B processors' estimate of the Rayleigh SNR (an erroneous factor in front of the solar background noise term). Therefore, in our OSEs we will have been giving too little weight to the Rayleigh winds in polar summer. This was resolved with L1Bp v7.08 and L2Bp v3.30 on 2 April 2020.

This simple error model, i.e. a scaling of the L2Bp estimated error, is perhaps too simplistic for the Mie winds where representativeness error is more important than for the Rayleigh winds. This has been investigated with the early FM-B data, as we describe in Section 4.3.4.4.

### 2.4.1.2 Quality control decisions and corrections

Being the first few months of data from a new observing system, it is not surprising that we applied various extra (non-nominal) corrections and QC decisions to try to maximise the impact of the available Aeolus data. The applied QC and corrections were done during the pre-processing and screening phase, before the data assimilation process and after the BUFR data has been read. The QC decisions and data corrections included:

- Only the Rayleigh-clear and Mie-cloudy winds are assimilated (i.e., Rayleigh-cloudy and Mie-clear are rejected due to their generally poorer quality).

- Observations with assigned observation errors (i.e. after scaling) greater than a threshold were rejected with the aim of removing gross errors without rejecting too many good observations (this requires further tuning in the future):
  - Rayleigh-clear:
    - if pressure < 90 hPa, reject if assigned observation error > 11 m/s
    - if 90 < pressure < 200 hPa, reject if assigned observation error > 7.7 m/s
    - if pressure > 200 hPa, reject if assigned observation error > 6.6 m/s
  - Mie-cloudy: reject if assigned observation error > 4.5 m/s
- The HLOS wind observation geometric heights were corrected by adding 250 m. This correction was required due to a known error in the LOS (Line-of-sight) pointing knowledge during the CP (star-tracker calibration issue). This error was resolved on 26 February 2019 in operational data and will be corrected in future reprocessed data.
- The Mie-cloudy winds were bias corrected by -1.35 m/s (global constant offset) to make them agree (in the global average) with the ECMWF model winds. This correction was only an approximation for the Aeolus data valid for the 12 September to 16 October 2018 period. The Mie bias may have been caused by imperfect calibration e.g. noise during the calibration procedure or errors in the processing algorithms.
- Specific pressure ranges for the Rayleigh channel were blacklisted to try to avoid biased HLOS winds that occur for specific range-bins (which was caused by hot pixels). This method worked reasonably well, but was found to be imperfect, due to the difficulty of fixed altitude range-bins varying in pressure space along the orbit. The blacklisting performed was:
  - For Rayleigh-clear to avoid:
    - range-bin 11 by rejecting data between 400-500 hPa for the whole period
    - range-bin 5 by rejecting data between 150-200 hPa after 4 November 2018
    - range-bin 15 by rejecting data between 700-800 hPa after 24 November 2018
  - For Mie-cloudy avoid:
    - range-bin 13 by rejecting data between 600-750 hPa after 21 October 2018
- Winds within 20 hPa (~160 m) of the ECMWF model's orography were discarded because occasionally ground returns were wrongly classified as wind observations.
- Rayleigh winds with range-bin thicknesses of 250 m were rejected due to excessive noise.
- Rayleigh winds with horizontal accumulation lengths less than 60 km and Mie less than 5 km were rejected since they tended to be outliers in O-B statistics.
- Specific periods, when the satellite AOCS (the star trackers) were commissioned and switched to the redundant side for calibration, led to some biased wind periods. These periods were blacklisted:
  - Data from 03:00 UTC on 25 September 2018 until 26 September 2018 14:51 UTC
  - Data from 9 November 2018 between 09:25 UTC and 15:25 UTC

- A method was employed to avoid duplicate observations that are present from overlaps between orbital dumps. The first occurrence of the observation is chosen (this is also applied in late FM-A and early FM-B periods).

No spatial thinning of the observations was applied. As mentioned in Section 2.2, a 5-sigma background forecast departure QC check is applied during the screening phase of data assimilation process.

After QC there were typically 40,000-50,000 HLOS winds assimilated per 12 hours during the period. This is effectively ~8% the number of Atmospheric Motion Vector (AMV) winds assimilated per 12 hours (600,000 wind components). Aeolus provided only less than 1% of the total number of observations assimilated in this CP OSE.

## 2.4.2 Late FM-A period OSEs

### 2.4.2.1 Experimental set-up

The applied code base was a tagged version of CY46R1 (operational at ECMWF on 11 June 2019) from 26 March 2019. The model outer loop and trajectory was set to  $T_{CO399}$  (~29 km) and the inner loops to  $T_{L95/159/255/255/255}$ . The nominal ECMWF operational set of satellite and conventional observations was assimilated. The 2.5-month period of the OSE from 2 April to 14 June 2019 allowed for more robust statistics compared to the CP period of around 1 month. This period is meteorological spring to early summer in the Northern Hemisphere and autumn to early winter the southern. The nominal assigned observation errors used a factor of 1.4 for the Rayleigh-clear winds and 1.2 for the Mie-cloudy winds. However, OSEs were run testing different scaling factors, which suggested that the Mie winds with a scaling factor 1.2 were over-weighted (i.e. a larger factor than 1.2 is required).

### 2.4.2.2 Quality control decisions and corrections

As already discussed in Section 2.1.2, manually determined AUX\_PAR\_2B settings allowed the L2B products to flag range-bins which were detected (via O-B monitoring) to be biased because of hot pixels. This resulted in roughly a quarter of range-bins being rejected.

Whilst the OSEs for this period were running, a lot more was learned about the behaviour of the Rayleigh wind biases e.g. we saw large changes in bias in the NH polar regions over a matter of days (this is discussed in Section 3.2.1). This led to the decision to implement a bias correction scheme using the ECMWF model as a reference (it is described in more detail for the early FM-B period that follows). For forecast verification it was found to be more reliable to verify against the ECMWF operational analysis ( $T_{CO1279}$ ) — since it is more accurate than our OSEs ( $T_{CO399}$ ), and Aeolus was not operationally assimilated during that period.

The QC decisions and observation weighting were the same as for the early FM-A period, apart from the 250 m correction of the observation altitude which was no longer needed.

## 2.4.3 Early FM-B period OSEs

### 2.4.3.1 Experimental set-up

The applied code base was a tagged version of CY46R1 from 3 December 2019 and the operational blacklist file dated 10 December 2019 was applied. The nominal ECMWF operational set of satellite

and conventional observations was assimilated. Many OSEs have been performed: Rayleigh-clear plus Mie-cloudy; Mie-cloudy only and modified Mie-cloudy assigned observation error.

The model outer loop and trajectory was set to T<sub>CO</sub>399 (~29 km) and the inner loops to T<sub>L</sub>95/159/255/255/255. The period tested is from 2 August 2019 until 31 December 2019, spanning later summer to early winter in the Northern Hemisphere and late winter to early summer in the Southern Hemisphere.

The nominal assigned observation errors were as follows: L2Bp estimated observation error scaling of 1.4 for Rayleigh-clear, 1.75 for Mie-cloudy. These were based on “Desroziers diagnostics” (Desroziers et al., 2005) and some tuning following running OSEs with various scaling factors. However, some testing of refinements to the Mie assigned errors were done, which is explained in Section 4.3.4.4.

### 2.4.3.2 Quality control decisions and corrections

The following are the nominal settings employed in the FM-B dataset OSEs:

- Bias correction to ECMWF model wind as function of orbit phase angle and longitude (done separately for Rayleigh-clear and Mie-cloudy winds – updated every few days based on previous week’s O-B statistics). The Mie bias correction did not require any longitudinal variation and was found to be much more stable with time than the Rayleigh.
- No specific time periods were blacklisted. However, in hindsight it was noticed that unusual biases on 3 September 2019 were associated with a temporary shift to star tracker B.
- For forecast verification it was found to be more informative to verify against the ECMWF operational analysis (T<sub>CO</sub>1279) — since it is more accurate than the lower resolution OSEs (T<sub>CO</sub>399), and Aeolus was not operationally assimilated for this period. Verification against operational analysis reveals the tropical Rayleigh impact in the tropics at shorter time ranges.
- QC decisions:
  - Only assimilate Rayleigh-clear and Mie-cloudy winds with valid overall confidence flag
  - Do not assimilate data within 20 hPa (~160 m) of the surface (to try to avoid any undetected ground returns)
  - Avoid Rayleigh winds at pressure > 850 hPa. It is unclear if this is necessary, but there were some indications of degradation when using boundary layer surface Rayleigh winds.
  - Do not use any Rayleigh winds with:
    - estimated errors (before error scaling) > 12 m/s if pressure ≤ 200 hPa (to try to allow data in the wintertime polar vortex)
    - estimated errors (before error scaling) > 8.5 m/s if pressure > 200 hPa
    - horizontal accumulation lengths < 60 km
    - vertical accumulation lengths < 300 m
  - Do not use any Mie winds with:
    - estimated errors (before error scaling) > 5 m/s

## 2.5 Forecast sensitivity observation impact (FSOI)

Forecast sensitivity observation impact (FSOI) (Langland and Baker (2004), Cardinali (2009) and Janiskova and Cardinali (2016)) is a method to measure how the assimilation of observations affects the short-range forecast error growth. There is no need for a “denial” experiment like in OSEs; FSOI measures the impact of observations in the context of all the other observations assimilated. At ECMWF the difference of global dry energy norm error at 36 hours and 24 hours is projected back onto the analysis. It relies on the accuracy of the model’s adjoint (with simplified dry and moist physical processes) and is therefore limited to short-range forecasts assessment. FSOI uses the analysis as the reference and like OSEs is prone to “own-analysis” verification issues. The short-range impact as measured by FSOI does not guarantee similar levels of impact on the medium range forecasts (as can be verified in OSEs). The impact of observations can be summed up over time and space in different subsets to compute the total contribution of the different components of the observing system towards the reduction in forecast errors. The relative impact of each observation type can be derived from this.

Since Aeolus has been operationally assimilated at ECMWF (9 January 2020) we have been able to assess its impact on short-range forecasts via the FSOI method. The FSOI suite runs operationally at ECMWF.

### 3 NWP monitoring results

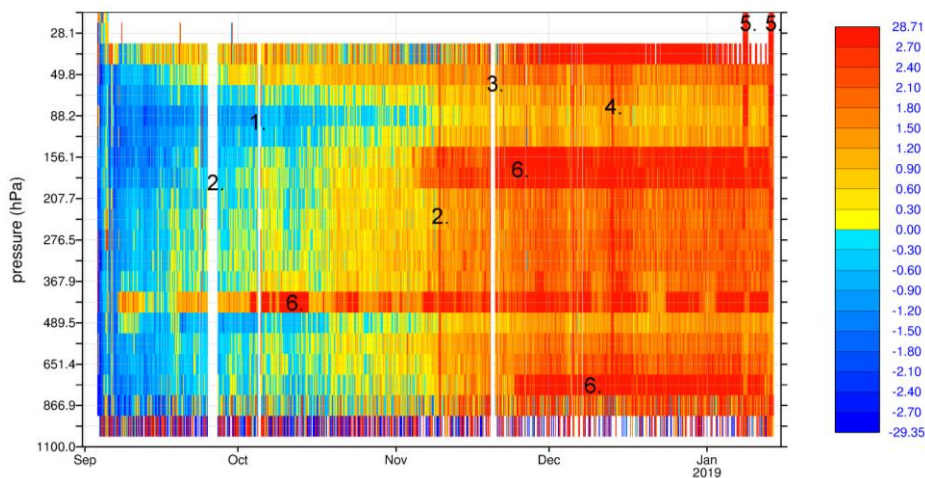
#### 3.1 NWP monitoring of Aeolus for the Commissioning Phase

##### 3.1.1 Rayleigh-clear HLOS wind O-B time variations and anomalies

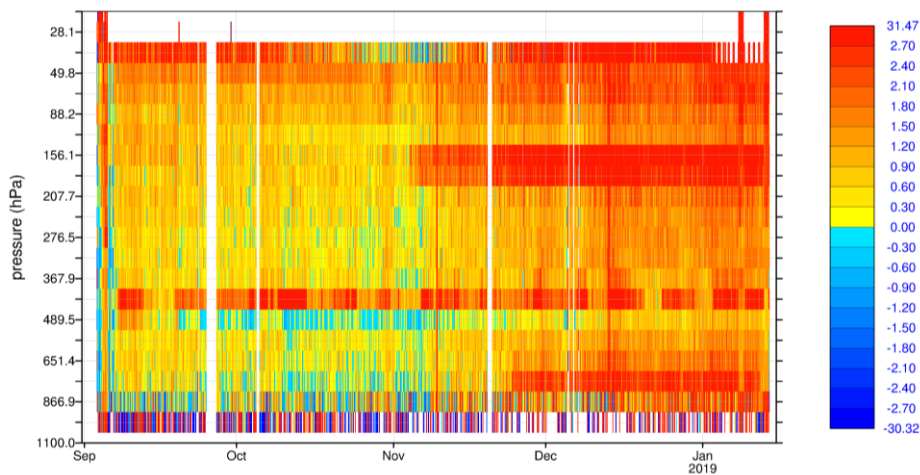
Time-series of Aeolus O-B statistics were calculated via an assimilation experiment (not operational monitoring) in which the L2B data is blacklisted but Aeolus departures are still calculated (see Section 2.3). Figure 8 shows the L2B Rayleigh-clear HLOS wind global statistics of mean O-B binned by time (in 3 hourly slots) and pressure (pressure bins chosen so that the pressure axis is linearly proportional to altitude, see Figure 7 for a reference). The mean of O-B was found to depend on whether the satellite is in the ascending or descending phase of its polar orbit, hence the statistics are split accordingly in Figure 8 a) and b).

Some anomalies and outages of the data are identified via the annotated numbers in Figure 8 a). The associated causes are listed below:

1. Satellite on-board software anomaly period
2. Star-tracker problem periods
3. Data gap due to a transition from reprocessed to operationally produced BUFR data
4. FM-A laser cold plate temperature test period
5. Testing of different vertical range-bin settings
6. Range-bins affected by enhanced dark current in memory zone pixels (“hot” pixels)



a)



b)

Figure 8. Global mean(O-B) as a function of time (every 3 hours) and pressure (a selection of pressure ranges from surface to near 24 km altitude) for the L2B Rayleigh-clear HLOS winds. The colour-scale has units of m/s. a) Ascending orbit phases and b) descending orbit phases. Numbered features in a) are referred to in the text.

In both ascending and descending orbit phases, there is a positive trend in the mean of O-B with time. No evidence was found to suggest that the ECMWF model caused the bias, therefore it is concluded to be due to L2B HLOS wind systematic errors. There are differences in bias between ascending and descending phases e.g. in September 2018 the ascending phase is negatively biased whereas the descending phase is positively biased. This was found to be at least partially due to a HLOS wind speed dependence to the bias resulting from imperfect L2Bp Rayleigh calibration (see Section 3.1.3.1). The ascending orbit phases measure on average positive HLOS winds and descending phases measure on average negative HLOS winds, due to the prevalence of westerly zonal winds in the extratropics. Therefore, a HLOS wind speed dependent bias (slow bias) manifests itself also as differences in bias between ascending (negative bias) and descending phases (positive bias). More recent testing using the calibration information applicable at the time (Rayleigh Response Calibration in mid-September 2018) resulted in a smaller wind speed dependent bias (linear slope error reduced by ~2%, corresponding to 1 m/s reduction in bias for a 50 m/s HLOS wind). An explanation for the orbit phase dependent biases of the Rayleigh was discovered in late 2019 and is explained in Section 3.2.1.

Wind biases associated with specific vertical range-bins are evident in the O-B statistics. This led the L1B processor team to discover an unexpected instrument problem, which is referred to as hot pixels. Increased dark current background and noise levels were found on specific pixels of the instrument's Accumulation Charge-Coupled Device (ACCD). This is thought to be triggered due to space environment radiation exposure (personal communication with ESA). The small changes in dark current background levels are enough to cause range-bin dependent wind biases, particularly for the Rayleigh channel. Hot pixel induced wind bias tends to fluctuate with time as the level of dark current varies, apparently randomly. The pattern mostly seen (by DLR's monitoring of this) is that the dark current levels raises to a very high level when the event is triggered, for then to fluctuate and stabilize after a while at a low elevation level. Some pixels however take a long time to stabilize or keep on

fluctuating. The positive bias associated with range-bin 11 (~400 hPa) during this period was caused by a hot pixel showing particularly strong fluctuations, as can be seen in Figure 8. In June 2019 ground segment processor updates went operational that use regular dark current calibration information (DUDE) to correct for this effect.

Figure 9 shows the global L2B Rayleigh-clear standard deviation of O-B as a function of time and pressure. This gives an impression of the observation random error changes with time, because the model short-range forecast errors are relatively stable. We show only the ascending orbit phase statistics, because the descending phase statistics are very similar. The random errors are very large near the surface because of the narrow 250 m range-bins and hence low signal levels (also attenuation of signal due to clouds contributes to low signal levels near the surface). The lowest standard deviations occur for range-bins around the 100 hPa level (~13-16 km). This is because of the use of 2 km thick range-bins around this pressure level, as compared to the 1 km thick-range-bins at levels below (see Figure 2). Doubling the range-bin thickness should reduce noise by ~40%, but at the cost of half the vertical resolution. The mid-tropospheric 1 km range-bins typically have O-B standard deviations of 4-5 m/s.

There is a general trend of increasing standard deviation with time, particularly at the upper levels, e.g., at 200 hPa from late November 2018 onwards. This is assumed to be caused mainly by a combination of increased solar background noise affecting the southern hemispheric observations (as the austral summer approached) and due to a decrease in the FM-A laser UV output energy with time (ESA, personal communication). It is yet not understood what caused the higher noise at the highest pressure bin in November 2018. The random errors are steadier for the mid-tropospheric levels than for higher altitudes. Higher altitudes have much less signal due to the exponentially decaying atmospheric density with height. Investigations showed that the upper range-bin random error increase is strongly related to increasingly poor L2Bp classification of measurement-level data into clear and cloudy conditions because of increasingly noisy L1B measurement-bin scattering ratios associated with the decreasing laser energy. An improvement in the standard deviation is evident in the last few days of Figure 9, due to a change in the L2B processor settings which improved the clear-cloudy classification.

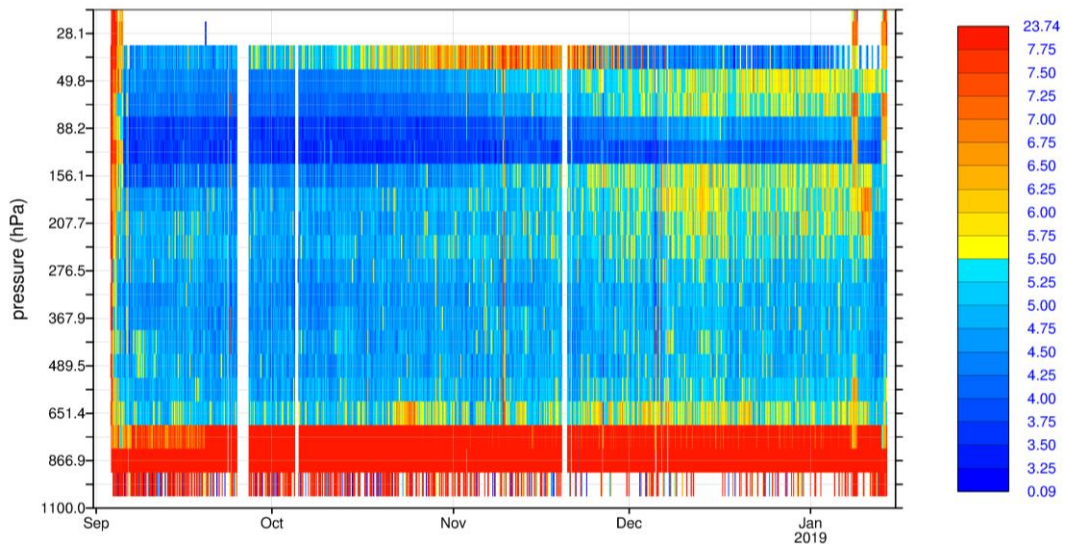


Figure 9. Global standard deviation of O-B as a function of time (every 3 hours) and pressure for the L2B Rayleigh-clear HLOS winds. The scale has units of m/s. Data for ascending orbit phases only.

Figure 10 shows the ascending phase Rayleigh-clear O-B statistics versus time for a mid-tropospheric pressure range (319-368 hPa, ~8 km) which was not affected by hot pixel induced biases. The statistics are split into a) Northern Hemisphere (NH) extratropics and b) Southern Hemisphere (SH) extratropics. This pressure range is roughly where the Rayleigh winds achieve their best precision with 1 km thick range-bins, taking account of lower signal at lower altitudes due to cloud attenuation. A quantitative assessment of the bias and random error variations with time can be deduced from Figure 10. The bias increase with time, as already mentioned, is evident in Figure 10. The bias settles in early December 2018, but to different levels in the NH and the SH; 2-3 m/s in the NH and 1 m/s in the SH. After an initial decrease with time, the standard deviation of O-B settles in the NH after October 2018, settling around the 4.2 m/s level. The initial decrease is thought to be because the solar background noise reduced as the boreal winter approached and hence solar background noise decreased. The standard deviation of O-B in the SH increased a little with time; probably due to a combination of decreasing UV laser energy and increasing solar background noise as the austral summer approached.

Generally, the L2Bp estimated error (green lines of Figure 10) mirrors the changes in the O-B standard deviation, proving that it is a useful error estimate. The Rayleigh HLOS wind errors are significantly larger than the 1.5-2 m/s ECMWF background forecast errors, hence the standard deviation of O-B is dominated by the Rayleigh observation error. Note that for the SH, the L2Bp estimated observation error appears to be too large for increased solar background conditions in late November onwards i.e. it exceeds the standard deviation of O-B. An explanation for this discrepancy was discovered in mid-2019 as being due to an error in the L2B Rayleigh SNR formulation. This is fixed in L1Bp v7.08 which should enter operations in the first quarter of 2020.

The early mission bias and random error fluctuations appear to settle by 12 September 2018, hence the chosen start date for the CP OSE. In the NH, the size of the bias became large around 16 October 2018, hence the chosen end date for the period (Section 2.4.1.1). In the SH the bias also increased with time, but with a smaller rate. The CP OSE chosen dates are also appropriate for the Mie winds as demonstrated in the next section.

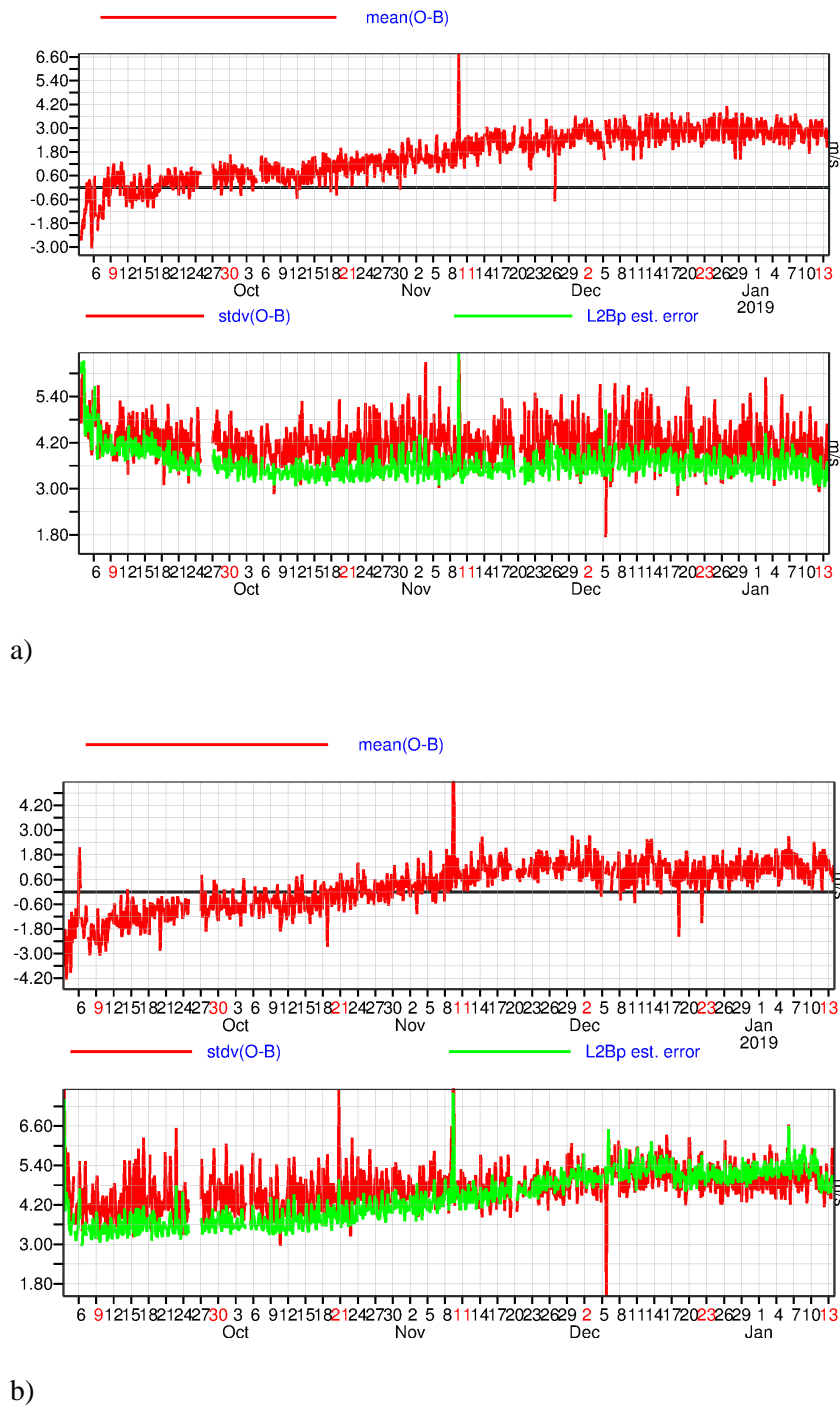
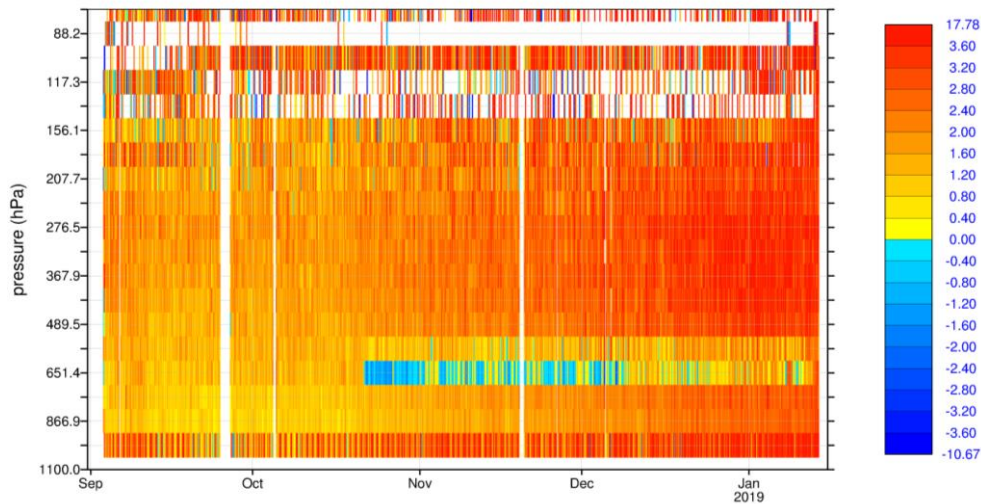


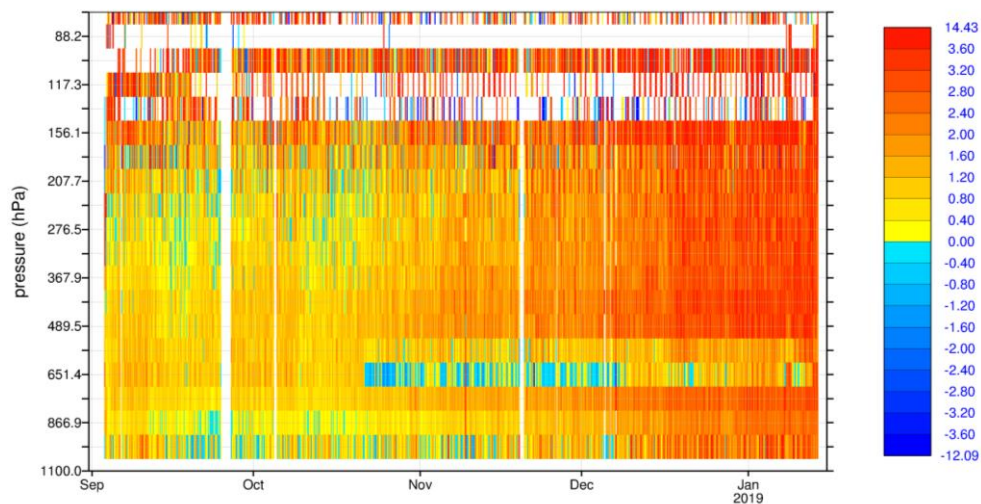
Figure 10. Time series (every 3 hours) of L2B Rayleigh-clear HLOS wind mean(O-B) (upper plot of each figure) and standard deviation of (O-B) (lower plot of each figure) for the pressure range 319-368 hPa for ascending orbit phases only. a) Northern Hemisphere extratropics (20-90 degrees latitude) b) Southern Hemisphere extratropics (-20 to -90 degrees latitude). The green line is the L2B processor estimated error derived from signal levels assuming shot-noise.

### 3.1.2 *Mie-cloudy HLOS wind O-B time variations and anomalies*

Figure 11 shows the L2B Mie-cloudy HLOS wind mean O-B statistics, split into ascending (a) and descending (b) orbit phases. The Mie winds are affected by the same instrument and/or operational anomalies illustrated by the numbers 1-5 in Figure 8 a) but are not repeated here. For both ascending and descending orbits there is a general positive trend in the bias with time (as also seen for the Rayleigh), but starting from an already small positive bias in September 2018 (there was no tuning to the ECMWF model for the Mie calibration). The descending phases are slightly less positively biased than the ascending, with the difference in September suggesting the Mie winds have a fast wind speed dependent bias with respect to the model, in contrast to the Rayleigh which had a slow bias for this period (this is confirmed in Section 3.1.3). A standout feature from Figure 11 is the appearance of negatively biased winds for observations at ~650 hPa from 21 October 2018 onwards. This is due to a hot pixel affecting Mie range-bin 13.



a)



b)

Figure 11. Global mean(O-B) as a function of time (every 4 hours) and pressure for the L2B Mie-cloudy HLOS winds (CAL/VAL dataset) during the period September 2018 to January 2019. The scale has units of m/s. a) Ascending orbit phases and b)) descending orbit phases.

Figure 12 shows the global L2B Mie-cloudy standard deviation of O-B as a function of time and pressure. Only ascending orbit phases are shown because the descending was very similar. As expected, the Mie winds have a higher precision than the Rayleigh winds, by comparing to Figure 9 (note the different colour scales). The standard deviations are smallest for the range-bins in the lower troposphere, which are 250 m range-bins with strong backscatter from optically thick boundary layer clouds. The very lowest range-bins are contaminated by ground return signals, hence the larger noise (this was

resolved in the next L2B processor version: v3.10). There is an obvious increase in standard deviation associated with range-bin 13's hot pixel which shows up at ~600-650 hPa. Apart from the hot pixel influence there is no obvious trend in the standard deviation with time.

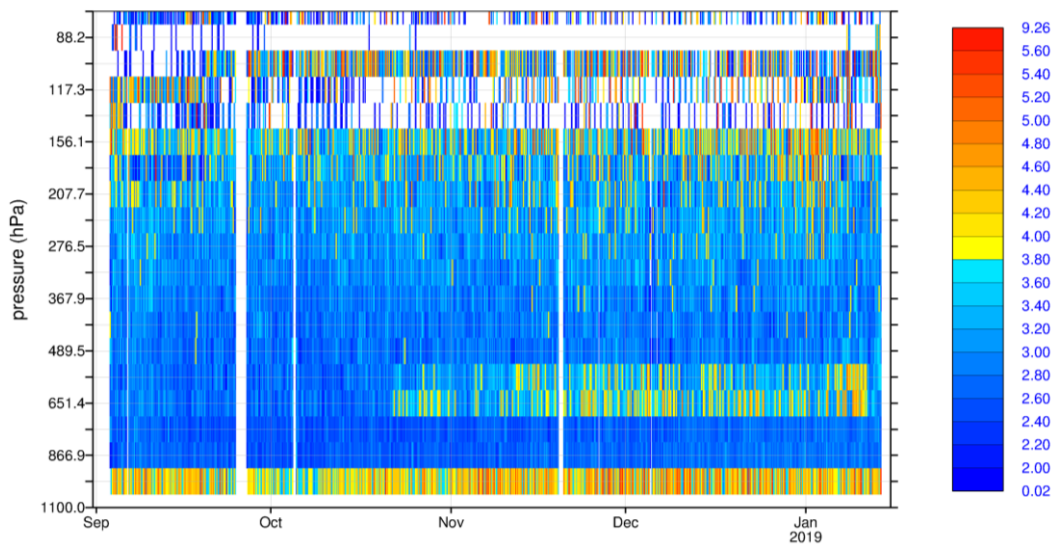
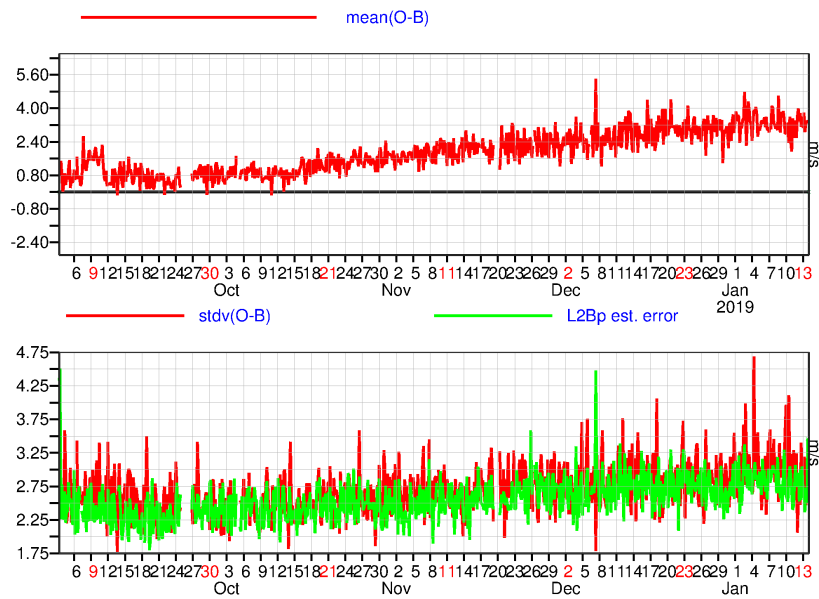
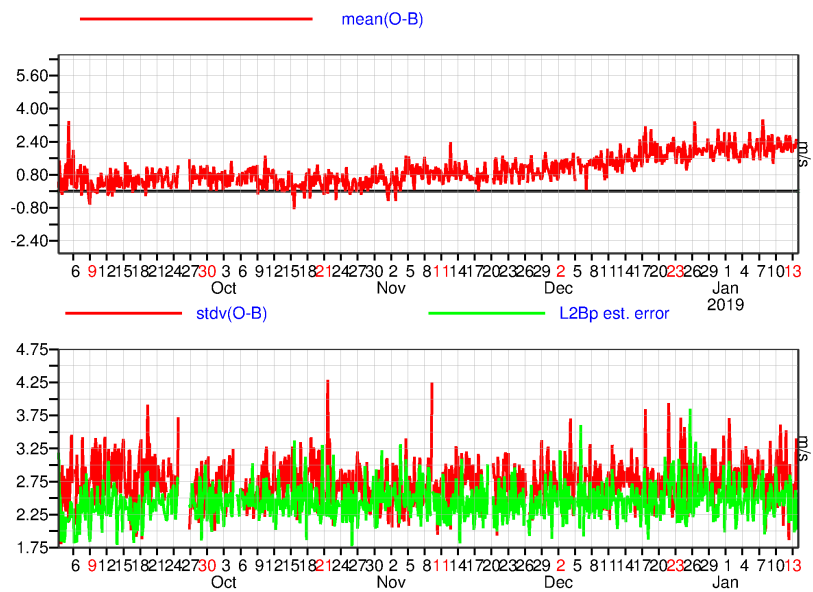


Figure 12. Global standard deviation(O-B) as a function of time (every 4 hours) and pressure for the L2B Mie-cloudy HLOS winds during the period September 2018 to January 2019. The scale has units of m/s. Data for ascending orbit phases only.

Figure 13 shows statistics for a pressure range in the lower troposphere (752-867 hPa, approximately 2 km altitude) with large samples of Mie winds resulting from strong backscatter off planetary boundary layer (PBL) cloud tops (and some aerosol); the figure is split into a) SH extratropics and b) NH extratropics (data for descending orbit phases only). This pressure range was not affected by hot pixels. It is evident that biases started to increase from early October 2018 in the NH, but much later in the SH; around late November 2018. The bias settled in January 2019 to ~3 m/s in the NH and ~2 m/s in the SH. This behaviour has some similarities with the Rayleigh development, but the details differ. Some of the bias drift with time may be related to an imperfect AOCS LOS velocity correction which was applied during this period, which changes with the seasons. It was turned off in operations with FM-B data. The random error in the NH shows a slight increase with time (which is not understood but may be due to seasonal changes in cloud conditions). In the SH the standard deviation of O-B is steady, which is promising for the mission lifetime for Mie winds given that the reported laser energy was around 20% lower in January 2019 than in September 2018. This suggests that the backscatter from clouds is sufficiently strong, such that the lower laser energy is not the limiting factor for the Mie random error. The magnitude and trends in L2Bp Mie estimated errors (green lines) correlates well with the standard deviation in O-B (red lines); suggesting it is a useful error estimate. Similar behaviour is found for other pressure ranges.



a)



b)

Figure 13. Time series (every 4 hours) of L2B Mie-cloudy HLOS wind mean(O-B) (top plot of each figure) and standard deviation of (O-B) (bottom plot of each figure) for the pressure range 752-867 hPa for descending orbit phases only, for the period 4 September 2018 to 15 January 2019. a) Northern Hemisphere extratropics (20-90 degrees latitude) b) Southern Hemisphere extratropics (-20 to -90 degrees latitude). The green line is the L2Bp estimated error derived from useful signal information.

3.1.3 Comparing the data quality in mid-September 2018 to early January 2019

3.1.3.1 L2B Rayleigh-clear

ALADIN’s FM-A reported laser UV energy per pulse dropped from approximately 61 mJ to 52 mJ from mid-September (15 September 2018) to early January 2019 (early January). Plots of O-B statistics as a function of altitude for the two periods are shown in Figure 14 (using the AUX\_MET method; see Section 2.3). There is a sample of around 80,000 observations in both cases (around 20 hours of data). The “robust standard deviation” in Figure 14 is the median absolute deviation (MAD) scaled by 1.4826 which is equivalent to the standard deviation for a normal distribution (Ruppert, 2010). The scaled MAD is less prone to outliers than the standard deviation, which is useful given that no first-guess check is applied in these plots.

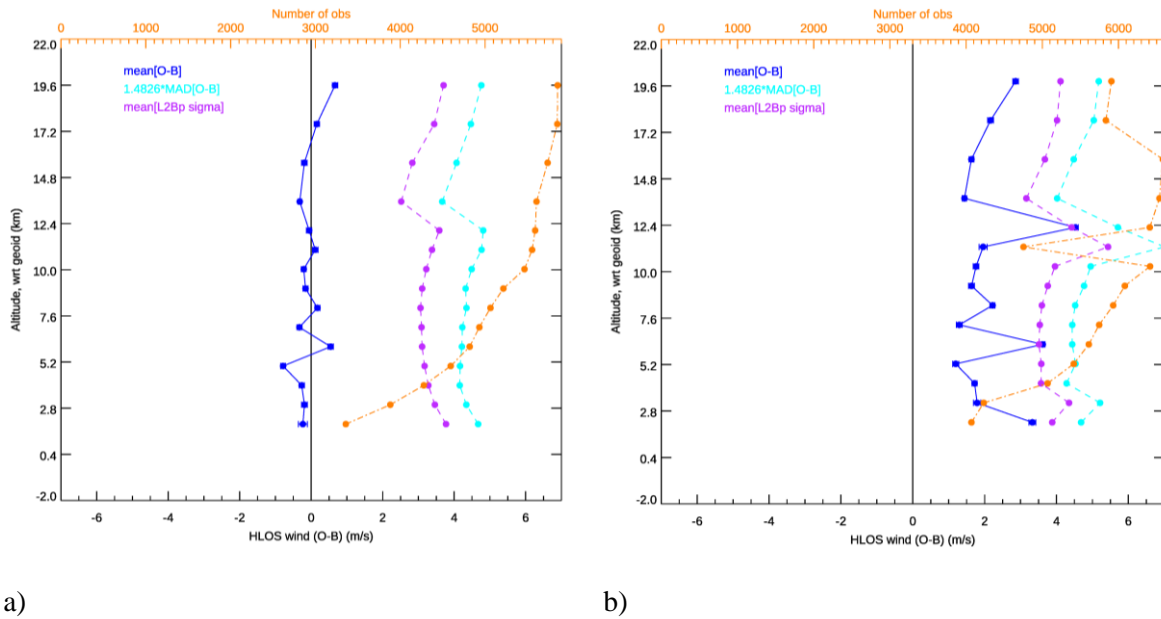


Figure 14. Global L2B Rayleigh-clear HLOS wind O-B statistics as a function of altitude. The dark blue line is the mean(O-B), the cyan line is the robust standard deviation of O-B, the purple line is the mean of the L2Bp estimated error and the orange line is the number of observations (top x axis). a) For mid-September 2018 b) for early-January 2019.

It is evident from Figure 14 that the accuracy and precision of the Rayleigh winds degraded with time during the CP. As already shown in Figure 8 and Figure 10, the Rayleigh winds were relatively unbiased in mid-September 2018 and became positively biased by early January 2019. The bias in early January 2019 shows spikes for several altitudes due the hot pixel affecting specific range-bins. The global average O-B bias in early January 2019 is about 2 m/s (discarding hot pixel affected levels). Given that global biases of ECMWF u-wind relative to radiosondes are rather small, at typically less than 0.3 m/s (as determined by radiosonde O-B departure statistics at ECMWF), then Aeolus Rayleigh observations must account for the bias change. The profile average robust standard deviation of O-B is 4.4 m/s in mid-September and 4.9 m/s in early January. Also, the counts are relatively reduced at specific range-bins in early January due to the applied 8 m/s estimated error QC rejecting more data than in September (overall 4% more rejections). Note that the L2Bp estimated random errors increase in the

summer Poles due to larger solar background noise estimated, and hence the QC rejections are not a strictly fair comparison.

As mentioned earlier, some of the degradation in the Rayleigh wind quality in early January 2019 is exacerbated by the L2Bp measurement-bin classification procedure performing worse than in mid-September 2018, as the noise of the L1B scattering ratios increased due to lower laser energy. The quality loss was later mitigated to a reasonable extent by retuning the L2B processor scattering ratio classification thresholds. Increasing the scattering ratio threshold to 1.6 from 1.25 allowed an increased number of genuinely clear measurement-bins into the calculation of Rayleigh-clear winds, hence reducing the noise. Also, some improvement was obtained by rejecting huge spikes in signal levels, which are thought to be due to cosmic radiation affecting the instrument. This led to the overall O-B robust standard deviation improving by about 0.3-0.4 m/s (as is evident in Figure 9 after the 11 January 2019).

Figure 15 shows the L2B Rayleigh-clear wind quality across the dynamic range of HLOS wind for the two periods. The linear correlation coefficient for mid-September from a) is 0.96 but is reduced slightly in early January to 0.95 via b). That is, the Rayleigh winds performed well over the dynamic range in both periods. To estimate the wind speed dependent errors, we plot the mean(O-B) as a function of B in c) and d) of Figure 15. The use of “Desroziers diagnostics” on conventional u-wind observation departures (radiosondes, aircraft) gives a global average value for the background forecast random error of  $\sigma_B = 1.6$  m/s (not shown). Errors in the independent variable (in this case the background HLOS wind) of a regression scheme leads to biases in the estimated fit coefficients; for a simple linear regression, an underestimate of the fit coefficient known as attenuation bias or regression dilution occurs (Frost, 2000). Because for the Rayleigh winds  $\sigma_B$  is significantly less than  $\sigma_O$  it is reasonable to have B as the independent variable. Simulations of the attenuation bias induced by the assumed  $\sigma_B$  produce a slow bias of -1.5% (not shown). The linear fit coefficient in c) shows a slope error of -4% in mid-September 2018. This is significantly more negative than the -1.5% that would be expected without any real wind speed dependent biases and therefore it can be assumed to be a real Rayleigh slow bias in mid-September 2018 of approximately -2.5%. This slow bias partially accounts for the ascending/descending orbit phase bias differences in September 2018 already noted from Figure 8. The linear fit coefficient in early January from d) is around -1%, so the slope error is closer to the expected -1.5% early January than in mid-September 2018. The reason for this is that the true Rayleigh response functions changed with time such that, by chance, the slope error improved with time by continuing to use the older but incorrect CP Rayleigh calibration file.

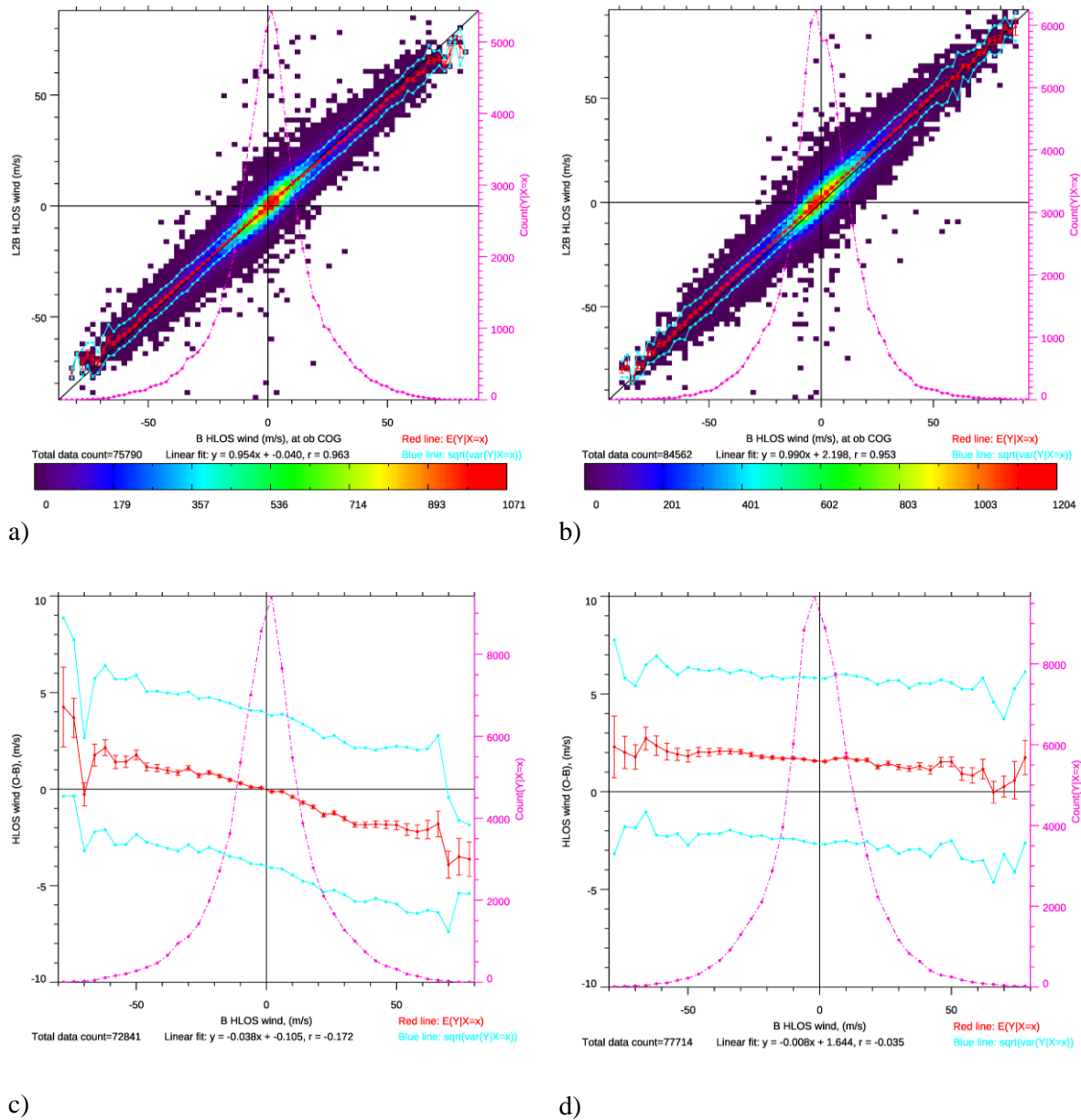


Figure 15. Global L2B Rayleigh-clear O-B statistics over the HLOS wind dynamic range. Dependence of L2B HLOS wind on background HLOS wind: a) in mid-September 2018 and b) in early-January 2019, as shown by 2D histograms. Dependence of mean(O-B) on background HLOS wind in c) mid-September 2018 and d) early-January 2019; the red-line is the mean(O-B) binned as a function of B (with the error bar showing the standard error of the mean), the cyan lines are the  $\pm$  standard deviation of O-B. The pink lines are the data count.

Later in the CP it was discovered that the Aeolus observation bias varies along the orbit; the variation with orbital phase angle (argument of latitude) is shown in Figure 16 for the Rayleigh winds. Zero degrees argument of latitude corresponds to the ascending node equator crossing point. The descending phase of the orbit is between 90 and 270 degrees, elsewhere it is ascending. It can be seen in mid-September 2018 a), that the bias was more positive in the descending phase and more negative

in the ascending phase; which concurs with the assessment of Figure 8 and Figure 15. There is also an orbital phase dependent bias in early January 2019 as shown in Figure 16 b) which peaks at the North Pole and is at its minimum at the South Pole. This has been shown (via L2B processor testing and personal communication with DLR) to be partially caused by an imperfect correction of the AOCS LOS velocity; but for the Rayleigh this is not the dominant source (the explanation for this was discovered after the CP, see Section 3.2.1). If the AOCS LOS velocity correction is switched off in the L2B processor the bias shows less variation with orbit phase in early-January 2019 (not shown). The reported satellite velocity correction maximum amplitude was small at  $\sim 0.16$  m/s HLOS in September 2018 but was up to 1 m/s HLOS in early January with a similar sinusoidal shape as a function of argument of latitude to the mean(O-B) bias. A similar variation of the bias on argument of latitude for the Mie winds in early-January is shown in Figure 19 b); since it applies the same AOCS LOS velocity correction. The cause of the imperfect satellite LOS velocity correction was found to be a bug in a coordinate transformation in the on-board software. This will be corrected on-ground for L1B 7.09.

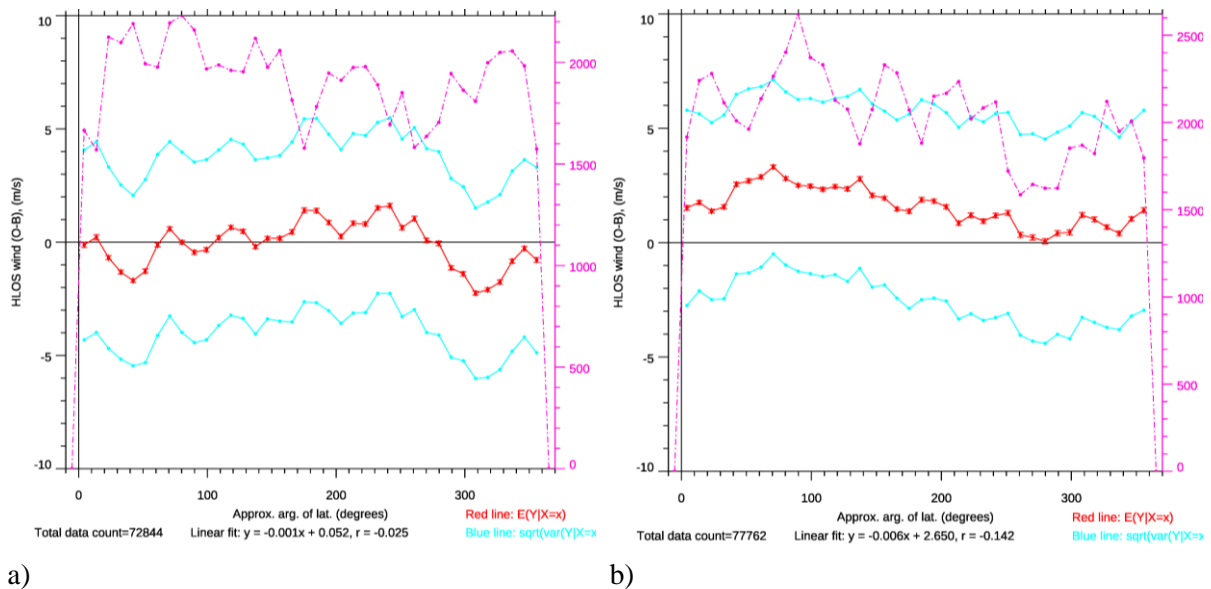


Figure 16. Dependence of the L2B Rayleigh-clear HLOS wind mean(O-B) on the orbital phase angle (argument of latitude) from zero degrees at the ascending node equator crossing point. The red-lines are the mean(O-B) binned as a function of argument of latitude (with the error bar showing the standard error of the mean), the cyan lines are the  $\pm$  standard deviation of O-B and the pink line is the count.

### 3.1.3.2 L2B Mie-cloudy

Global L2B Mie-cloudy O-B statistics for mid-September 2018 and early January 2019 are shown in Figure 17. The average bias in mid-September 2018 was 1.2 m/s, as is also evident in Figure 11. This bias grew significantly and by early January 2019 had reached 4 m/s (after excluding the negatively biased data due to the hot pixel at roughly 3 km (range-bin 13)). The Mie-cloudy random error as assessed by the L2Bp estimated error is almost identical in mid-September 2018 and early January 2019 (at 1.65 m/s), however the profile average robust standard deviation increased from 3.25 m/s to 3.49

m/s, which may be associated with the hot pixel (see the peak in robust standard deviation at ~3 km). To summarise, the Mie random error for the two periods is similar and does not show an obvious effect of the laser energy decrease, as also shown in Figure 12. As already discussed, it is assumed that the backscatter signal from clouds is sufficiently strong for the emitted signal level decrease to not be the limiting factor for Mie random errors.

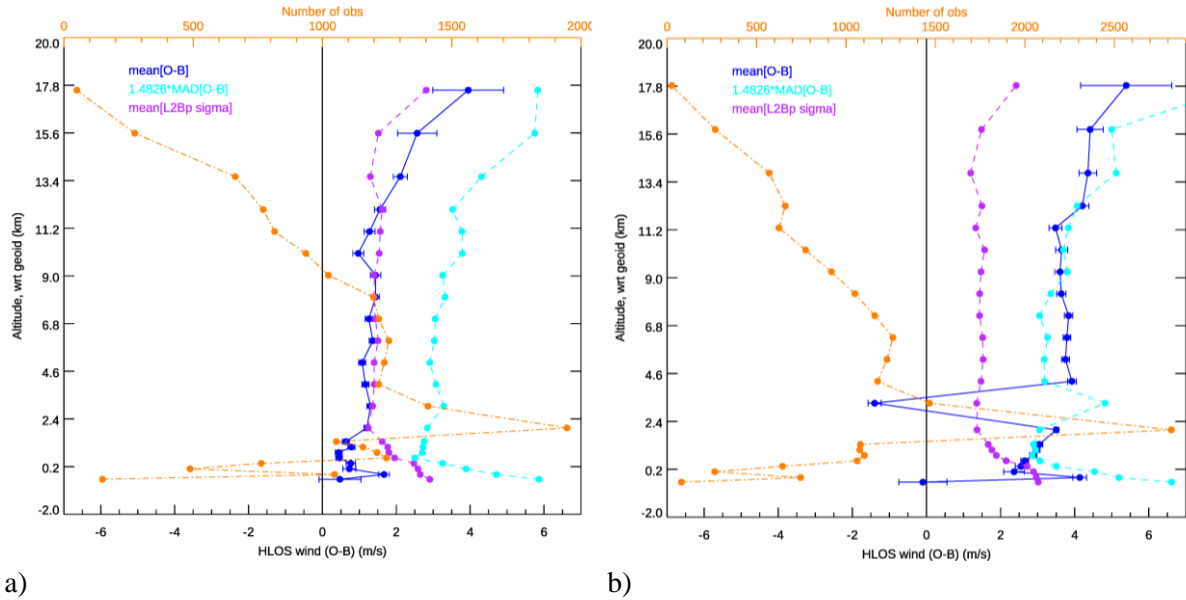


Figure 17. Global L2B Mie-cloudy HLOS wind O-B statistics as a function of altitude. The dark blue line is the mean(O-B), the cyan line is the robust standard deviation of O-B, the purple line is the mean of the L2Bp estimated error and the orange line is the number of observations (read off top axis). a) For mid-September 2018 b) for early-January 2019.

The Mie-cloudy HLOS wind quality over the HLOS wind dynamic range is shown in Figure 18. High correlation coefficients are found: 0.97 in mid-September a) and 0.96 in early January b). The HLOS wind dependence of the bias shows a fast bias (the linear fit shows a wind speed dependent bias which has larger magnitude winds than the ECMWF model) in mid-September with a linear fit of +5%, see c). Note that the independent variable is chosen to be  $(O+B)/2$  rather than B alone, because the Mie observation random errors are of similar magnitude to the model background errors, therefore to decrease the effect of errors in the independent variable for the regression it is beneficial to average. The fast bias also occurs in early-January but is smaller at +3%, see d). It is unclear if the fast bias of the Mie observations relative to the model is a problem with the Mie calibration or in the model winds in the cloudy areas that the Mie samples. It should be noted that Mie-cloudy winds sample different atmospheric conditions to Rayleigh-clear winds, which could lead to differences in the O-B statistics e.g. model wind biases could differ in cloudy conditions, or in boundary layer cumulus clouds.

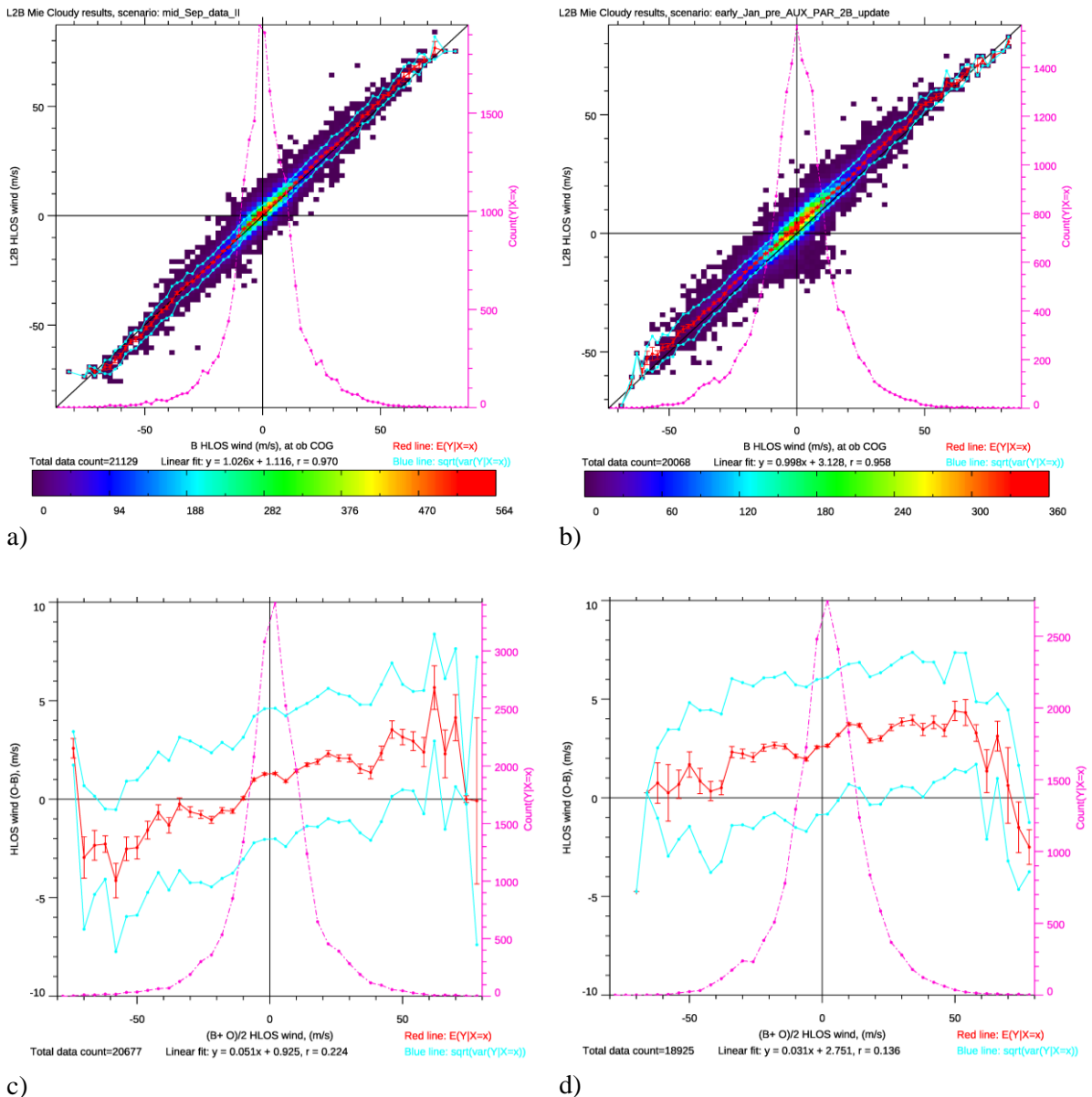


Figure 18. Global L2B Mie-cloudy O-B statistics over the HLOS wind dynamic range. Dependence of L2B HLOS wind on background HLOS wind a) in mid-September 2018 and b) in early-January 2019, as shown by 2D histograms. Dependence of mean(O-B) on background HLOS wind in c) mid-September 2018 and d) early-January 2019; the red-line is the mean(O-B) binned as a function of B (with the error bar showing the standard error of the mean), the cyan lines are the  $\pm$  standard deviation of O-B.

The Mie-cloudy bias as a function of argument of latitude is shown in Figure 19. The dependence in mid-September 2018, Figure 19 a), is thought to be mostly a result of the fast bias (reported above) given the variations in the average HLOS wind along the orbit. The behaviour in early January 2019, Figure 19 b), shares a similar pattern to the applied satellite LOS velocity correction and it thought to be mostly due to this imperfect correction (as discussed earlier for the Rayleigh).

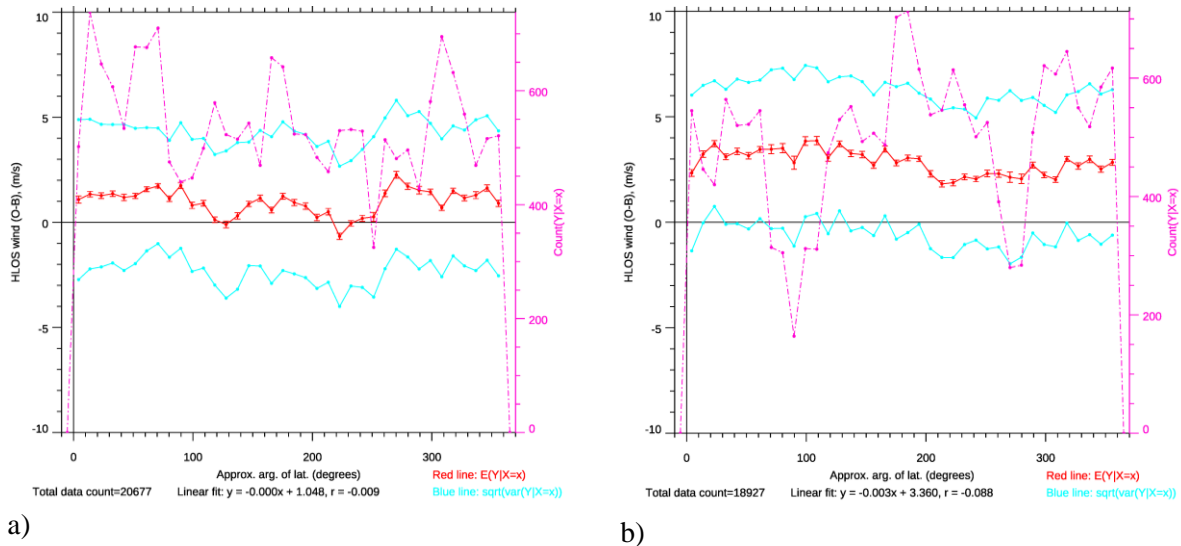


Figure 19. Dependence of the L2B Mie-cloudy HLOS wind mean(O-B) on the orbital phase angle (called argument of latitude) from zero degrees at the ascending node equator crossing point. The red-lines are the mean(O-B) binned as a function of argument of latitude (with the error bar showing the standard error of the mean), the cyan lines are the  $\pm$  standard deviation of O-B and the pink line is the count.

### 3.1.4 Aeolus HLOS wind random error assessment during the CP

The NWP model background forecast random error varies geographically, for ECMWF being largest at the tropical tropopause and smallest in the NH mid-latitudes based on Ensemble Data Assimilation spread statistics (not shown). The global average value for the background u-wind component is estimated to be 1.6 m/s (1- $\sigma$ ) using “Desroziers diagnostics” (estimated for September 2018), see Section 3.1.3.1 (a similar number is derived for the v-component, hence this applies also for the HLOS wind component). From this estimate and our O-B standard deviations in Section 3.1.3, an approximate global average level of random error of the Aeolus L2B HLOS winds is calculated as follows:

$$\sigma_O = \sqrt{\sigma_{O-B}^2 - \sigma_B^2}$$

This is derived assuming that the observation and background errors are uncorrelated. This estimate of Aeolus observation error includes the representativeness error due to mismatch between what the observation represents and what the model can represent, given, for example, the point-like observation operator.

*Table 1. Estimating the global average Aeolus L2B observation error during the CP.*

<b>Observation type</b>	<b>Average HLOS wind O-B robust standard deviation (m/s)</b>	<b>Average observation (1-sigma) estimate (m/s)</b>
<b>L2B Mie-cloudy</b>	3.4	3.0
<b>L2B Rayleigh-clear</b>	4.6	4.3

These results show that the Aeolus L2B HLOS Rayleigh wind random error levels are larger than the pre-launch mission requirements (Ingmann and Straume, 2016).

### 3.2 Understanding biases and longer-term monitoring of Aeolus; from December 2018 until April 2020

Aeolus was introduced into the ECMWF operational data assimilation for monitoring purposes (i.e. blacklisted, so no weight given in the analysis) in early December 2018. This section explains the origins of a significant source of Aeolus bias thanks to detailed monitoring investigations using the operational monitoring and investigations of the quality of the data versus time.

#### 3.2.1 M1 mirror temperature dependent biases

During the Commissioning Phase of Aeolus, comparisons between the Aeolus winds and NWP model winds showed there were significant biases that differed between ascending and descending orbit phases (see Section 3.1). These kinds of biases were expected before launch and were hoped to be taken care of by the Harmonic Bias Estimator (HBE) which uses the ground returns to provide the zero wind reference to calibrate against. However, as we moved into the first Northern Hemisphere Spring in April 2019 it was noticed that the biases increased significantly over the North Pole during the month; see Figure 20. The bias changed by around 4 m/s over the North Pole over four weeks (around 4 radians on this plot).

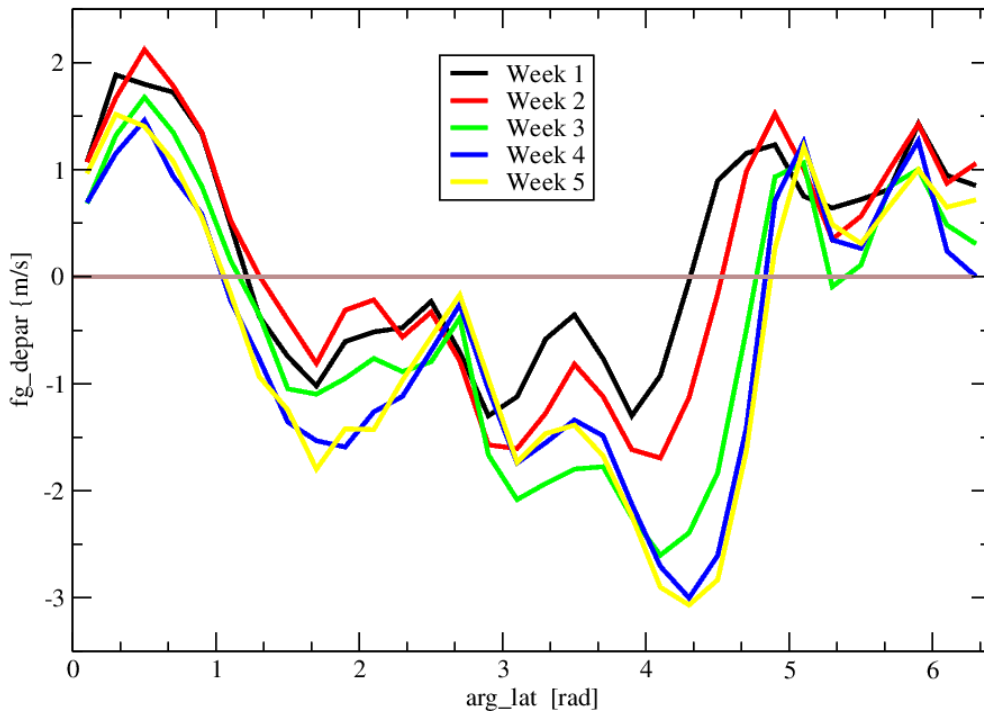
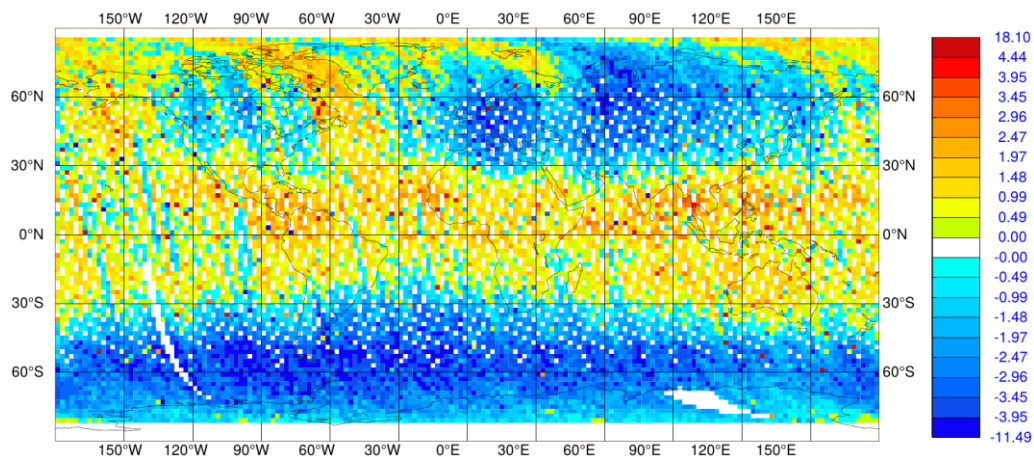


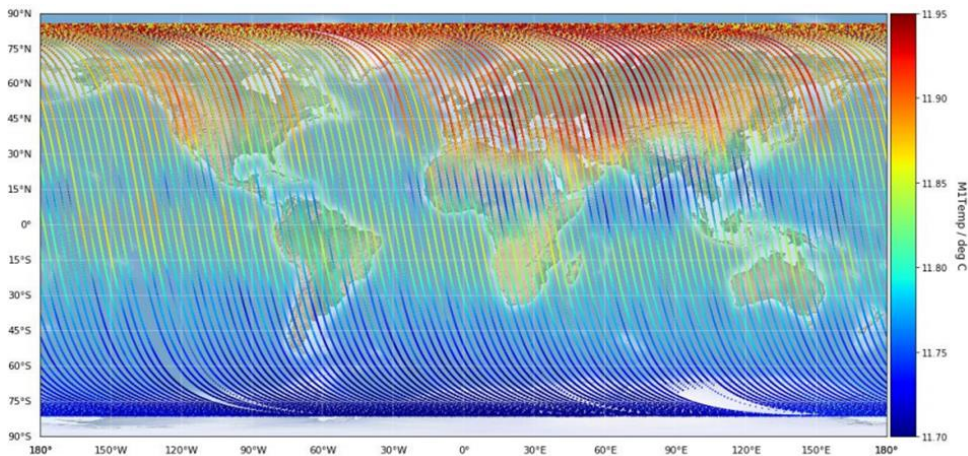
Figure 20. Behaviour of L2B Rayleigh-clear mean(O-B) as a function of a “pseudo” argument of latitude (the “pseudo” argument of latitude is not the true value, but a proxy for it based on the time of the data and the nominal orbital period) for April 2019, one bias curve per week. A dramatic change in the bias occurred over a matter of four weeks for the North Pole region (near 4 radians on the x-axis).

In August 2019, with early FM-B data, we also noticed that there was a large longitudinal, latitudinal and orbit phase variation to the biases, which was reasonably constant over a weekly time scale. It was decided to compare the available housekeeping information to the sub-orbital time

variation of the bias to try to understand what is causing them. Figure 21 shows an example of the monitoring results which led to the discovery that the Rayleigh wind biases have some dependence on the M1 (primary) mirror temperatures. Consistent negative biases were found in the Antarctic region where M1 temperatures were low, but in the NH midlatitudes negative biases were associated with regions where M1 temperatures were high. After further investigations we identified a strong relationship between the M1 temperatures and the bias. This allowed a bias correction procedure to be conceived using a linear combination of the M1 mirror thermistor temperatures as predictors and the NWP model as a reference. A temperature function which is the average of temperatures at the outer rim of the M1 mirror minus the average of those near the centre was discovered to provide very high linear correlation e.g. for an example from 8 August 2019 see Figure 22.



a)



b)

Figure 21. a) L2B Rayleigh-clear mean(O-B) from 6 August 2019 to 7 September 2019 between 0-400 hPa b) M1 mirror average temperature (degrees Celsius) for a similar period (courtesy of Fabian Weiler, DLR).

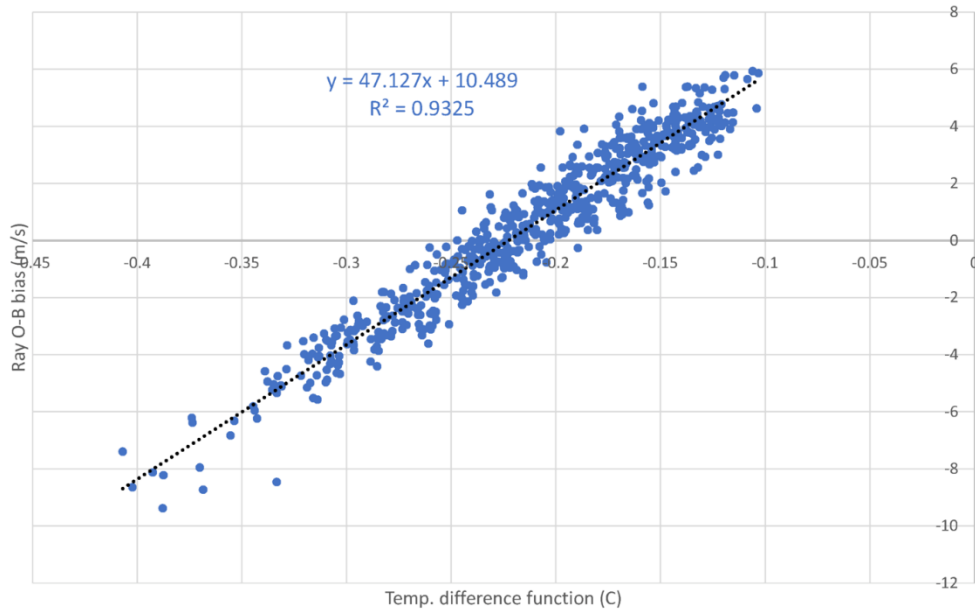


Figure 22. Dependence of L2B Rayleigh-clear mean O-B (bias) on M1 temperature function (mean of outer minus mean of inner temperatures) for data on 8 August 2019. Each blue point represents a 2 minute long sample. The linear fit (black dotted line) is given in the plot. There is a high Pearson's correlation coefficient of 0.93

The M1 mirror temperatures vary along the orbit in response to varying top of atmosphere radiation (short and long wave) and the mirror's thermal control in response to this. The temperature variations (of only up to 0.3 K) are assumed to cause small changes in the pointing of the received laser light from the atmosphere. The spectrometers are sensitive to the change in angle of the incoming laser light and therefore produce an apparent frequency shift and hence wind bias.

Thermal variations were already considered as a source of bias pre-launch along with e.g. line-of-sight pointing errors, but it was assumed that the biases would be a truly harmonic function with orbit phase angle (argument of latitude). In practice we found that the bias was not harmonic, but very scene dependent. Also, an issue with the harmonic bias method is the use of ground returns as the reference, which are (perhaps due to relatively low SNR for Aeolus) only available from high albedo ground conditions which are limited to the poles. Therefore, we do not have a full picture of the zero wind bias across the globe.

It turns out that most of the Rayleigh bias is due to M1 temperature variations, very little comes from, e.g. line-of-sight pointing errors, hence the M1 bias correction works very well. An example of how well the M1 bias correction works for Rayleigh-clear HLOS winds, during an eight-hour period, is shown in Figure 23. Biases ranging from  $\pm 6$  m/s varying along the orbit are reduced to typically  $\pm 1$  m/s.



Figure 23. L2B Rayleigh-clear HLOS wind bias versus time (between 16:00 and 23:59 UTC) on 9 August 2019, in 2-minute samples of mean(O-B) for all wind observations. The red line is before any bias correction and green is after an M1 bias correction using the linear regression coefficients calculated from the previous day (8 August 2019), as shown in Figure 22.

An operational M1 bias correction has been applied in the L2B processor since 20 April 2020 using a multiple linear regression method developed by DLR (Fabian Weiler) using all the thermistors available on the M1 telescope. Either the mean of O-B (from the ECMWF model) or zero wind correction (ZWC) values can be used as the reference, however NWP seems to be a more reliable reference in testing so far (by DLR).

Also, there are calibration drifts due to internal drifts in the instrument (e.g. laser pointing) with time (over days-weeks) which lead to a global bias drift with time. The M1 telescope temperature based bias correction scheme also deals with global offset bias drift by being recalibrated every day – using NWP as a reference (today’s regression is used to correct tomorrow’s biases). The new bias correction scheme using the instrument temperatures as predictors was implemented as part of the L2B processing, removing the need to bias correct Aeolus winds in ECMWF’s data assimilation system. In hindsight we now can confirm that similarly complex Rayleigh biases existed during the Commissioning Phase as shown in Figure 24. However, it appears that FM-B biases have a greater sensitivity to M1 temperature changes than for FM-A, perhaps indicating a greater sensitivity perhaps to angular changes on the spectrometer for the FM-B laser. This will be investigated further as part of reprocessing activities.

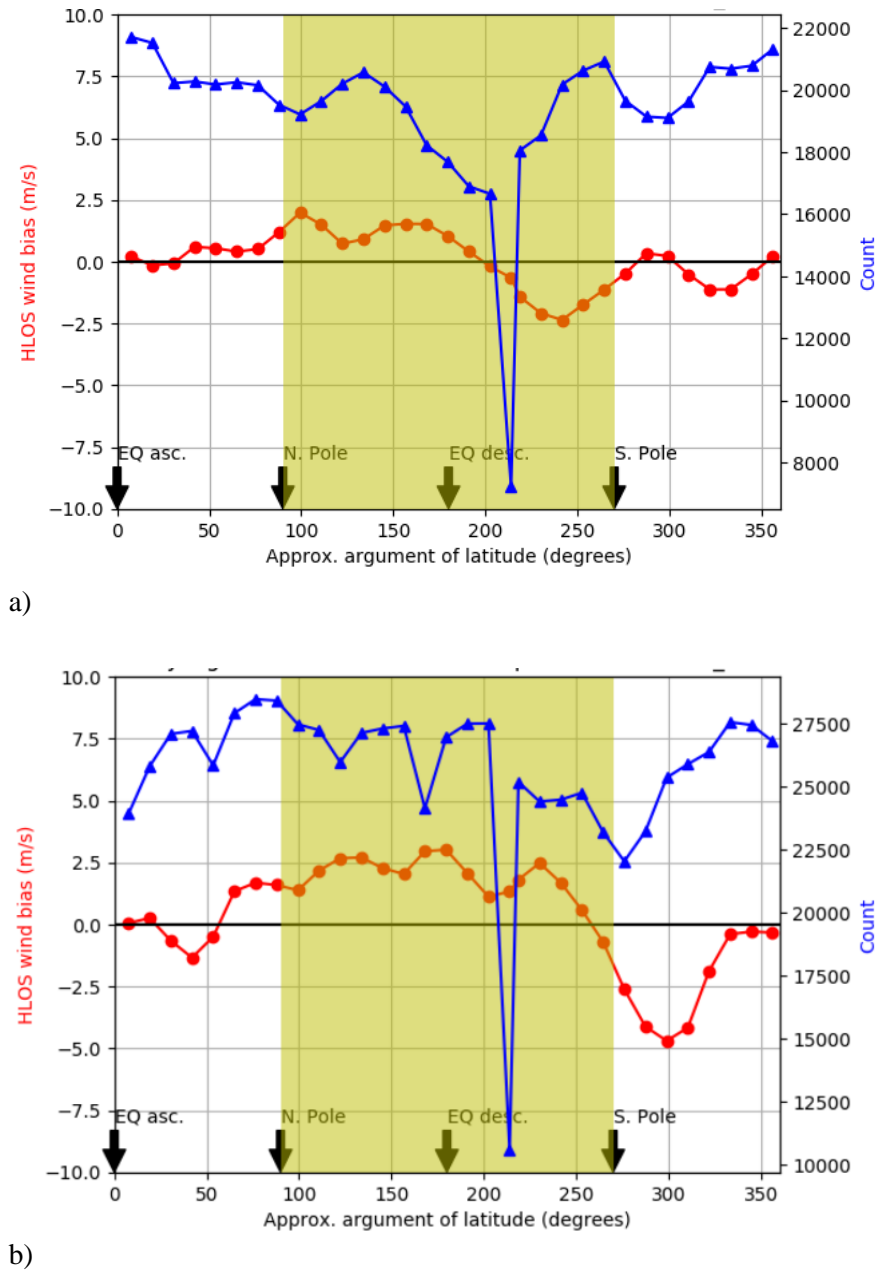


Figure 24. Dependence of L2B Rayleigh-clear mean(O-B) i.e. bias on orbit phase angle (argument of latitude) for a) early FM-A data from 12-19 September 2018 and b) early FM-B data from 12-19 September 2019.

### 3.2.2 Longer term trends in L2B Rayleigh-clear statistics

Monitoring of L2B Rayleigh-clear HLOS wind O-B statistics (via ECMWF operational monitoring) for the whole period available since early December 2018 is shown in Figure 25. The QC applied was reasonably relaxed (reject data if  $abs(O-B) > 15$  m/s) in the attempt to more clearly see trends in random error quality, which can be very sensitive to QC decisions. The L2Bp estimated error is not used for QC.

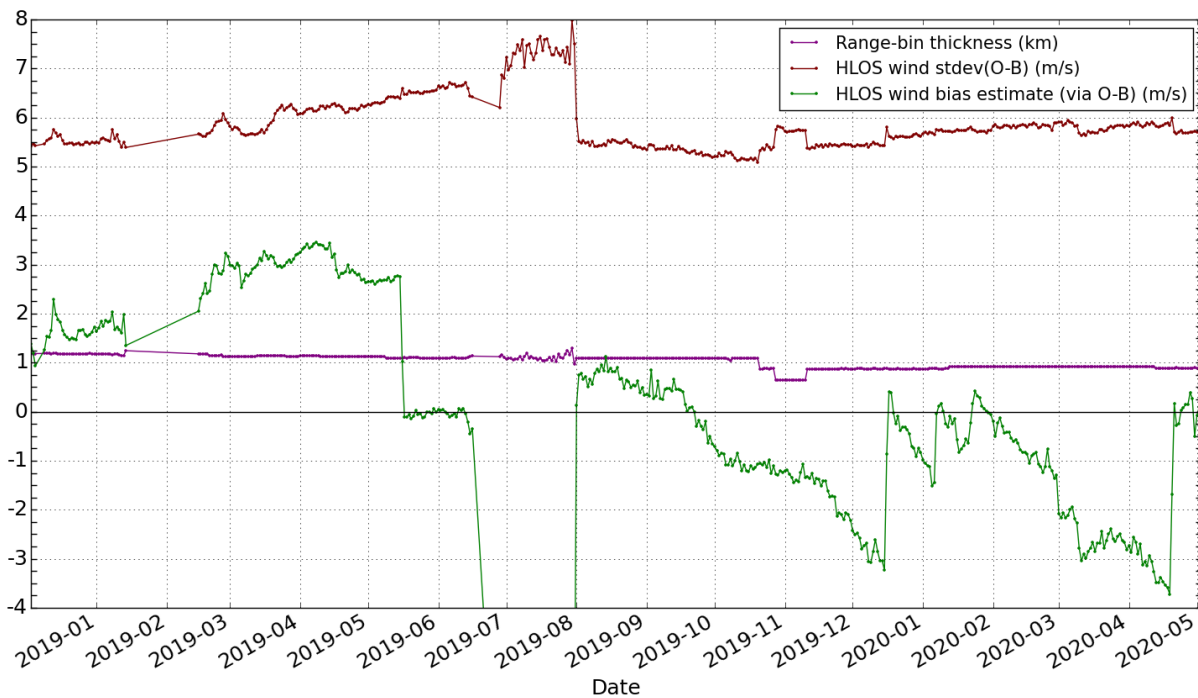


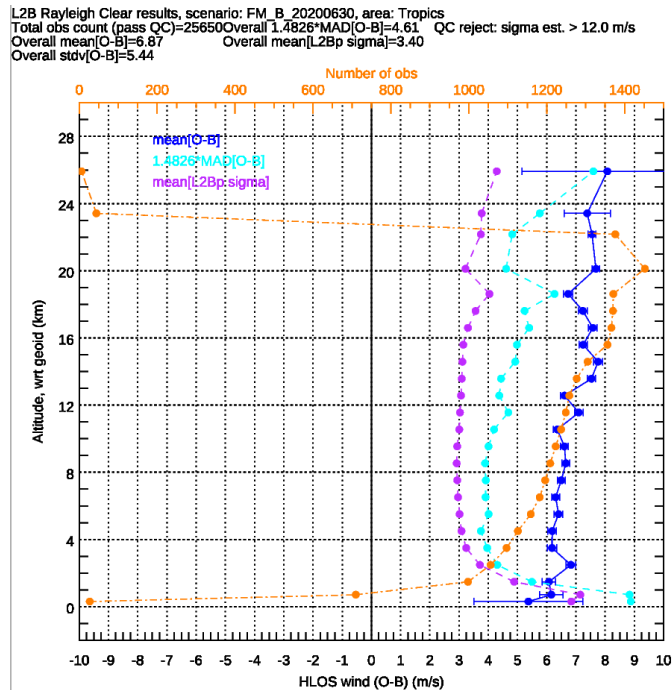
Figure 25. Time series of global and all pressure levels L2B Rayleigh-clear O-B statistics via operational monitoring from early December 2018 until early May 2020. The QC applied was reasonably relaxed; reject data if  $\text{abs}(O-B) > 15 \text{ m/s}$ .

Features which stand out in the statistics are:

- Global average bias (green line) went more positive after the gap in FM-A data in February 2019. The bias then remained reasonably steady (and positive) until a new calibration file was implemented in May 2019, moving it close to zero.
- The missing bias (green line) after FM-B was switched on in late June 2019 was due to the initial operational calibration files being those for FM-A and therefore inappropriate, leading to a very negative bias, which is off the scale of the plot. The bias for FM-B data (from 2 August 2019 onwards when new calibration files were implemented operationally) has been changing at a large rate of around  $-3 \text{ m/s}$  per month. The positive bias jumps on 16 December 2019 and 7 January 2020 occurred due to the application of manual bias corrections to the L2B data. The jump after (around 22 January 2020) was due to an internal reference anomaly. DLR investigations have shown that the negative bias drift for FM-B is due to a drifting internal reference Rayleigh response which is not matched in the atmospheric Rayleigh response (which is relatively stable); suggesting unstable laser pointing. The improvement in bias since 20 April 2020 is due to the M1 temperature bias correction scheme.
- The Rayleigh standard deviation of O-B i.e. random error depends on many factors, such as:
  - Changes in emitted atmospheric path signal
  - Seasonal changes in solar background noise (this is larger in a global average sense in summer periods, and the NH polar summer has larger solar background noise than the SH due to the pointing of the satellite).

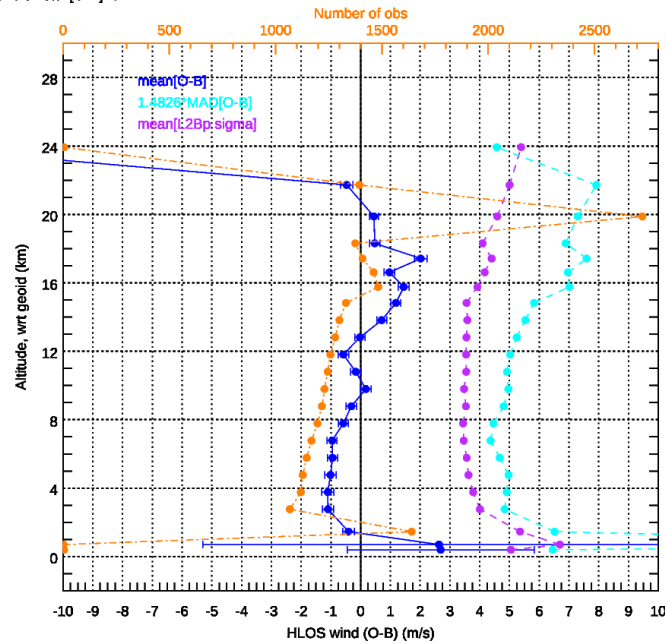
- Seasonal changes in the M1 mirror temperatures induced biases (worse in NH summer)
- Changes in range-bin settings and ground processing versions (the latter will be resolved via reprocessing).
- The random error drifted to larger values for late FM-A period. This is thought to be due to increasing solar background noise, increasing percentage of hot pixels, a fast reduction in atmospheric signal levels due to laser energy decreases and seasonal changes in the M1 mirror temperature dependent bias variations.
- With initial FM-B the Rayleigh random error improved significantly compared to late FM-A. Since then the FM-B random errors have varied to a large extent for the reasons listed above (but not due to hot pixels; these are corrected). There is a trend to larger random errors in late 2019 and early 2020. DLR have confirmed the atmospheric signal for FM-B has dropped by 35% since late June to March 2020, which would increase random errors by at the least 16% (and more when solar background noise is considered). The FM-B random errors in April 2020 are similar in magnitude to those for FM-A in April 2019.

Evidence for FM-B’s atmospheric signal loss influence on wind random errors in shown in Figure 26. Here tropical (less influenced by solar background noise) mid-tropospheric L2B processor estimated error has increased from 30/6/19 (early FM-B) to 13 February 2020 from roughly 3.0 to 3.5 m/s (which is a 16% increase) which is roughly agreeing with expectation due to a ~30% drop in atmospheric signal levels in this period. The effect on robust standard deviation of O-B is more like at 25% increase in noise.



a)

L2B Rayleigh Clear results, scenario: orbit\_8552\_8564\_sappa\_area: Tropics  
 Total obs count (pass QC)=27187 Overall 1.4826 MAD(O-B)=5.78 QC reject: sigma est. > 12.0 m/s  
 Overall mean(O-B)=0.07 Overall mean[L2Bp sigma]=3.98  
 Overall stdv(O-B)=6.77



b)

Figure 26. L2B Rayleigh-clear statistics versus altitude for the tropics (within  $\pm 30$  degrees latitude) for a) 30 June 2019, i.e. early FM-B and b) 13 February 2020.

### 3.2.3 Longer term trends in L2B Mie-cloudy statistics

Monitoring of L2B Mie-cloudy HLOS wind O-B statistics for the whole period since early December 2018 is shown in Figure 27. The QC applied was reasonably relaxed (reject data if  $\text{abs}(\text{O-B}) > 10$  m/s) in the attempt to more clearly see trends in random error quality, which is very sensitive to QC decisions.

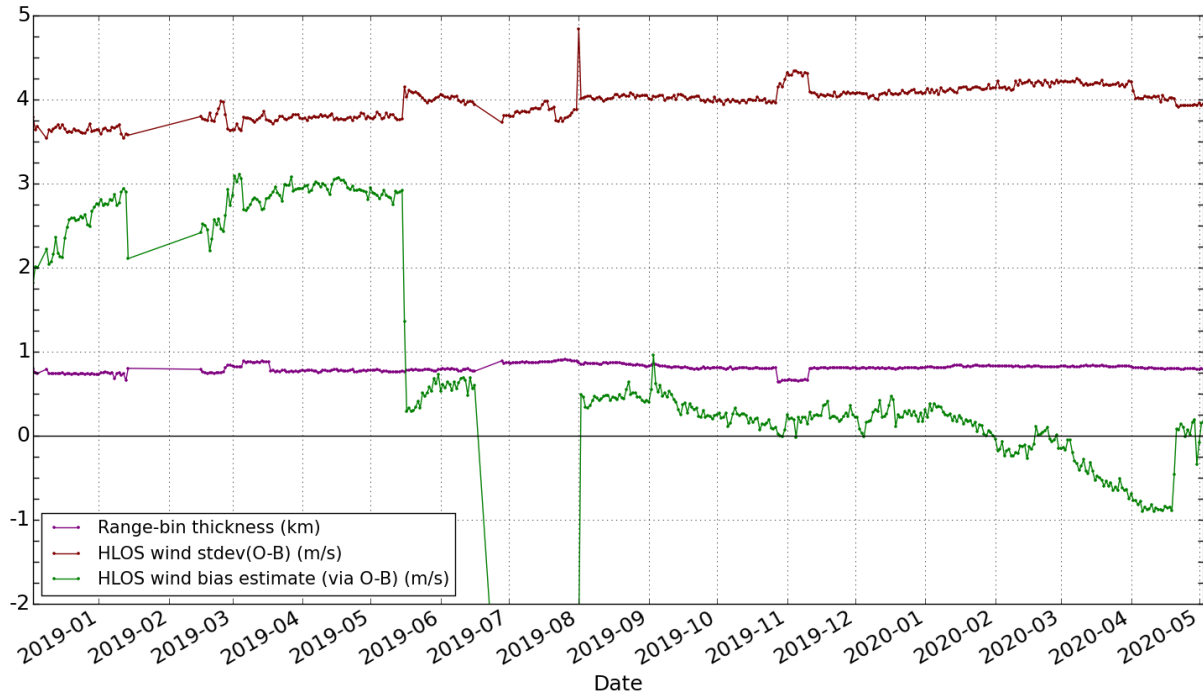


Figure 27. Time series of global and all pressure levels L2B Mie-cloudy O-B statistics via operational monitoring from early December 2018 until early May 2020. The QC applied was reasonably relaxed, reject data if  $\text{abs}(O-B) > 10 \text{ m/s}$ .

Some features which stand out in the statistics are:

- Global average bias had a positive trend for FM-A, although it settled in April 2019 onwards. The bias then dropped by 2.5 m/s when a new MRC file was implemented in May 2019.
- The global bias for FM-B data (since appropriate calibration files were implemented in August 2019) was reasonably stable and  $< 1 \text{ m/s}$  until January 2020, since then it has been drifting to negative values. The improvement in bias since 20 April 2020 is due to the M1 temperature bias correction scheme.
- The Mie random error appears to have increased with time during the mission. Some of this may be explained by imperfect MRC files.

## 4 Results of Aeolus NWP impact assessment at ECMWF

### 4.1 Commissioning Phase OSE results

For the experiment assimilating Rayleigh-clear and Mie-cloudy (referred to as “Rayleigh+Mie”, see Section 2.4.1.1), the 4D-Var analysis showed the expected behaviour and was pulled towards Aeolus observations, as shown by the smaller standard deviation and mean of O-A relative to O-B statistics in Figure 28. The analysis pulls much closer (relatively) to the Mie winds compared to the Rayleigh winds due to the Mie winds significantly smaller assigned observation errors (less than half the Rayleigh wind values). However, there are about five times as many Rayleigh winds as Mie winds assimilated and the Rayleigh winds are sampled in much larger fraction of the atmosphere. Global average statistics such as in Figure 28 show relatively small biases (as expected during this period of known low bias, see Section 2.4.1.2). However, there does appear to be some positive global average bias for upper levels for both the Mie winds and the Rayleigh winds, and at lower levels for the Mie winds. There is a negative bias at around 500 hPa for the Rayleigh winds, which is also seen in Figure 8, which is not understood (but perhaps is a range-bin affected by hot pixels that was not successfully quality controlled).

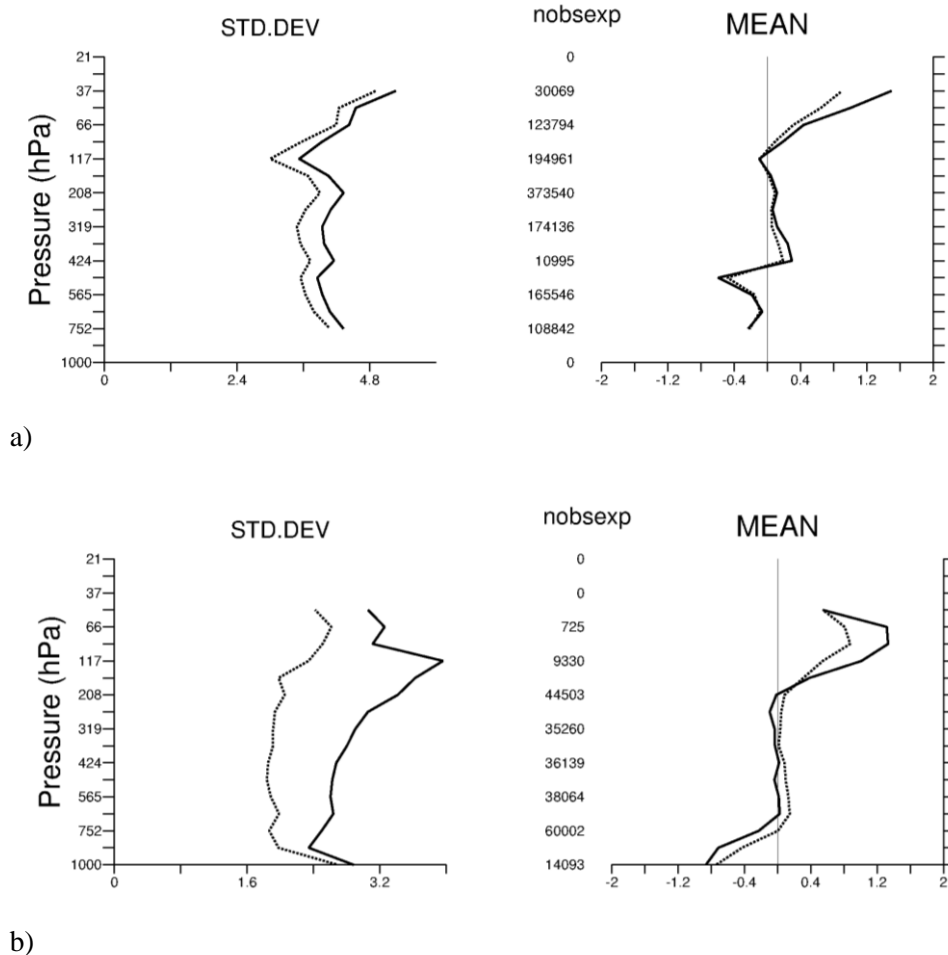


Figure 28. Aeolus global O-B (solid) and O-A (dotted) departures statistics as a function of pressure when L2B Rayleigh-clear plus Mie-cloudy HLOS winds are assimilated. The variable on the x-axis

*is HLOS wind (m/s). The standard deviation is shown on the left, and the mean on the right and the sample size is listed in the middle. The L2B Rayleigh-clear statistics and in a) and the L2B Mie-cloudy statistics are in b). The period is from 12 September 2018 to 16 October 2018.*

Assimilating Rayleigh winds has a notable effect on the mean analysis state for the u-wind component, as shown in Figure 29 (in both a) Rayleigh+Mie and b) Mie only experiments). Note that the effect of Mie winds on the mean state is much smaller. The effect is strongest in the tropics for Rayleigh+Mie where the generally easterly winds are increased by 0.5 m/s in the zonal average (as checked but not shown). This change leads to an increase in bias with respect to tropical radiosonde u-wind mean(O-B) (not shown), hence it is assumed to be caused by Aeolus observation bias and not by a trustful correction of model bias. Interestingly the bias is improved against radiosonde v-wind. The systematic u-wind changes persist in the longer forecast ranges e.g. 8 day (192 hour) forecasts.

The Rayleigh wind speed dependent slow bias (see Figure 15 c) is -2.5% for most of September 2018. Such a bias should reduce the tropical easterly wind speed and not increase it. On closer inspection, it was found that for the small wind speeds present in the tropics, the descending orbit phase is positively biased relative to the ascending phase by about 2 m/s (not shown). It appears that the descending phase bias is causing the tropical easterlies to become stronger. The cause of this descending bias is not yet understood; however, in the orbital phase dependence of the bias is different in January 2019. The slight decrease by 0.03 m/s in the polar vortex (polar night jet) in the SH, is however thought to be due to the Rayleigh slow bias as shown in Figure 15 c).

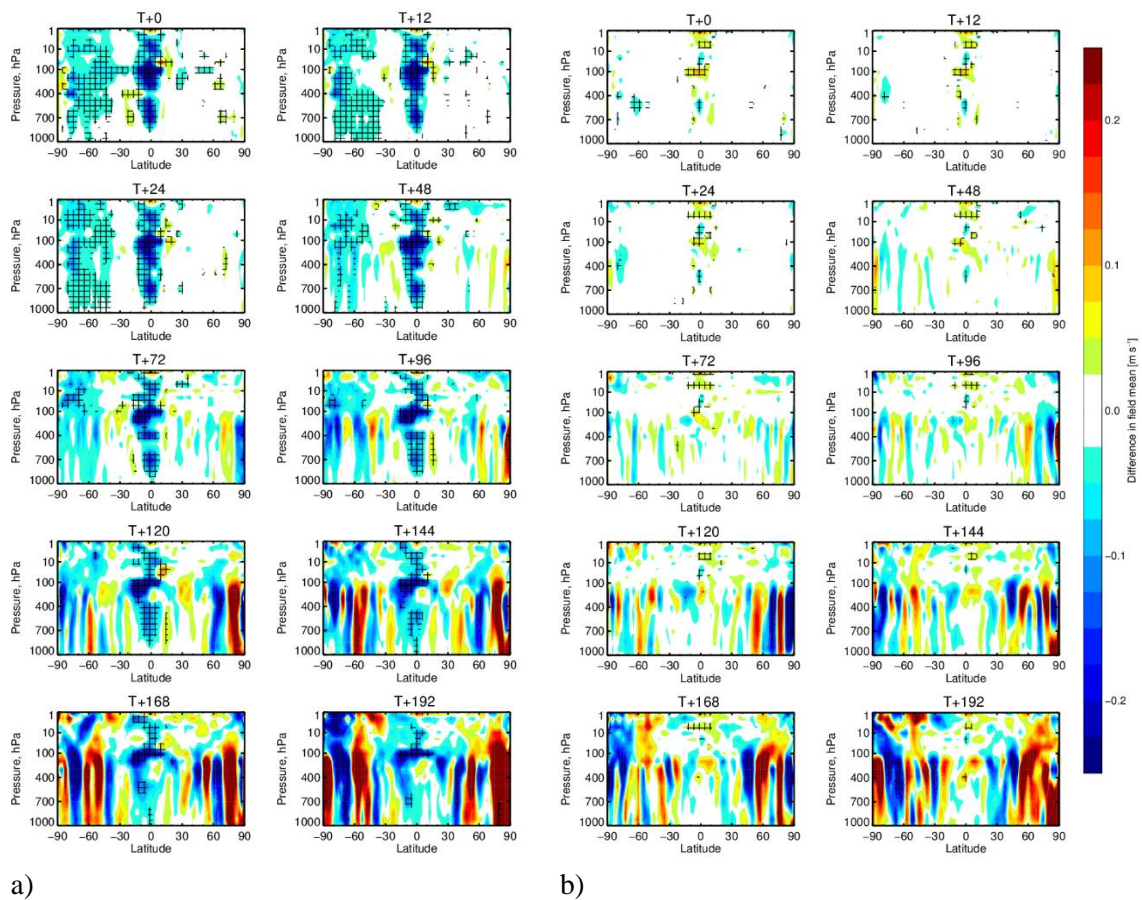


Figure 29. The zonal mean change in analysis ( $T+0$  hours) and forecast ( $T+12$  to  $T+192$  hours)  $u$ -wind fields resulting from assimilating a) L2B Rayleigh-clear and Mie-cloudy HLOS winds and b) L2B Mie-cloudy winds only. The period is from 12 September 2018 to 16 October 2018.

The impact of Aeolus in this relatively short OSE is most robustly demonstrated via the short-range forecasts (up to 12-hour forecasts) fit to other assimilated observation types; this is shown in Figure 30. The other observation types shown consist of: conventional wind observations (radiosondes, pilots, aircraft and radar wind profilers); AMSR-2 (Advanced Microwave Scanning Radiometer 2) all sky radiances; radiosonde temperature; aircraft temperature; geostationary satellite radiances; GPSRO (Global Positioning System radio occultation) and AMSU-A (Advanced Microwave Sounding Unit-A) radiances (mostly temperature information). For the Rayleigh+Mie experiment, the fit to conventional wind observations (which is dominated by the very large sample of aircraft wind observations) shows an improvement of around 1% in the SH extratropics at 300 hPa ( $\sim 8$  km). The improvement in the tropics is roughly 0.7%, with only a small improvement evident in the NH extratropics. Note that the fit to  $u$  and  $v$ -winds from radiosondes only (not shown) is larger e.g. up to 1% in the NH, 2% in the tropics and 1% in the SH extratropics; perhaps because aircraft follow flight paths restricted in spatial coverage meaning that the forecast winds are much better along those flight paths. The assimilation of only the Mie winds (red lines) seems to provide a reasonable fraction of the Rayleigh+Mie impact (black lines). Wind improvements of order 1% in SH extratropics and tropics are comparable to the impact of

other satellite observation types such as infrared sounders, AMV (atmospheric motion vectors) or GPSRO in troposphere as shown in OSE denial experiments from recent years at ECMWF (Bormann et al., 2019).

Globally it is seen that the fit to radiosonde and aircraft temperatures is improved by 0.5% at 300-400 hPa. The fit to GPSRO is improved by 0.8% at 11 km. In terms of humidity and cloud information there is an improvement of 0.8% against some channels of AMSR-2 and improvements in other humidity sensitive observations such as e.g. MHS (Microwave Humidity Sounder) and geostationary infrared imagery. The only observation type to show a clear degradation are the microwave temperature sounders in the lower stratosphere i.e. AMSU-A and ATMS (Advanced Technology Microwave Sounder). AMSU-A channel 11, which peaks around 25 km, shows the worst degradation, but note that Aeolus provided winds only up to around 20 km altitude for this period, hence the degradation does not seem to be the direct effect of its assimilation. Interestingly it must be the Rayleigh winds that cause this degradation, because the Mie only experiment does not show the negative impact against AMSU-A.

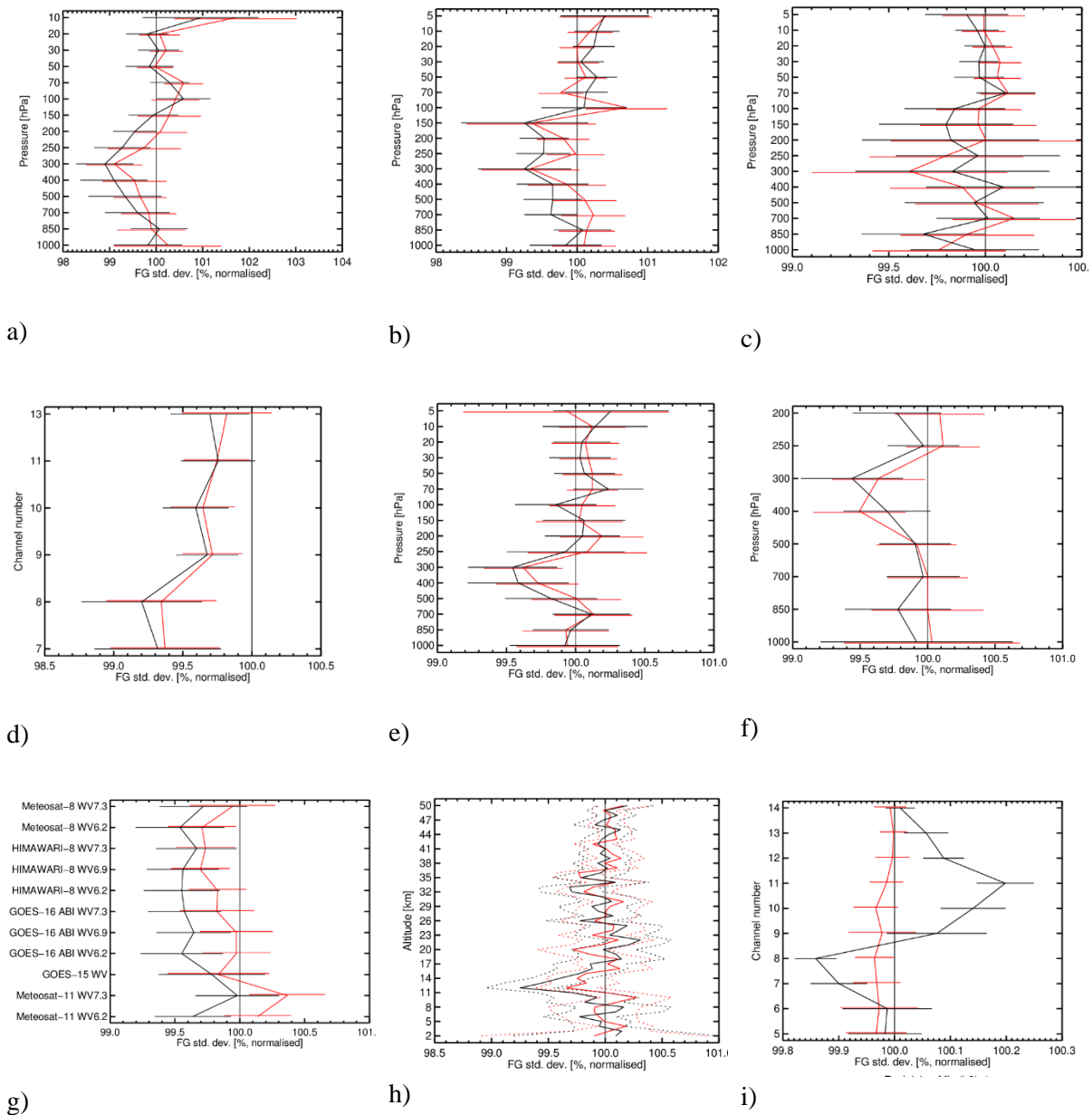


Figure 30. Change in standard deviation of O-B departures (12 hour forecasts) resulting from assimilating Aeolus HLOS wind observations, normalised so that the control is 100%. Values below 100% show an improved fit from assimilating Aeolus and above 100% show a degraded fit. The observation types are a) conventional vector wind in the SH extratropics, b) conventional vector wind in the tropics, c) conventional vector wind in the NH extratropics, d) global AMSR-2 all sky radiances, e) global radiosonde temperature, f) global aircraft temperature, g) global geostationary satellite radiances, h) global GPSRO bending angle and i) global AMSU-A radiances. The black lines are the Rayleigh+Mie experiment and the red lines are the Mie only experiment. Horizontal bars show the 95% confidence range. The period is from 12 September 2018 to 16 October 2018.

The impact of Aeolus on the longer forecast ranges, verified against own analyses, is shown in Figure 31 (both experiments) and Figure 32 (the Rayleigh+Mie experiment only). There is a tendency to positive impact for the Rayleigh+Mie experiment in the SH extratropics at longer forecast ranges of order 2%; and in the tropics at higher altitudes. The impact on the 500 hPa geopotential heights in the SH extratropics also looks promising (not shown). However, the confidence intervals suggest the impact is mostly not statistically significant. A longer reprocessed L2B dataset without bias drift (e.g. six months) should allow for a more robust assessment of the longer-range forecast impact. The impact of the Mie only experiment looks to be neutral, as can be seen in Figure 31, in contrast to the short-range forecast fit to other observation types; this result is not yet understood. The apparent degradation in the shorter range forecasts (red areas in Figure 32) is a typical feature of verification against own analyses, when adding a new observation type which adds variability to the forecasts, and given the improved fit of short-range forecasts to other observation types it is not of great concern.

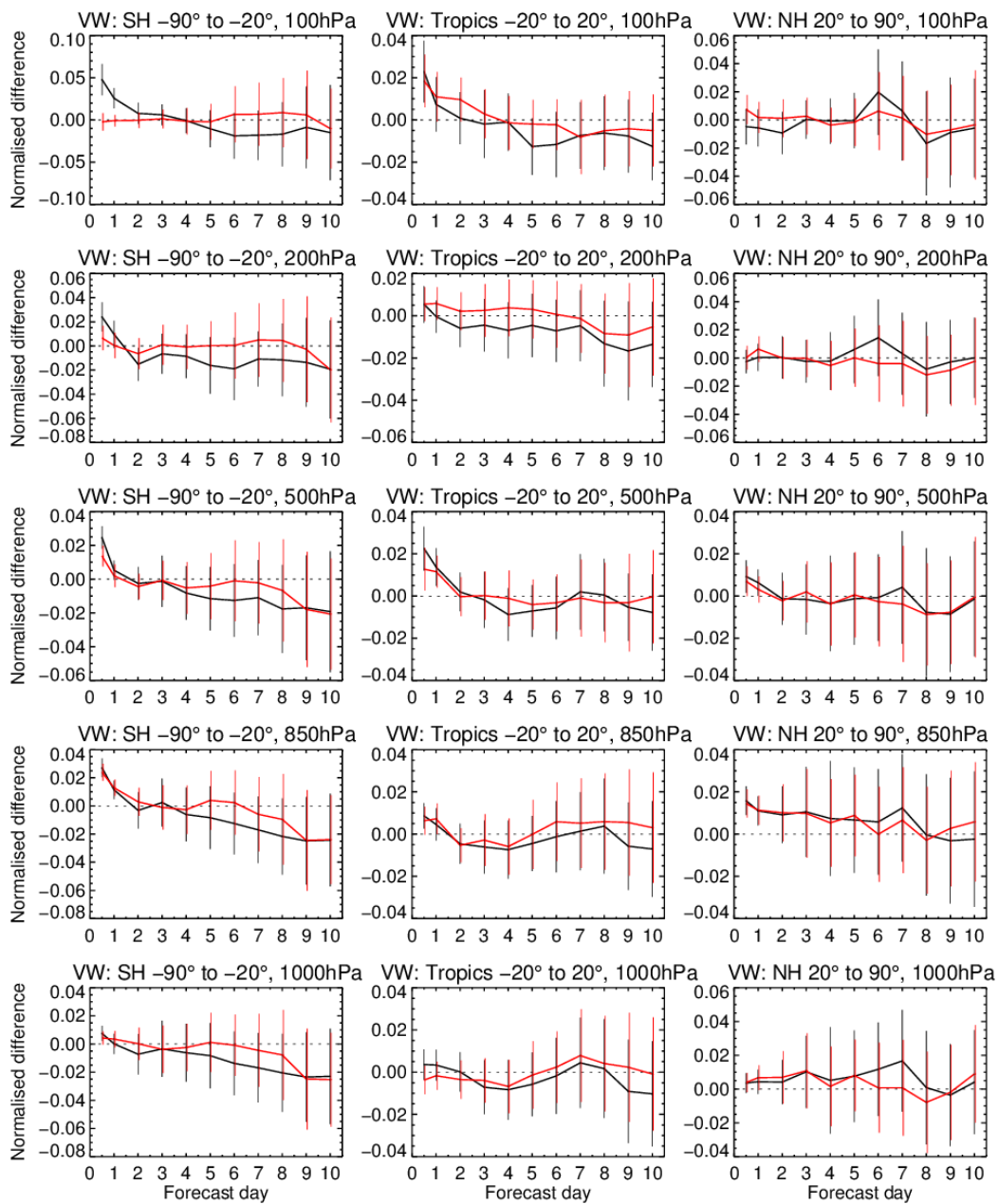


Figure 31. Normalised change in the RMS (root mean square) error in wind vector for different vertical levels (from 100 to 1000 hPa, top to bottom) and for SH, tropics and NH (left to right). The black line is for the Rayleigh plus Mie experiment and the red line is for the Mie only experiment. The period is from 12 September 2018 to 16 October 2018. Confidence ranges are 95%. Negative values indicate a reduction in error from assimilating Aeolus. Verified against own analyses.

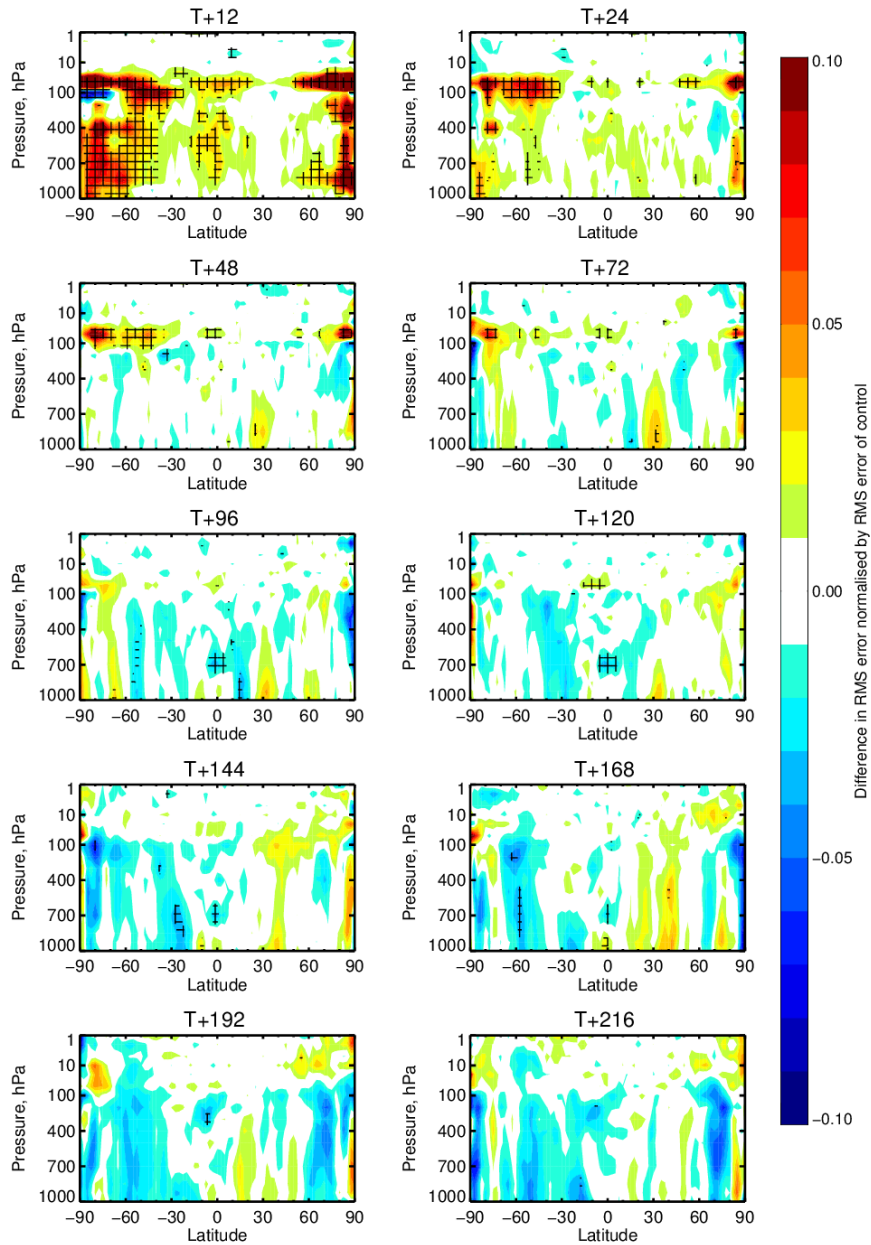


Figure 32. Zonal average normalised change in the RMS (root mean square) error of wind vector for the Rayleigh plus Mie experiment for the period 12 September 2018 to 16 October 2018. Negative values (blue) indicate a reduction in error from assimilating Aeolus and red values an increase in error. Verified against own analyses. Note that the scale is rather large  $\pm 10\%$  which usually occurs when the experiment has not run for long enough.

## 4.2 Late FM-A OSE results

Here we show the results of the experiments performed for the late FM-A period. The description of the dataset is in Section 2.1.2 and the quality control decisions for the OSE experiments are described in Section 2.4.2.

### 4.2.1 Experiments without bias correction

First, we show the results obtained before a bias correction scheme was considered.

Figure 33 shows a map of the 20-day average in April 2019 of the standard deviation of the differences of 200 hPa zonal wind analyses with and without Aeolus, respectively. The largest effects of Aeolus data on the wind analyses are in tropical convectively active areas (along the inter tropical convergence zone) and further south over the Pacific Ocean in extratropical frontal zones (as shown by the satellite imagery of Figure 34, a snapshot in early April 2019). There are also peaks in the south-eastern United States, which was convectively very active for this period, and in the extratropical frontal zones in the northern hemispheric oceans.

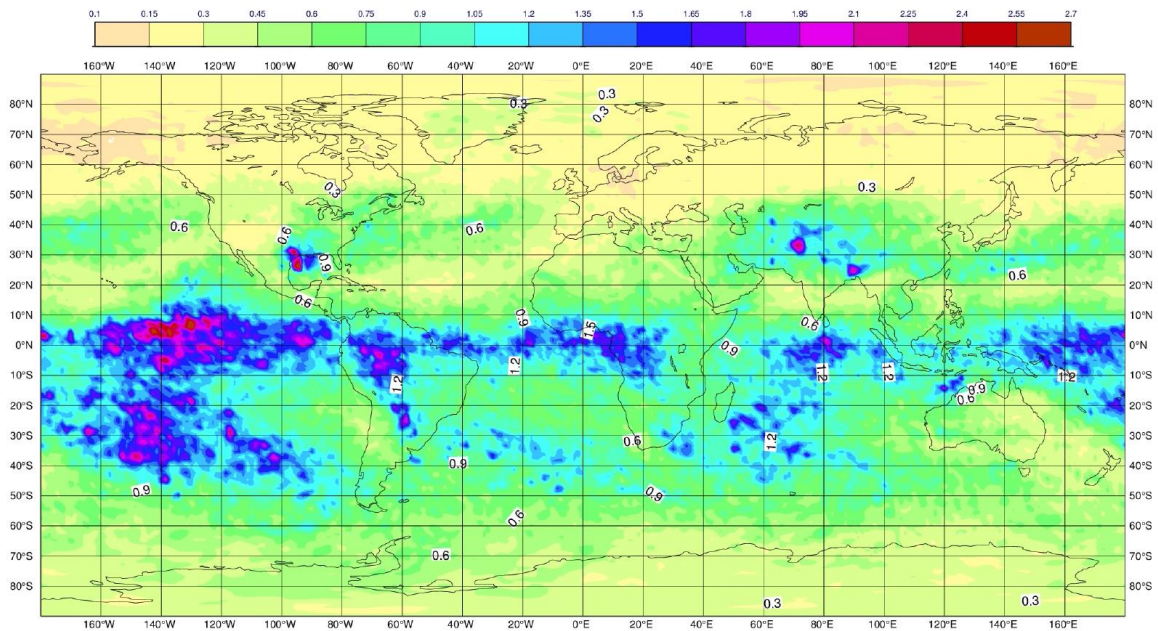


Figure 33. Standard deviation of the differences of  $u$ -wind component at 200 hPa between analysis using Aeolus and control not using Aeolus HLOS winds averaged over the period 4-23 April 2019. Unit of colour-scale is m/s. The scale is from 0.1 to 2.7 m/s.

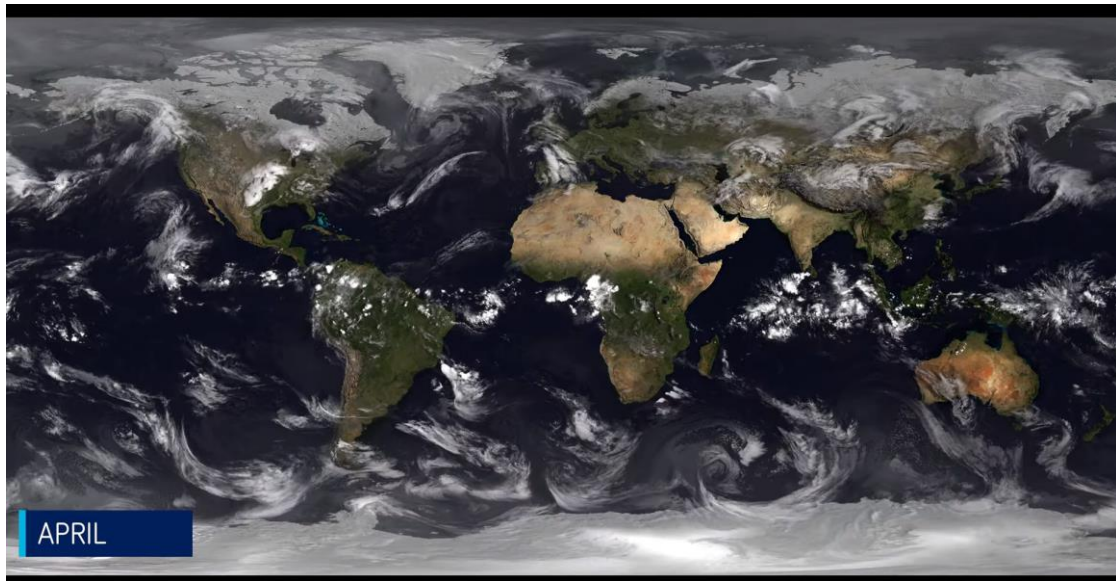
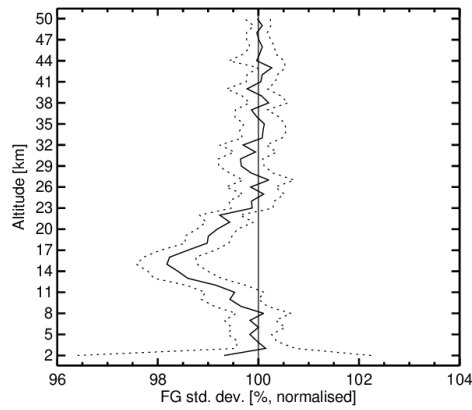


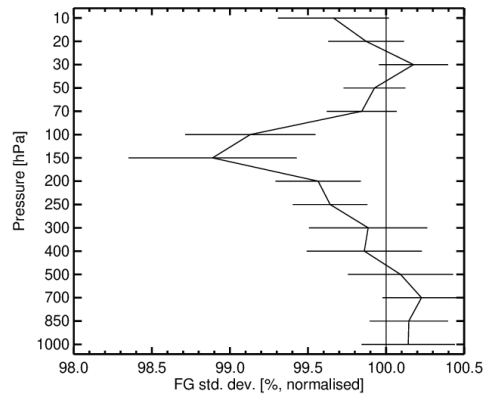
Figure 34. Composite of satellite imagery courtesy of EUMETSAT, an example in early April 2019.

The impact of Aeolus late FM-A data (without bias correction) on short-range forecasts is shown in Figure 35, as assessed by the fit to other observations. Impact was most positive in the tropics. In a), the strong (2%) improvement in fit to GPS radio occultation data in tropical upper troposphere indicates an improvement in temperature; this peaks at about 15 km altitude. The tropical impact is also seen in the fit to in situ wind observation in b), for which the positive impact peaks at 150 hPa (upper troposphere). In c) the fit to AMSU-A radiances in the global sense is most improved for channel 9, which has a peak sensitivity to temperatures at roughly 17 km. The pattern of degraded fit to AMSU-A radiances seen in early FM-A experiments is not seen, which is probably because of thinner range-bins in upper troposphere and lower stratosphere; therefore, reducing the observation operator error (in which we assume no vertical averaging of the winds). Statistical significance for these results is improved compared to the early FM-A period which is likely due to the larger sample of forecasts. The results show that Aeolus is improving short-range temperature and wind forecasts in the upper troposphere. However, there appears to be less impact in mid-troposphere than Sep-Oct 2018 and not so much impact on humidity. This may be due to overweighting the much more numerous 10 km horizontal resolution Mie winds or possibly due to thicker Mie range-bins. For this first experiment of late FM-A the scaling of observation error was 1.4 for the Rayleigh and 1.2 for the Mie. An experiment should be considered (from reprocessed datasets) to assess if we can obtain more NWP impact from a larger sample of higher resolution Mie winds or from longer horizontal averaging and fewer winds.

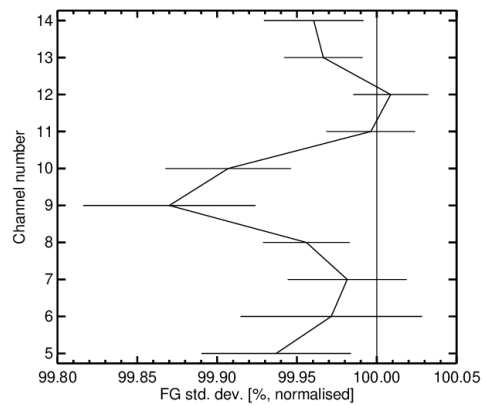
It is reassuring that positive impact can still be obtained from Aeolus for this period in which the FM-A laser energy was rather low (40-50 mJ).



a)



b)



c)

Figure 35. Change in standard deviation of O-B departures resulting from assimilating Aeolus HLOS wind observations (Rayleigh-clear and Mie-cloudy), normalised so that the control is 100%. Values below 100% show an improved fit from assimilating Aeolus and above 100% show a

degraded fit. The observation types are a) GPS radio occultation in the tropics, b) conventional vector wind in the tropics and c) global AMSU-A radiances. Horizontal bars show the 95% confidence range. The period is from 2 April 2019 to 14 June 2019.

The impact of Aeolus late FM-A data (with no bias correction) on longer range forecasts as verified against operational analyses is shown in Figure 36. The results are made up of 128 to 147 samples (with more samples for short-range forecasts). The impact is more positive (blue) than negative (red) for days 2-4 but lacks statistical significance. There seems to be more negative impact in the NH extratropics for days 5-7.

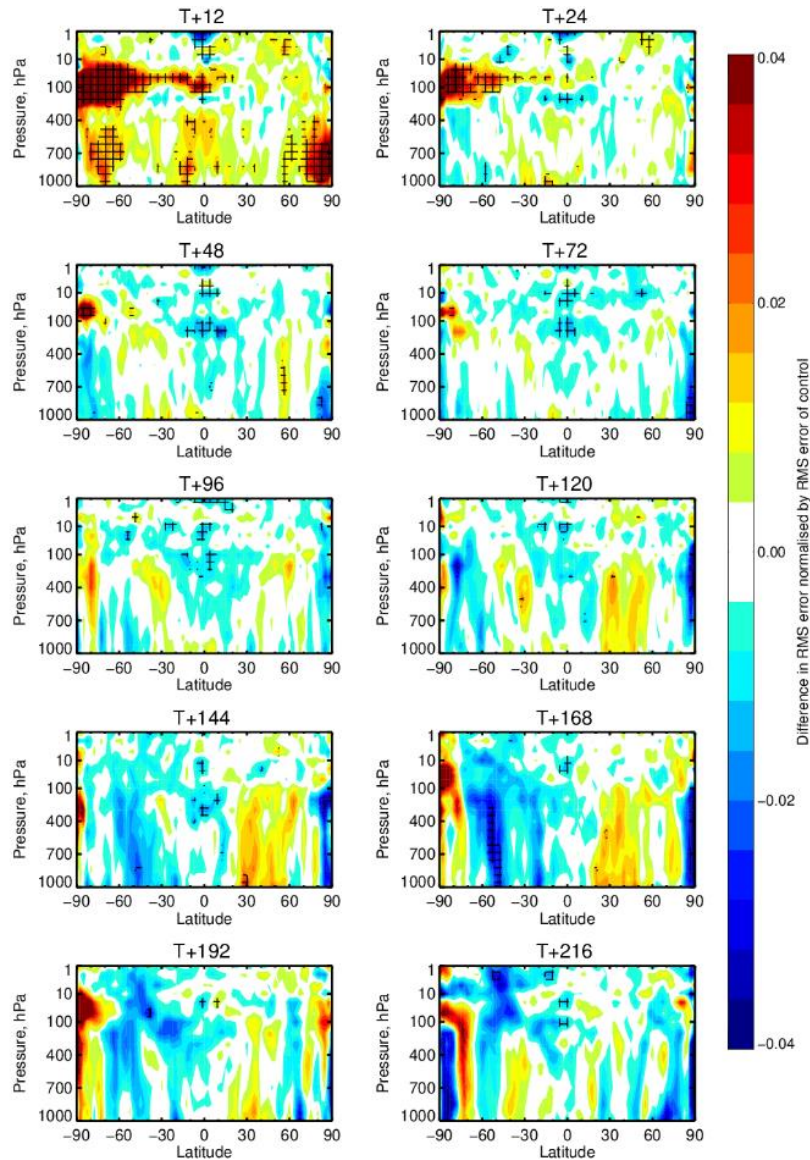


Figure 36. Zonal average normalised change in the RMS (root mean square) error of wind vector for the Rayleigh-clear plus Mie-cloudy experiment (with no bias correction applied) for the period 2 April 2019 to 14 June 2019. Negative values (blue) indicate a reduction in error from assimilating Aeolus and red values an increase in error. Verified against operational analyses. Cross-hatching indicates 95% confidence.

#### 4.2.2 Experiments with bias correction

As shown in the O-B monitoring of Section 3.2.1, the L2B Rayleigh-clear bias was found to vary strongly with argument of latitude for this late FM-A period and the magnitude of the bias became large in the April-June 2019 period, changing a lot in the NH extratropics. To try to correct for this, a bias correction scheme was developed in the ECMWF IFS code using the ECMWF model as a reference. It was implemented via look-up tables of mean(O-B) versus argument of latitude, for which the bias seemed to have strong dependence on. With FM-B data it was noticed that the Rayleigh biases can also vary significantly with longitude in certain latitude bands. The bias correction scheme does not vary with altitude. The bias correction look-up table is applied in the BUFR to ODB (Observation Database) step. Further information on the bias correction is provided in Section 2.4.3.2. The bias correction look-up tables were calculated from operational monitoring (i.e. bias with respect to the operational short-range forecasts); typically using a week's mean O-B statistics. It was found that weekly updates of the bias correction seemed a reasonable refresh rate for the Rayleigh channel. The Mie biases were found to be much more stable with time so less frequent updates were required, however some dependence on argument of latitude existed.

The ECMWF bias correction scheme was found to improve the impact of Aeolus on short-range forecast skill, as can be seen in the fit of short-range forecasts to some important observation types sensitive to temperature, humidity and winds (ATMS and in situ vector wind observations), see Figure 37. The black line (with bias correction) being more to the left than the red line (without bias correction) demonstrates an improvement in Aeolus impact.

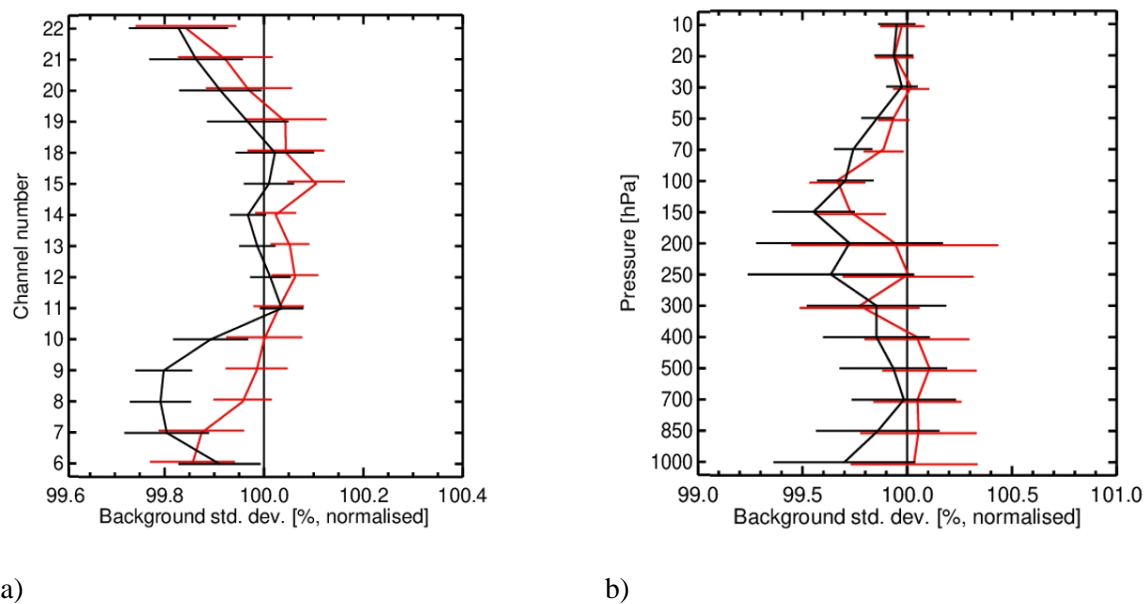


Figure 37. Change in standard deviation of O-B departures resulting from assimilating Aeolus HLOS winds with the bias correction scheme (black line) and without the bias correction (red line) normalised so that the control (without Aeolus) is 100%. Values below 100% show an improved fit from assimilating Aeolus and above 100% show a degraded fit. The observation types are a) global ATMS radiances b) global conventional vector winds. Horizontal bars show the 95% confidence range. The data period is from 2 April 2019 to 14 June 2019.

The ECMWF bias correction look-up table was also found to improve the impact of Aeolus on longer range forecast skill, as can be seen by comparing the impact with the bias correction (Figure 38) to that without it (Figure 36), for vector wind forecast skill as verified against operational analyses. The bias correction leads to larger areas of statistically significant impact in the tropics (cross-hatched areas), particularly at days 2-5 in the upper troposphere. The negative impact at day 5 without bias correction (although not statistically significant) is mitigated to be more neutral with the bias correction. This improvement in NH skill is likely due to the avoidance of the dramatic change in Rayleigh bias that occurred in the NH during the period of the experiment (see Section 3.2.1). The positive impact of bias correction is demonstrated more quantitatively in Figure 39; since the black lines (with bias correction) are more negative (i.e. positive impact) than the red lines (without bias correction).

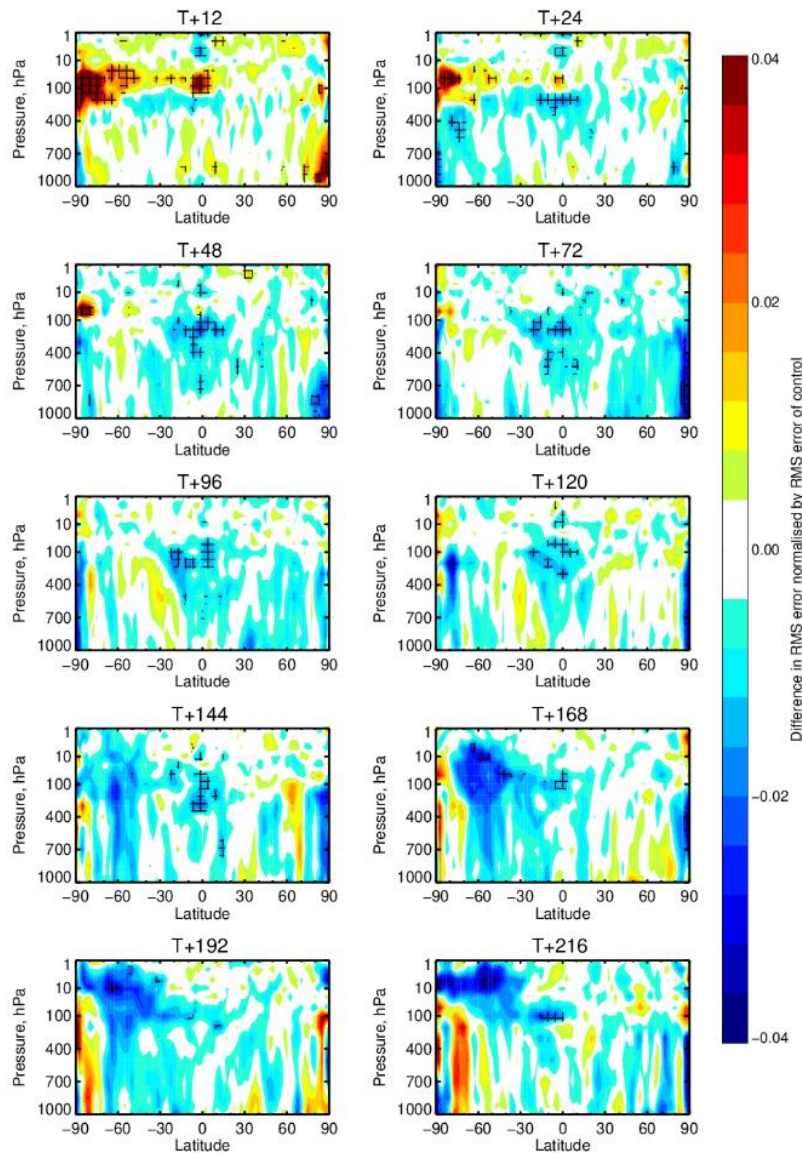


Figure 38. Zonal average normalised change in the RMS (root mean square) error of wind vector for the Rayleigh-clear plus Mie-cloudy experiment for the period 2 April 2019 to 14 June 2019 with the ECMWF bias correction scheme applied (dependence of argument of latitude only). Negative

values (blue) indicate a reduction in error from assimilating Aeolus and red values an increase in error. Verified against operational analyses. Cross-hatching indicates 95% confidence.

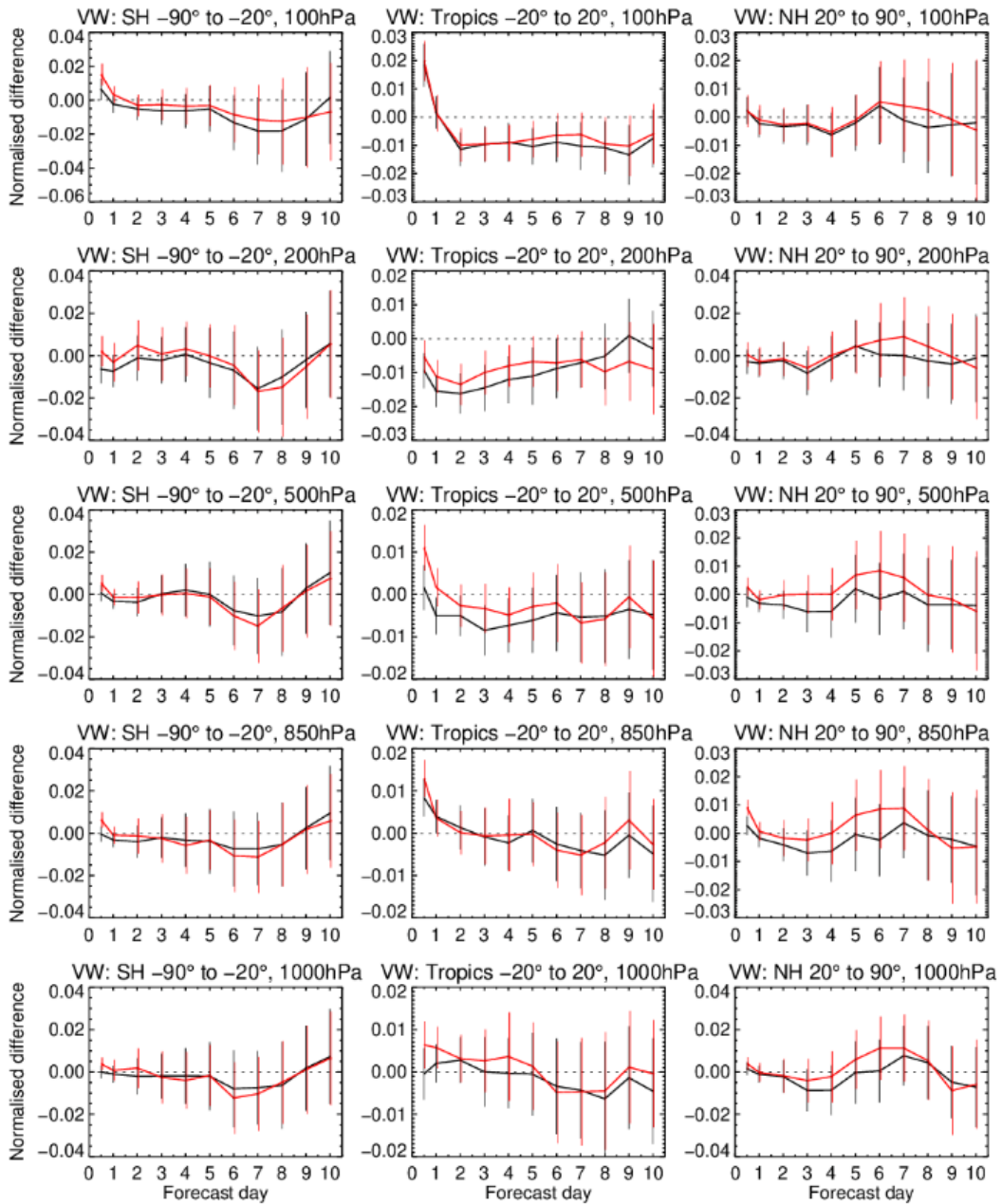


Figure 39. Normalised change in the RMS (root mean square) error in wind vector for different vertical levels (from 100 to 1000 hPa, top to bottom) and for SH extratropics, tropics and NH extratropics (left to right). The black line using the bias correction scheme and the red line is without the bias correction scheme. The period is from 2 April 2019 to 14 June 2019. Confidence ranges are 95%. Negative values indicate a reduction in error from assimilating Aeolus relative to a control without Aeolus. Verified against operational analyses.

Despite having to reject a quarter of the range-bins (blacklisted due to observed hot pixels in the range-bins) and having a rather low reported laser energy, the late FM-A period data was (with a bias correction) still able to provide some useful improvement in forecast skill. The short-range forecasts were statistically significantly improved throughout the troposphere when verified against other observations. The tropical wind forecasts were statistically significantly improved by 1.5% at day 2 dropping to 1% by day 6 at 200 hPa when verified against operational analyses. However, the test period was not long enough, or the impact was not large enough, for the promising improvements in the SH and NH to show statistical significance.

### 4.3 Early FM-B Aeolus impact experiments

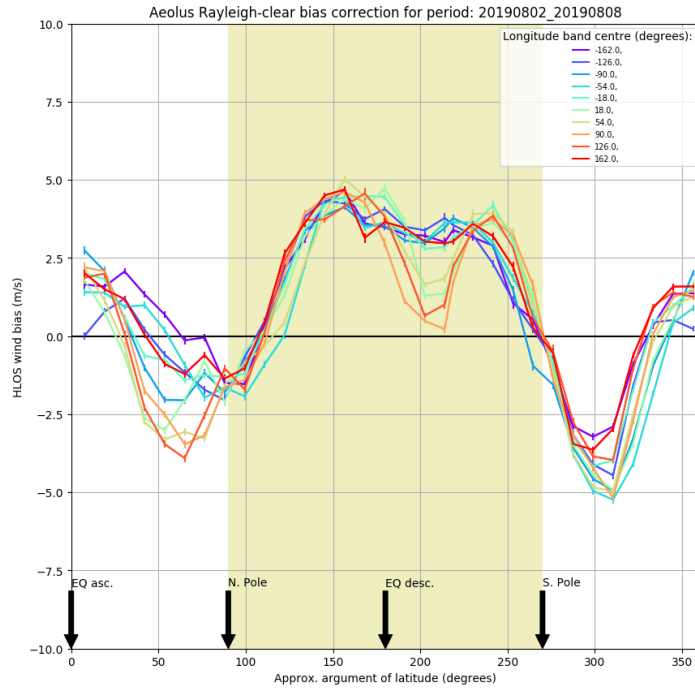
Here we show the results of the experiments performed for the early FM-B period. The early FM-B period data sets is described in Section 2.1.3 and the design and settings for the OSE experiments are described in Section 2.4.3.

#### 4.3.1 Bias correction scheme

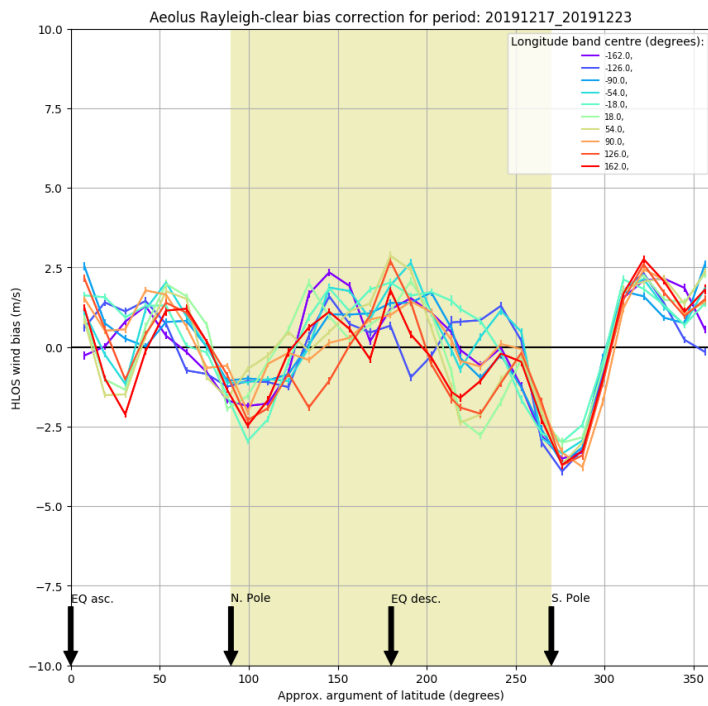
Following the positive impact of the data assimilation bias correction scheme when applied to the late FM-A period OSEs, as discussed in Section 4.2.2, it was decided to continue testing the method with the data assimilation of FM-B data. Initially the bias correction scheme continued to be used as a function of argument of latitude only, however as evidence mounted from FM-B O-B monitoring results, see Section 3.2.1 it was decided that a longitudinal dependence to the bias correction was needed, leading to an extra dimension to the look-up table.

Figure 40 (Rayleigh-clear) and Figure 41 (Mie-cloudy) show examples of how the biases varied with argument of latitude and longitude (for Rayleigh only) for two weeks in August and December 2019. The Rayleigh biases had a larger range of  $\sim 9$  m/s in early August 2019 compared to that in mid-December 2019 of  $\sim 6$  m/s. As discussed in Section 3.2.1 it was later identified that these biases changes are the result of changes in top of atmosphere radiation to which the main ALADIN telescope is exposed. The longitudinal structure has more variability in December 2019.

No clear evidence was found to support the need for a longitudinal dependence for the Mie biases. The structure of Mie bias with argument of latitude has changed with the seasons, but the cause for this is unknown. In the early FM-B OSEs we correct the Mie bias using the mean(O-B) as a function of argument of latitude only. It would be interesting to see the impact of only a global constant offset bias relative to an argument of latitude dependent bias; just in case the biases are due to the ECMWF model. This has not yet been investigated.

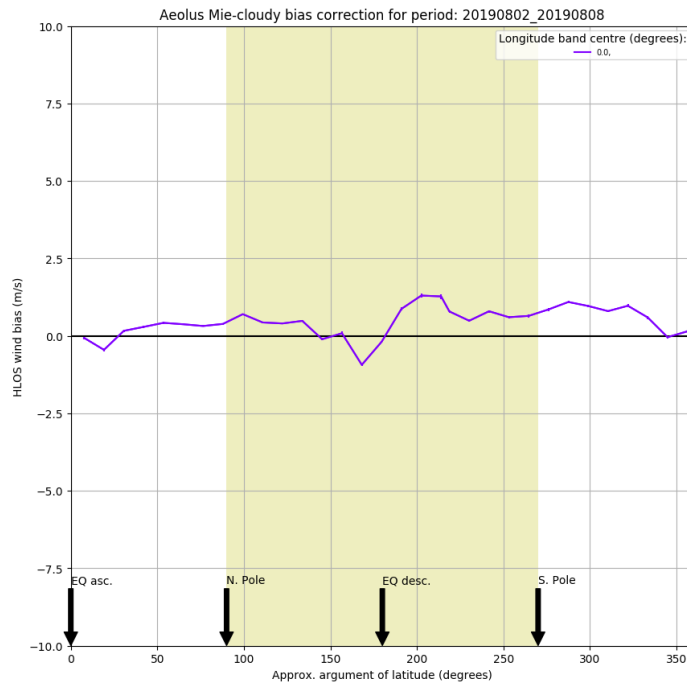


a)

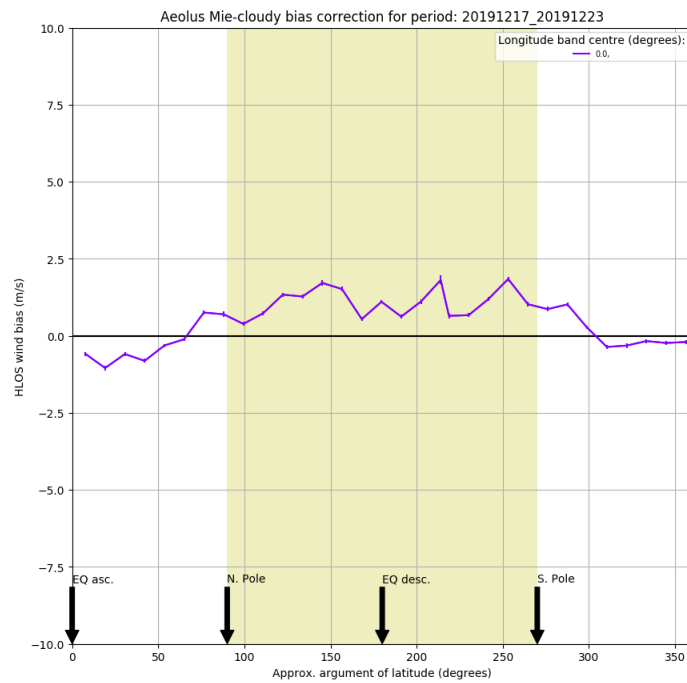


b)

Figure 40. The bias corrections determined for the Rayleigh-clear HLOS winds for the argument of latitude and longitude dependent bias correction; a) calculated for the week from 2-8 August 2019 and b) calculated for the week from 17-23 December 2019. Different longitude bands are shown by different coloured lines (as labelled).



a)



b)

Figure 41. The bias corrections determined for the Mie-cloudy HLOS winds for the argument of latitude dependent bias correction; a) calculated for the week from 2-8 August 2019 and b) calculated for the week from 17-23 December 2019. No longitude dependence to the bias correction was considered here.

#### 4.3.2 Changes to the analysis from assimilating Aeolus

Figure 42 shows a map of the average standard deviation of the differences of 250 hPa zonal wind analyses with and without Aeolus assimilation (both Rayleigh-clear and Mie-cloudy). The largest effects of Aeolus occur in the tropics in convectively active areas (along the Inter Tropical Convergence Zone) and further south over the Pacific Ocean, associated with extratropical frontal zones (and perhaps the Warm Conveyor Belt). This is a similar pattern to the results for the late FM-A period, as shown in Figure 33. The same metric but at 700 hPa (Figure 43) shows Aeolus induced changes reach closer to the poles and again in convectively active areas in the tropics. In the upper troposphere, the largest magnitude changes to u-wind occur at 150 hPa over the East Pacific convective region in a distinct line, with standard deviation reaching 4 m/s, see Figure 44. Interestingly the wind field is changed quite a lot at very high altitudes (1 hPa, ~48 km), which of course is far above the direct influence of Aeolus, which is perhaps due to changes in gravity waves propagation due to Aeolus' influence in the troposphere, see Figure 45. The patterns in v-wind component are very similar in geographical patterns (not shown).

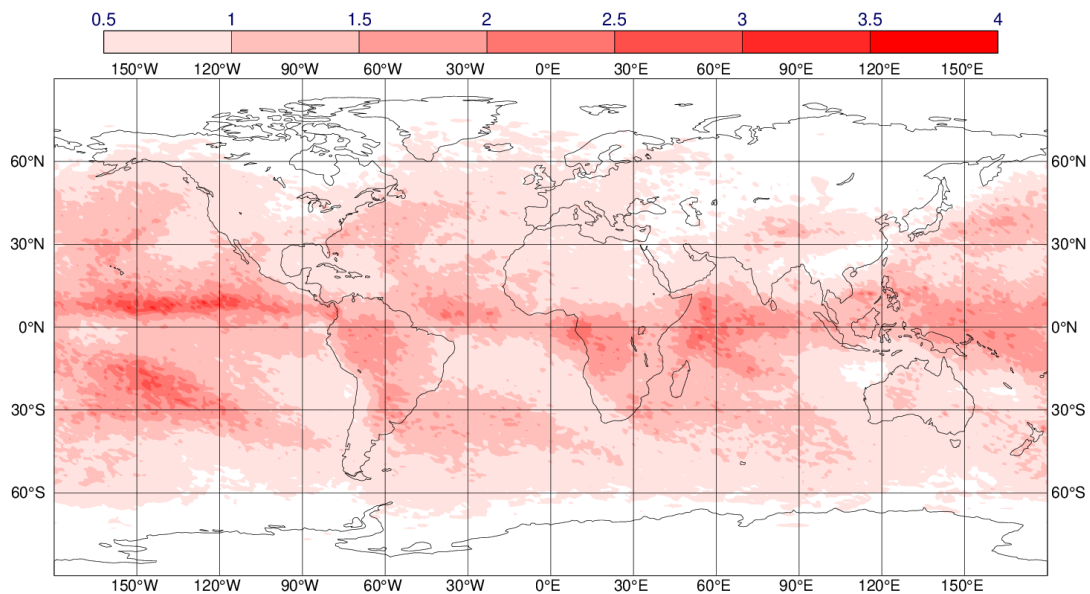


Figure 42. Standard deviation of the differences of u-wind component (m/s) at 250 hPa between the analysis using Aeolus (Rayleigh-clear and Mie-cloudy) and the control not using Aeolus HLOS winds averaged for the period 2 August to 31 December 2019.

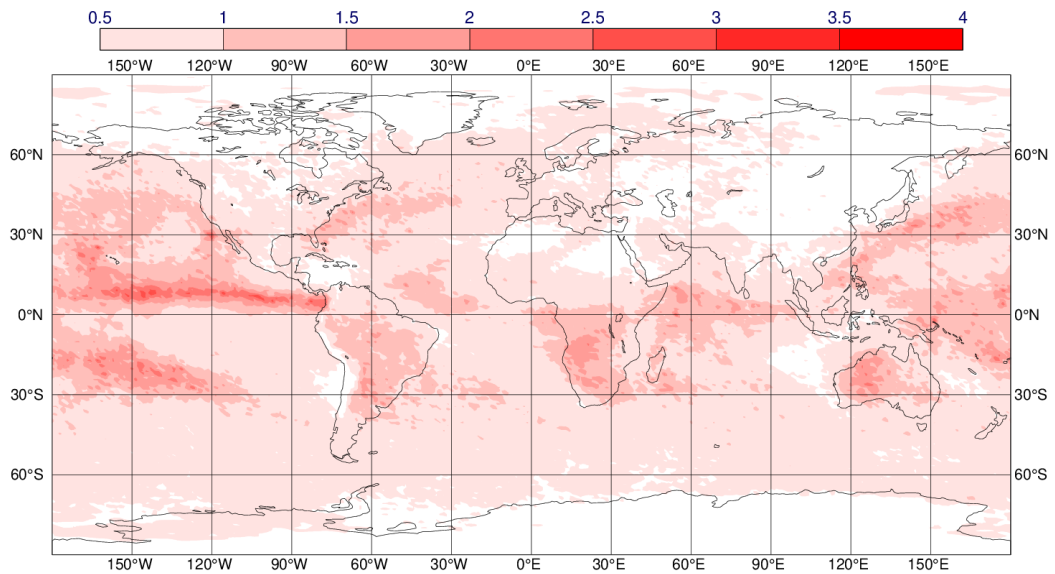


Figure 43. Standard deviation of the differences of  $u$ -wind component (m/s) at 700 hPa between the analysis using Aeolus (Rayleigh-clear and Mie-cloudy) and the control not using Aeolus HLOS winds averaged for the period 2 August to 31 December 2019.

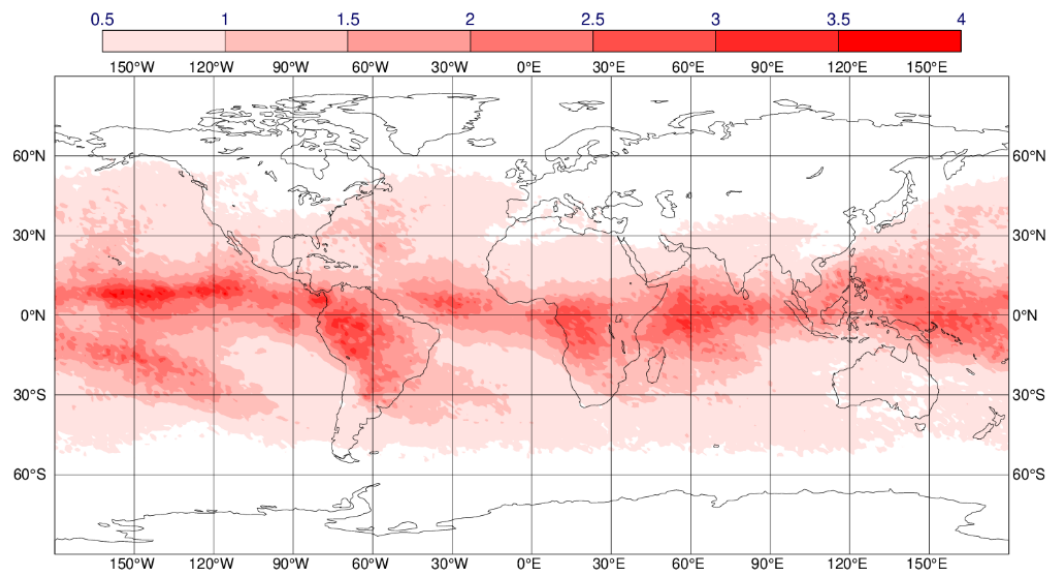


Figure 44. Standard deviation of the differences of  $u$ -wind component (m/s) at 150 hPa between the analysis using Aeolus (Rayleigh-clear and Mie-cloudy) and the control not using Aeolus HLOS winds averaged for the period 2 August to 27 December 2019.

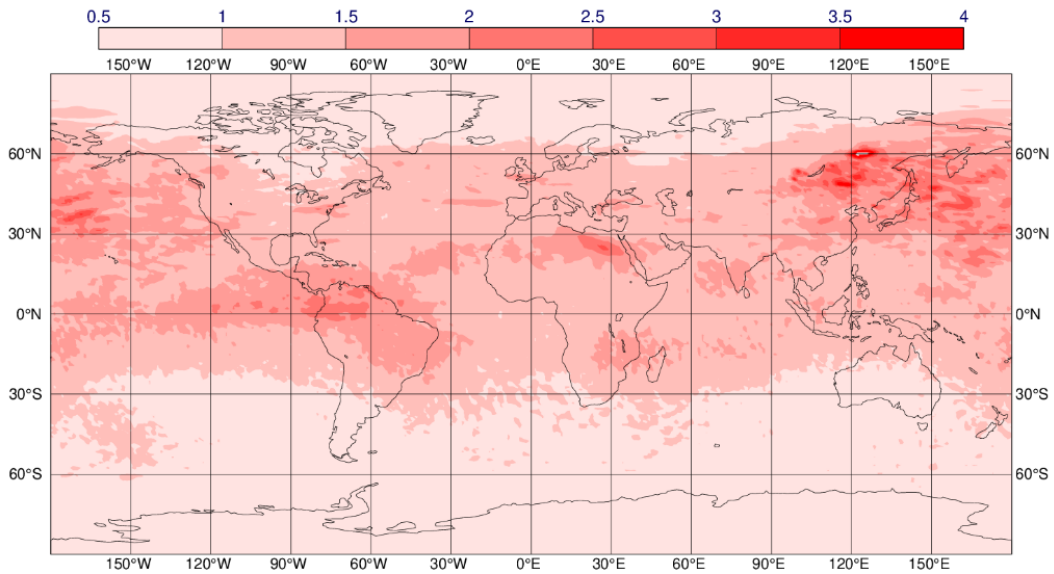


Figure 45. Standard deviation of the differences of  $u$ -wind component (m/s) at 1 hPa between the analysis using Aeolus (Rayleigh-clear and Mie-cloudy) and the control not using Aeolus HLOS winds for the period 2 August to 27 December 2019.

Figure 46 shows the zonal average plots of the systematic (mean) change in wind field after assimilating Aeolus. There is a complicated structure of mean changes in the wind in the tropics and an apparent slowing down of the westerly flow in the Southern Hemisphere at  $-60$  to  $-70$  degrees latitude. The tropical changes are largest around 100 hPa, whereas for the extratropics they are largest at 400 hPa.

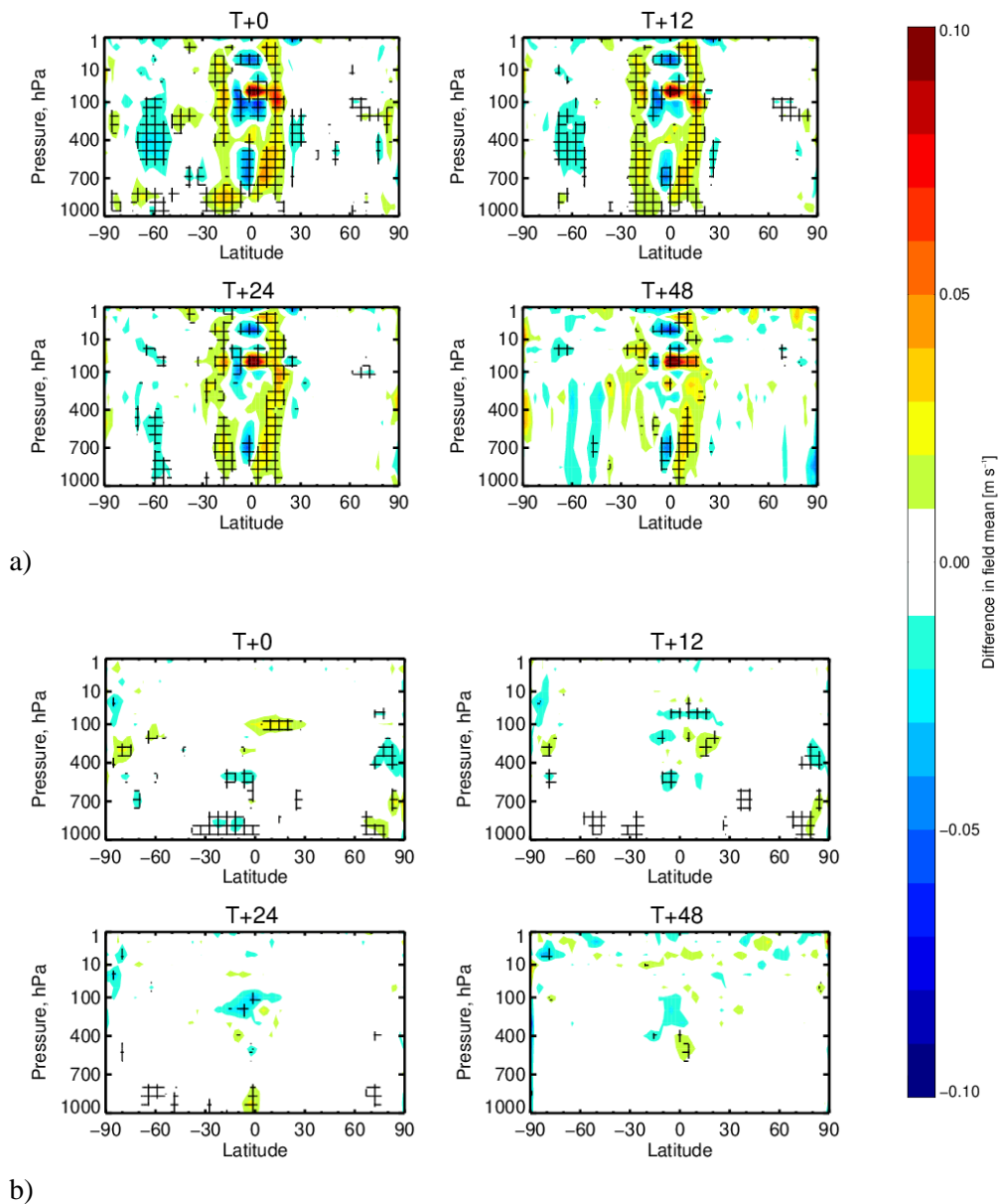


Figure 46. The zonal mean change in the analysis ( $T+0$  hours) and the forecasts ( $T+12$  to  $T+48$  hours) a)  $u$ -wind and b)  $v$ -wind fields because of assimilating Aeolus (Rayleigh-clear and Mie-cloudy). For the period from 12 August 2019 to 31 December 2019.

Figure 47 shows that the mean change in the tropical zonal wind at 100 hPa occurs in longitudinal bands with opposite signs. The changes tend to persist throughout the forecast range. There is also an interesting pattern of mean changes with alternating sign over Antarctica (yet to be explained), which is evident in both wind components.

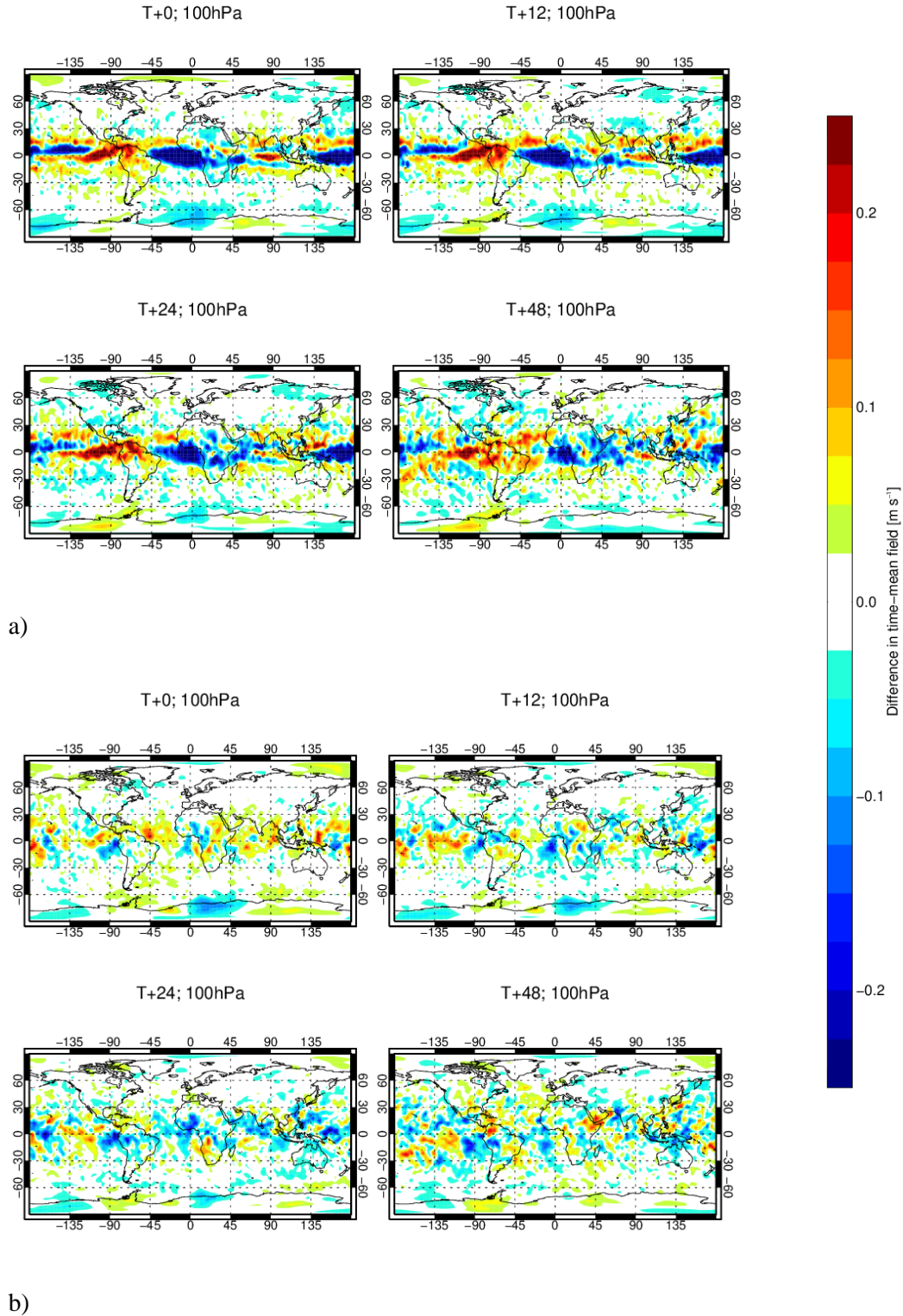
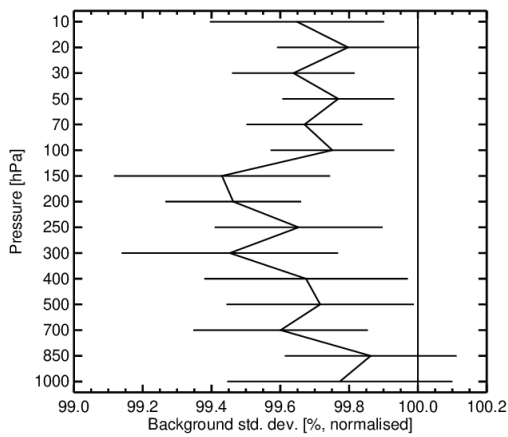


Figure 47. Maps of the mean change in the analysis ( $T+0$  hours) and the forecasts ( $T+12$  to  $T+48$  hours) at 100 hPa for a)  $u$ -wind and b)  $v$ -wind resulting from assimilating Aeolus. For the period from 12 August 2019 to 31 December 2019.

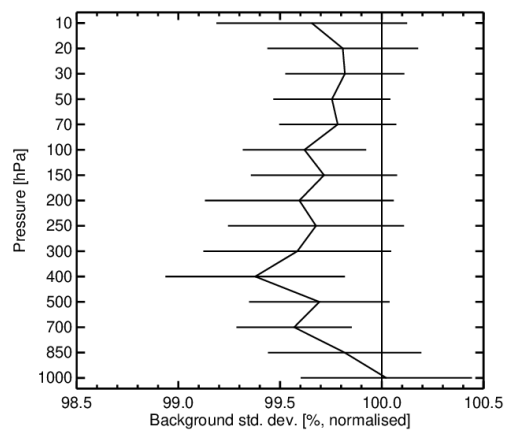
### 4.3.3 Short-range forecast impact

#### 4.3.3.1 Rayleigh-clear and Mie-cloudy

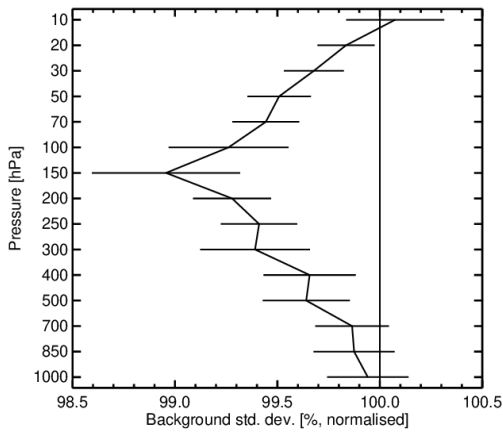
The impact of Rayleigh-clear and Mie-cloudy data on the short-range forecasts (12 hours) as verified by the fit to other observation types is shown in Figure 48 and Figure 49. Figure 48 focusses on in situ wind observations and radiosonde temperature observations. Aeolus improves the short-range forecast fit to vector wind and temperatures by typically less than 1%. The largest impact is in the tropics, with the peak impact at 150 hPa (around 1%), but positive impact is present throughout the troposphere and lower stratosphere. The impact throughout the troposphere and lower stratosphere in the SH extratropics is consistent with altitude, with a peak impact of 0.5%. The impact in the NH extratropics is positive above 150 hPa for wind, but otherwise neutral.



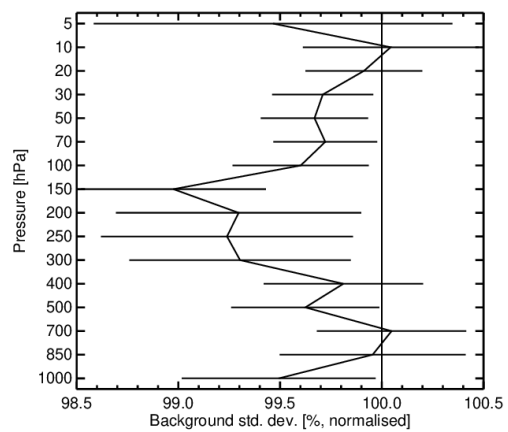
a)



b)



c)



d)

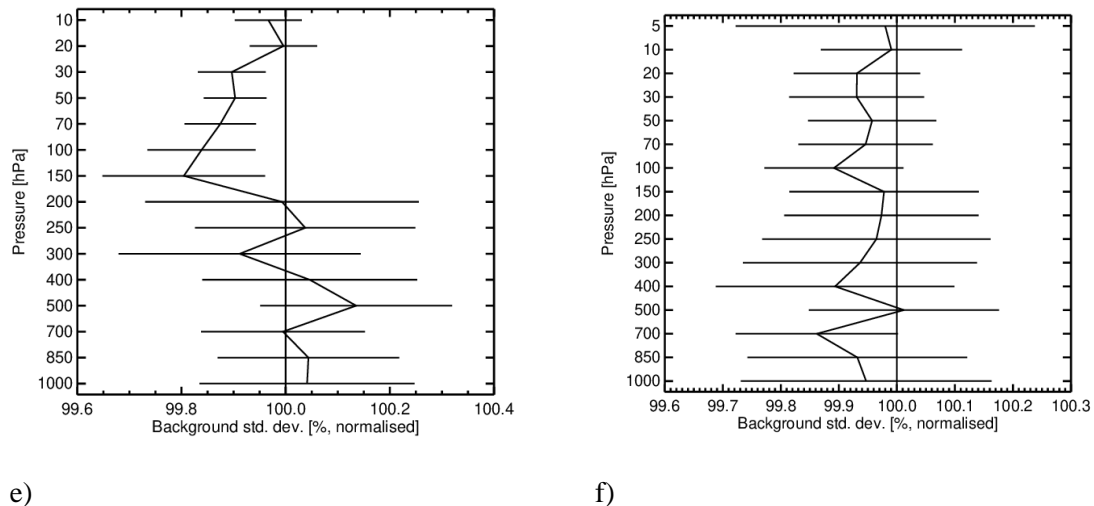
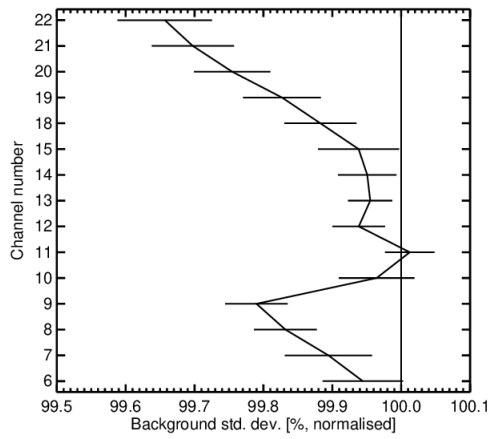
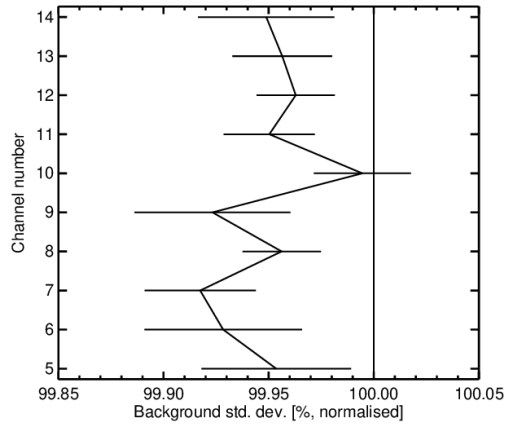


Figure 48. Change in standard deviation of O-B departures resulting from assimilating Aeolus HLOS wind observations (Rayleigh-clear and Mie-cloudy), normalised so that the control is 100%. Values below 100% show an improved fit from assimilating Aeolus and above 100% show a degraded fit. The observation types are a) conventional data vector wind in the SH extratropics, b) radiosonde temperatures in the SH extratropics, c) conventional data vector wind in the tropics, d) radiosonde temperatures in the tropics, e) conventional data vector wind in the NH extratropics and f) radiosonde temperatures in the NH extratropics. Horizontal bars show the 95% confidence range (Student's *t*-test). For the period from 12 August 2019 to 31 December 2019.

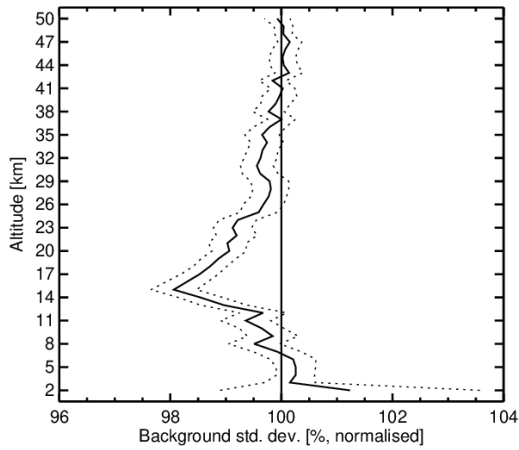
Figure 49 shows the short-range forecast fit to a large range of satellite observations. Aeolus improves the fit to global microwave sounding temperature sensitive channels (for ATMS and AMSU-A) and to ATMS humidity sensitive channels (18-22). GPS radio occultation fits are improved by 2% at ~14-15 km in the tropics (upper troposphere), with the positive impact seen throughout much of the troposphere and lower stratosphere; this is similar to equivalent plot for the late FM-A data (see Figure 35a). Relative to the infrared sounding instrument CrIS, Aeolus shows improvements in temperature sensitive channels in the upper troposphere and lower stratosphere and in channels sensitive to the surface temperature and humidity. The change relative to AMVs is positive at 200-250 hPa and near the surface; but there is a small negative impact at 700 hPa (perhaps associated with the top of boundary layer clouds). The fit to geostationary water vapour imagery is improved, as is the fit to the FY-3B microwave humidity sounder. Finally, in the NH, there are improvements relative to scatterometer winds (ASCAT) and wave height altimeter data (RALT).



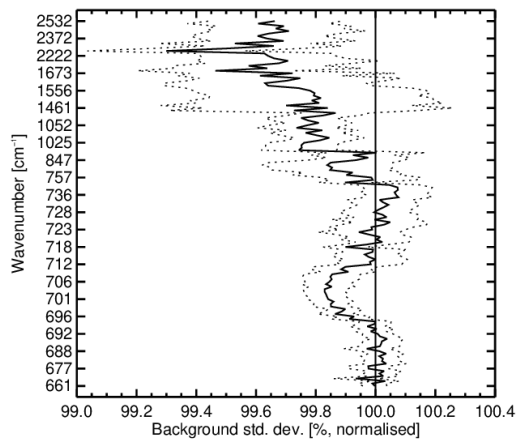
a)



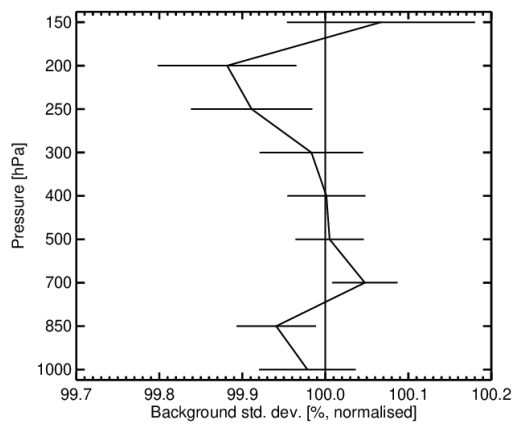
b)



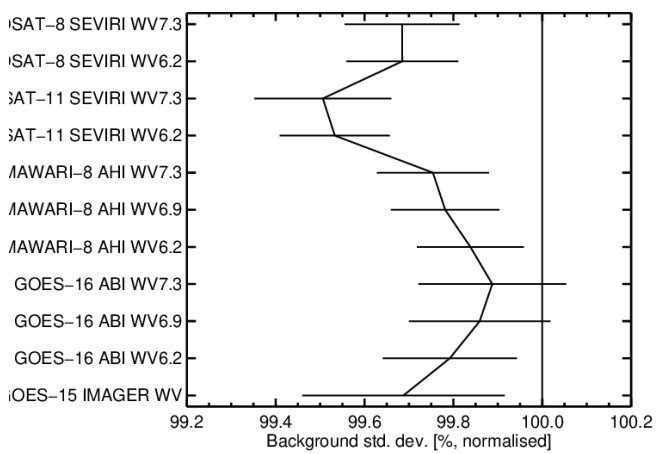
c)



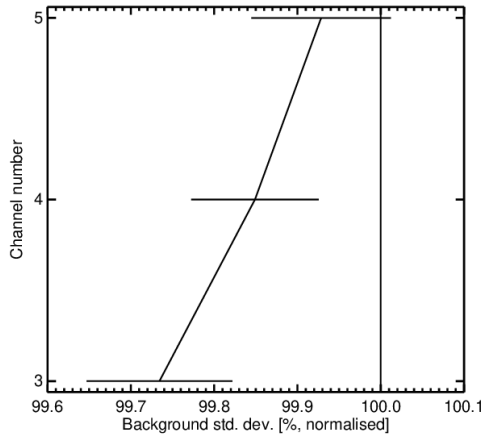
d)



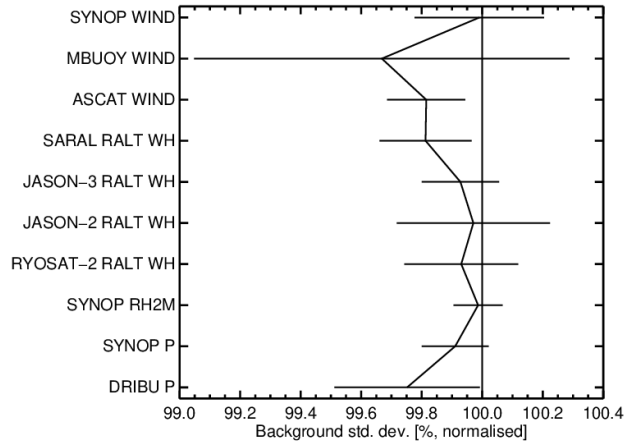
e)



f)



g)



h)

Figure 49. Change in standard deviation of O-B departures resulting from assimilating Aeolus HLOS wind observations (Rayleigh-clear and Mie-cloudy), normalised so that the control is 100%. Values below 100% show an improved fit from assimilating Aeolus and above 100% show a degraded fit. The observation types are a) ATMS global statistics, b) AMSU-A global statistics, c) GNSS radio occultation in the tropics, d) CrIS global statistics, e) AMVs global statistics, f) geostationary imagery global statistics, g) FY-3B MWHS global statistics and h) various surface observation types in the NH. Horizontal bars show the 95% confidence range (Student's t-test). For period from 12 August 2019 to 31 December 2019.

Aeolus FM-B data is improving the short-range forecast wind, temperature and humidity. The magnitude of the impact is consistently of a good magnitude for one satellite, when compared to the magnitude of the impact of other satellite data in OSEs from recent years at ECMWF, e.g. Bormann et al. 2019.

Assimilating Aeolus leads to small changes which in the mean fit to tropical conventional wind data (mostly radiosondes sampling the maritime continent), as shown in Figure 50. These changes mostly bring the forecast closer to radiosondes, which is a good indication that the mean analysis changes from Aeolus are moving the analysis closer to the truth (as shown in Figure 46 and Figure 47). This is reassuring given that the bias correction scheme relied on the model which has biases in the tropics, but perhaps these biases vary significantly with pressure are not significant for the profile average bias correction. In previous years we have seen significant mean differences between the ECMWF and Met Office model wind fields in tropical upper troposphere.

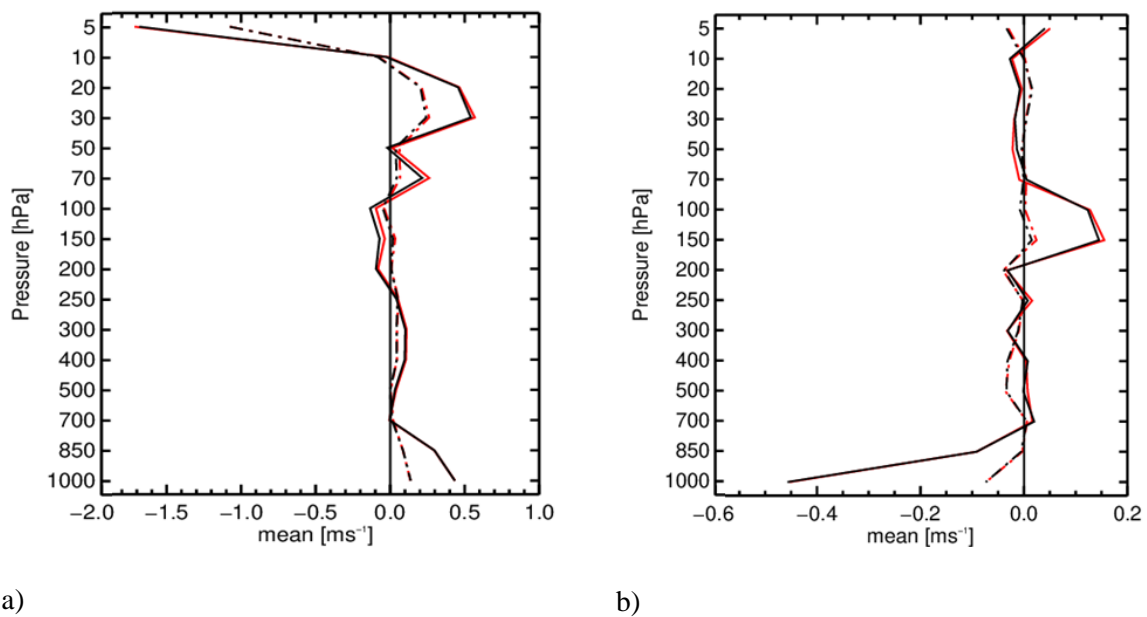


Figure 50. The mean(O-B) fit to conventional wind data (mostly radiosondes) in the tropics for a) u-wind component and b) v-wind component. The red line is the control (without Aeolus) and the black line is when Aeolus is assimilated. For period from 2 August 2019 to 31 December 2019.

#### 4.3.3.2 Mie-cloudy only

The short-range forecast impact relative to ATMS microwave radiances of assimilating Mie-cloudy winds only in comparison to assimilating Rayleigh-clear and Mie-cloudy is shown in Figure 51. The black line is when assimilating only Mie-cloudy winds and the red line is when assimilating both Rayleigh-clear and Mie-cloudy winds. The impact of Mie-cloudy winds on its own is not wholly positive relative to ATMS (and AMSU-A, not shown). The addition of Rayleigh-clear winds changes the negative impact to positive impact. Mie-cloudy winds are degrading the fit to the stratospheric temperature sensitive channels (channels 12-15, with weighting functions peaking around 20-35 km) and for the humidity sensitive channel near the surface (channels 18). However, the impact of the Mie-cloudy on tropospheric temperature i.e. channels 6 to 9 (below 10-12 km) is positive. Splitting into NH extratropics, tropics and SH extratropics (not shown), the stratospheric temperature degradation is strongest in the SH extratropics. With Mie-cloudy winds in the SH extratropics typically only reaching 16 km this is clearly an indirect effect, which could be due to gravity wave propagation from the troposphere to the stratosphere being affected by Mie-cloudy winds altering the flow at low levels. Figure 45 showed how Aeolus affected the model's winds at very high altitude in the SH extratropics in areas associated with orographically (and perhaps frontal) generated gravity waves. The high peaking microwave radiances are very sensitive to the temperature variability associated with orographically driven gravity waves.

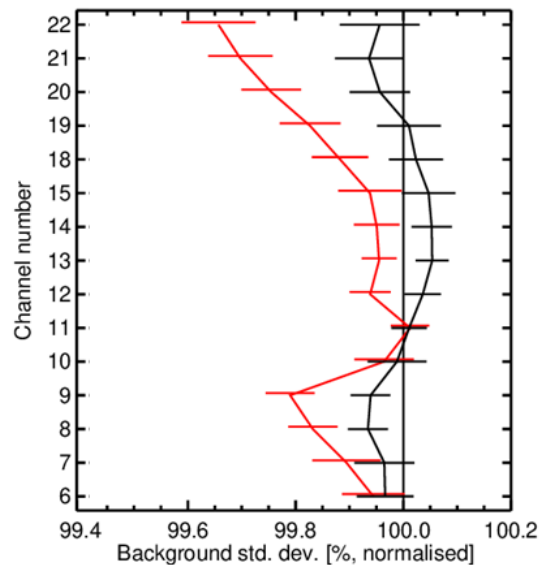


Figure 51. Change in standard deviation of O-B departures relative to global ATMS microwave radiances resulting from assimilating Aeolus HLOS wind observations, normalised so that the control is 100%. The red line is with both Rayleigh-clear and Mie-cloudy used and the black line is with only Mie-cloudy. Values below 100% show an improved fit from assimilating Aeolus and above 100% show a degraded fit. For the period 2 August 2019 to 31 December 2019.

#### 4.3.4 Medium-range forecast impact

##### 4.3.4.1 Rayleigh-clear and Mie-cloudy

Figure 52, Figure 53 and Figure 54 show the combined impact of Aeolus Rayleigh-clear and Mie-cloudy winds for the period from 2 August 2019 until 31 December 2019 on vector wind, verified against ECMWF operational analyses in which Aeolus was not assimilated. The impact on 2 to 4-day forecasts looks to be mostly positive with statistical significance in the tropical troposphere. The percentage improvements are on the order of 1-2% in the tropics. In the extratropics the impact up to the lower stratosphere is less than 1% for the whole area, but the impact is focused poleward of 60 degrees. The positive impact has similar patterns to that shown for the late FM-A period (Figure 38), but has a larger magnitude at days 2 to 4. This may be due to the smaller Rayleigh random error for early FM-B compared to late FM-A, or perhaps a seasonal effect.

The apparent negative impact at T+12 around 100 hPa and in the lower troposphere and at T+24 hours around 100 hPa is thought to be an artefact of the extra variability that Aeolus adds to wind forecasts in poorly observed areas when verifying against analyses. This is corroborated by the short-range forecast fit to observations being improved. There may however be an element of overweighting or improper use of the data causing some part of this, e.g. in the lower stratosphere.

There is negative impact in the SH extratropics for 5-day forecasts and beyond, particularly in the stratosphere e.g. 10 hPa (~30 km). It is unclear what is causing this, but it may be associated with the Mie-cloudy wind related gravity wave issue discussed in Section 4.3.3.2. Another possible explanation is that there are large gradients in Rayleigh wind bias in this region, which perhaps were not corrected well enough via our argument of latitude and longitude based bias correction method. It will be interesting to see if the M1 mirror temperature dependent bias correction method (see Section 3.2.1) can improve this. This will be evaluated when the reprocessed dataset for this period becomes available in

September 2020. The late FM-A period showed hints of positive impact in the same region (see Figure 38).

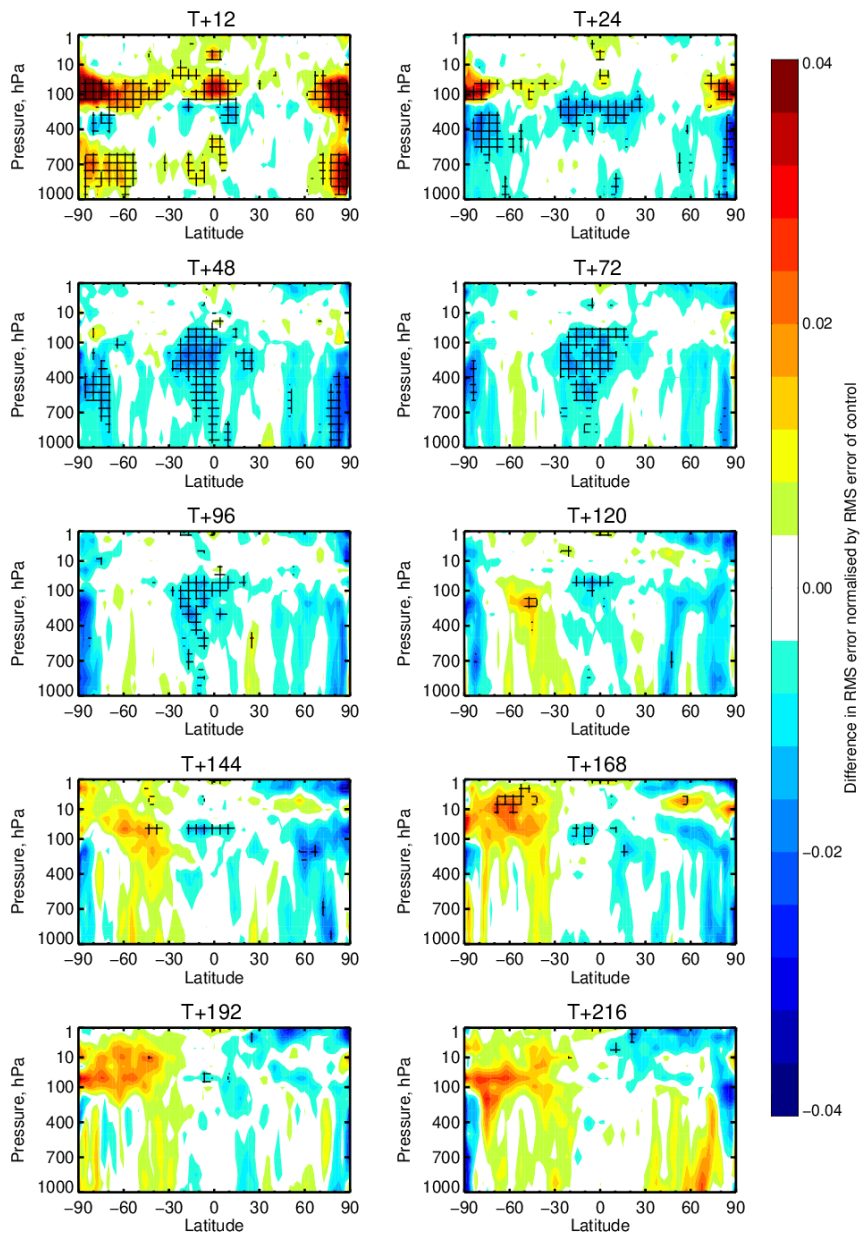


Figure 52. Zonal average normalised change in the RMS (root mean square) error of wind vector from assimilating Aeolus (Rayleigh-clear and Mie-cloudy) for the period 2 August 2019 to 31 December 2019. Negative values (blue) indicate a reduction in error from assimilating Aeolus and red values an increase in error. Verified against operational analyses. Cross-hatching indicating 95% confidence.

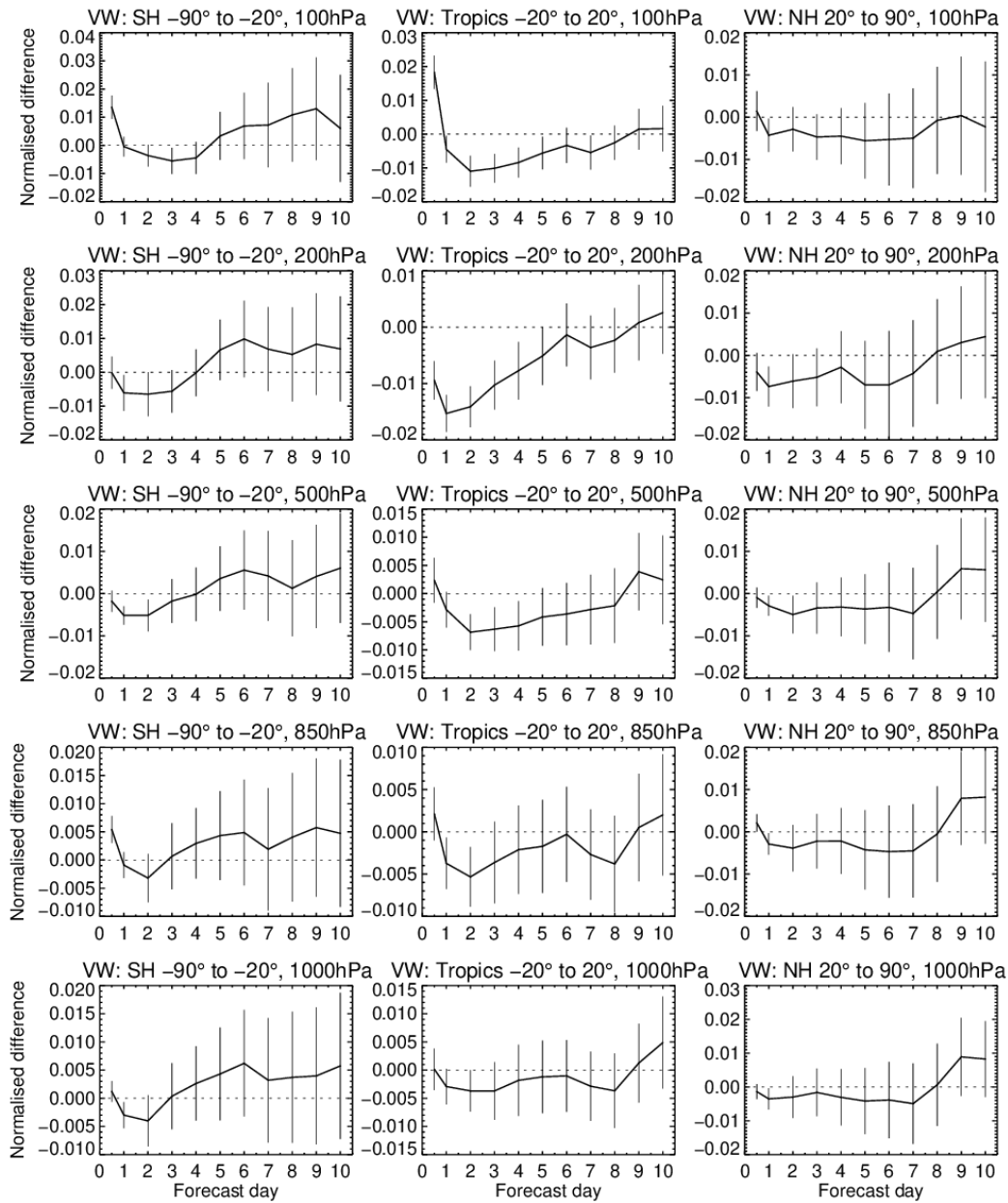


Figure 53. Normalised change in the RMS (root mean square) error in vector wind for different vertical levels (from 100 to 1000 hPa, top to bottom) and for SH extratropics, tropics and NH extratropics (left to right) from assimilating Aeolus (Rayleigh-clear and Mie-cloudy). The period is from 2 August 2019 to 31 December 2019. Confidence ranges are 95%. Verified against operational analyses. Negative values indicate a reduction in error from assimilating Aeolus.

The map of vector wind impact at 200 hPa is shown in Figure 54. The positive impact (blue colours) tend to in the tropics, over oceans and other areas that a relatively lacking in wind profile observations. The negative impact in the south Pacific seems to grow with propagate westward with time.

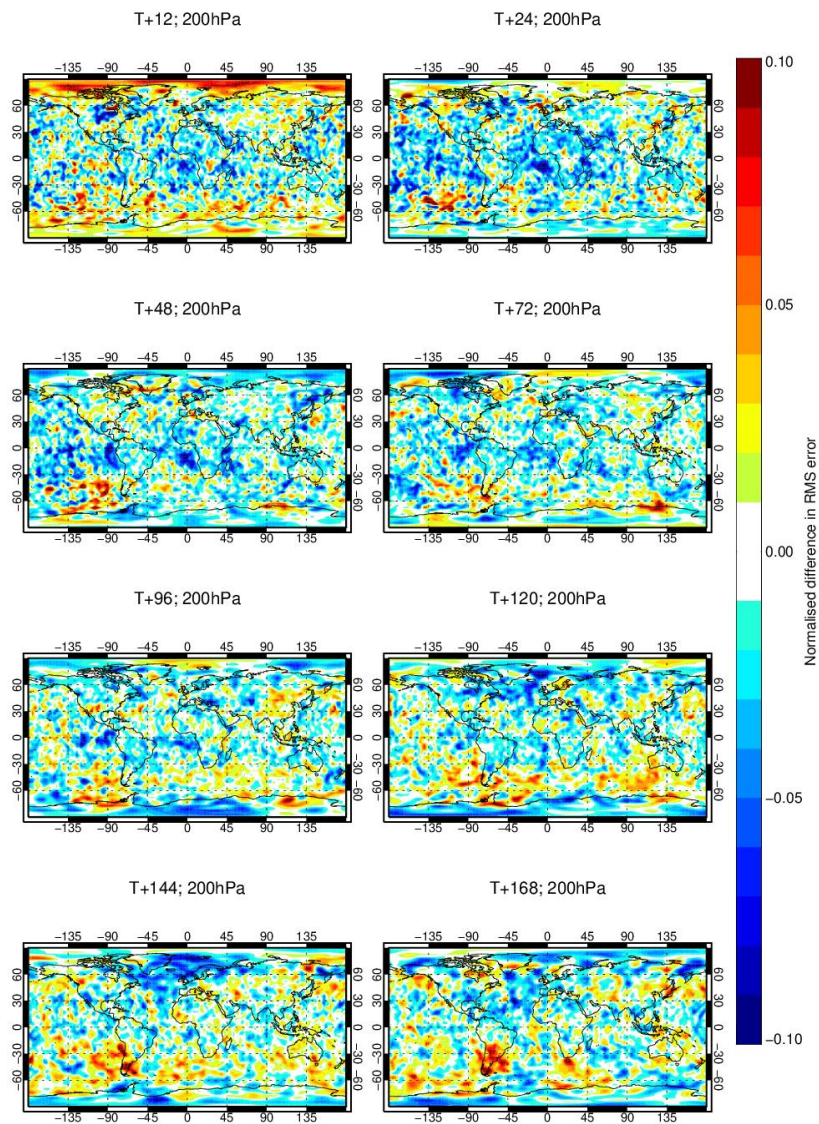


Figure 54. Maps of normalised change in the RMS (root mean square) error of wind vector at 200 hPa from assimilating Aeolus (Rayleigh-clear and Mie-cloudy) for the period 2 August 2019 to 31 December 2019. Negative values (blue) indicate a reduction in error from assimilating Aeolus and red values an increase in error. Verified against operational analyses.

Other variables are effected in a similar pattern to the wind impact as shown in Figure 55 to Figure 57 (temperature, relative humidity and geopotential height).

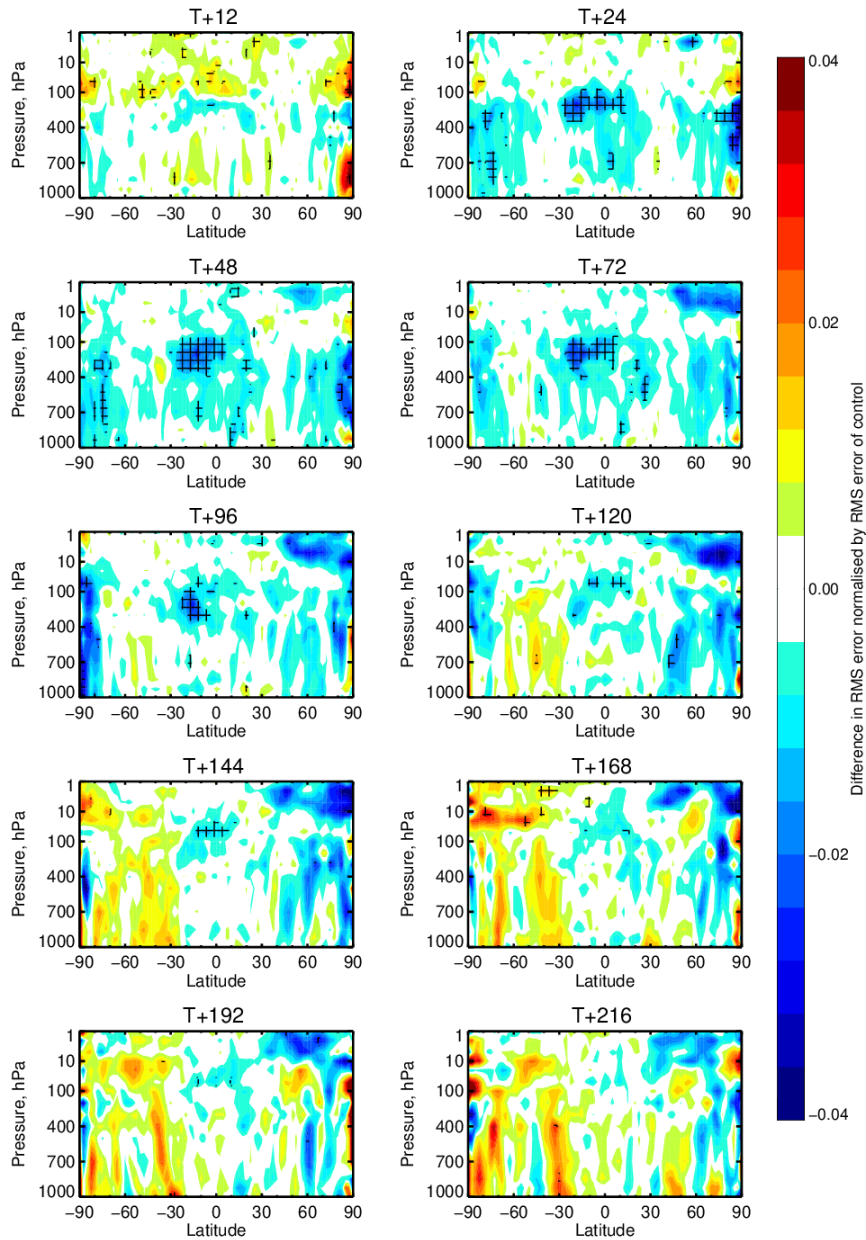


Figure 55. Zonal average normalised change in the RMS (root mean square) error of temperature from assimilating Aeolus (Rayleigh-clear and Mie-cloudy) for the period 2 August 2019 to 31 December 2019. Negative values (blue) indicate a reduction in error from assimilating Aeolus and red values an increase in error. Cross-hatching indicating 95% confidence. Verified against operational analyses.

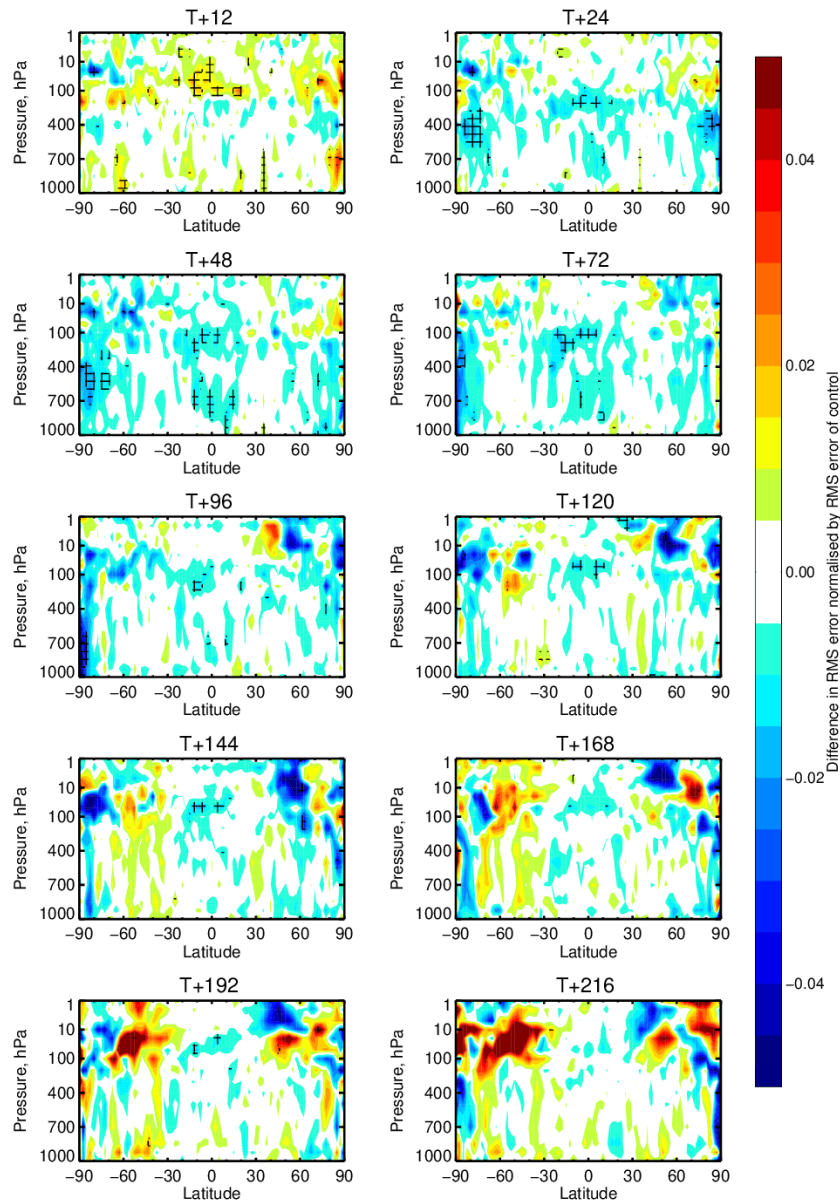


Figure 56. Zonal average normalised change in the RMS (root mean square) error of relative humidity from assimilating Aeolus (Rayleigh-clear and Mie-cloudy) for the period 2 August 2019 to 31 December 2019. Negative values (blue) indicate a reduction in error from assimilating Aeolus and red values an increase in error. Cross-hatching indicating 95% confidence. Verified against operational analyses.

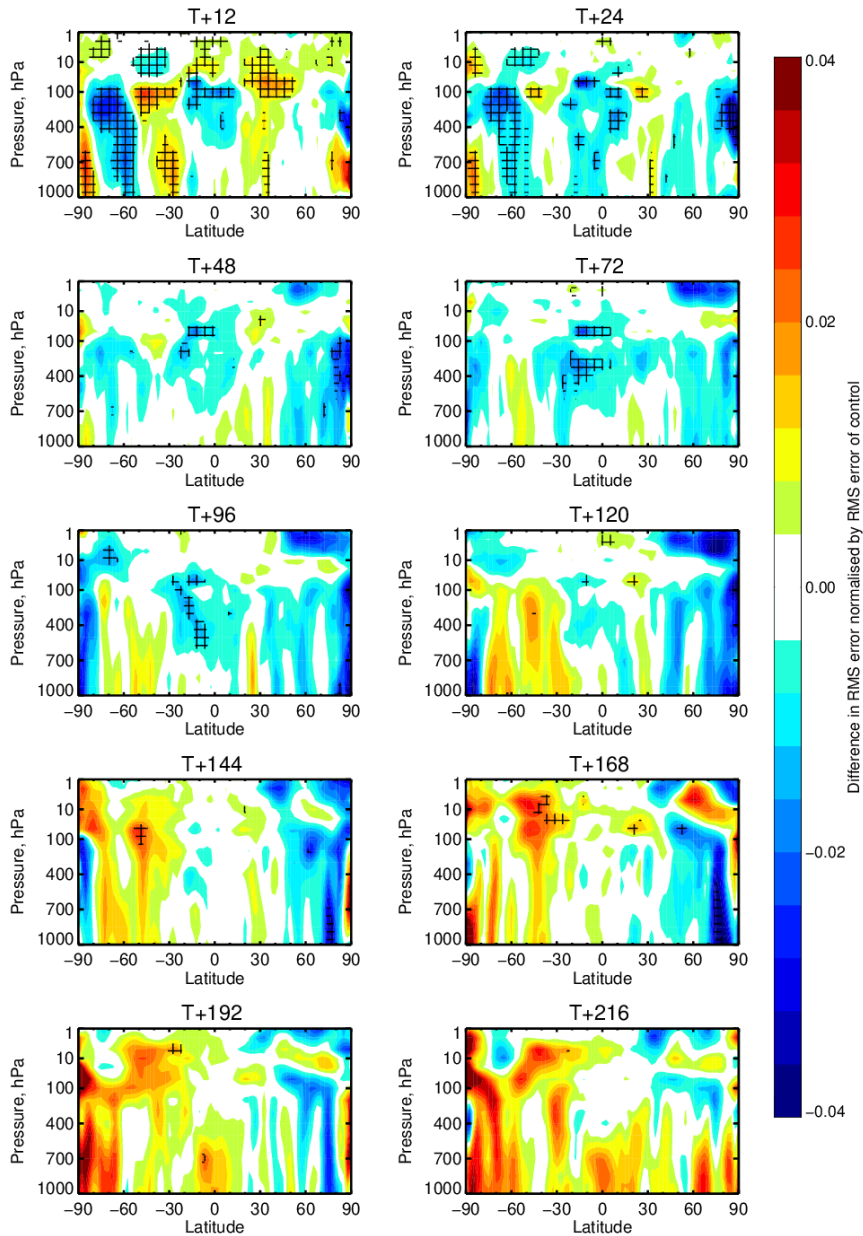


Figure 57. Zonal average normalised change in the RMS (root mean square) error of geopotential height from assimilating Aeolus (Rayleigh-clear and Mie-cloudy) for the period 2 August 2019 to 31 December 2019. Negative values (blue) indicate a reduction in error from assimilating Aeolus and red values an increase in error. Cross-hatching indicating 95% confidence. Verified against operational analyses.

#### 4.3.4.2 Impact of Aeolus in the stratosphere

The nominally used Aeolus vertical range-bin settings provide clear-air winds (Rayleigh scattering) up to 20-25 km (50-20 hPa) altitude, therefore sampling the lower stratosphere. Aeolus is limited to 24 range-bins, therefore, to keep the vertical resolution reasonable in the troposphere, the maximum possible altitude of 30 km is not applied. The Rayleigh winds become increasingly noisy with altitude due to the exponential drop in the backscatter (proportional to density). These noise aspects and the limited number of range-bins means the stratospheric range-bin resolution typically is set to 1-2 km.

The highest cloudy-air winds (Mie scattering) are typically due to scattering from water/ice clouds at around tropopause level. An exception is Polar Stratospheric Clouds for which decent quality Mie winds can reach ~25 km, particularly over Antarctica. The flexible vertical sampling of Aeolus is raised over the winter poles to sample the Polar Night Jet.

The strongest stratospheric impact of Aeolus at ECMWF occurs in the tropical lower stratosphere; see Figure 58, which shows the impact for vector winds at 50 hPa (~20 km). The positive impact on wind and temperature persists into the medium range. Positive impact in the extratropical stratosphere relative to convective wind observations is also evident particularly above 150 hPa (see Figure 48 a and e). The tropical impact is corroborated with short-range forecast verification against GNSS radio occultation (see e Figure 49c) — with impact reaching 35 km. The impact is also positive relative to ATMS (microwave radiances) channels 13 to 15 which peak between 20–40 km (Figure 49a). The positive impact occurs at significantly higher altitudes than Aeolus observes directly. The mechanism for this could be via Aeolus changing the mean wind field at lower altitudes leading to a better propagation gravity waves from troposphere to stratosphere.

For the same time period, Figure 47 shows the mean change in the zonal wind due to Aeolus at 100 hPa and Figure 44 shows the standard deviation of changes in zonal wind due to Aeolus at 150 hPa (where the effect is largest). The changes are strongest in convectively active areas of the tropics; with a pattern perhaps suggesting a modification to the Walker Circulation. Large random changes are also present at 1 hPa (Figure 45) which must be associated with gravity waves. Research continues to understand these changes.

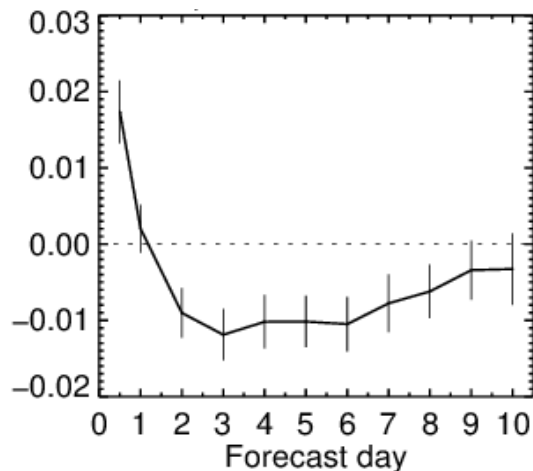


*Figure 58. Normalised change in the root mean square error in vector wind at 50 hPa in the tropics from assimilating Aeolus (Rayleigh-clear and Mie-cloudy). The period is from 2/8/2019 to 31/12/2019. Confidence ranges are 95%. Verified against operational analyses. Negative values indicate a reduction in error from assimilating Aeolus.*

#### 4.3.4.3 Mie-cloudy only

The impact of assimilating Mie-cloudy winds (with the nominal observation error assignment as described in 2.4.3) on vector wind forecasts is shown in Figure 59; this should be compared to the impact of the combined Rayleigh-clear and Mie-cloudy winds in Figure 52. Mie winds show hints of positive

impact for days 2-4 but it is lacking in statistical significance. Therefore, we conclude that the Rayleigh winds are provided the majority of Aeolus' positive impact. This concurs with the short-range forecast fit to observations in Figure 51. Despite the much larger noise of Rayleigh winds compared to Mie winds, the Rayleigh winds much greater spatial coverage and smaller representativeness error leads to a greater positive impact than seen for the Mie winds.

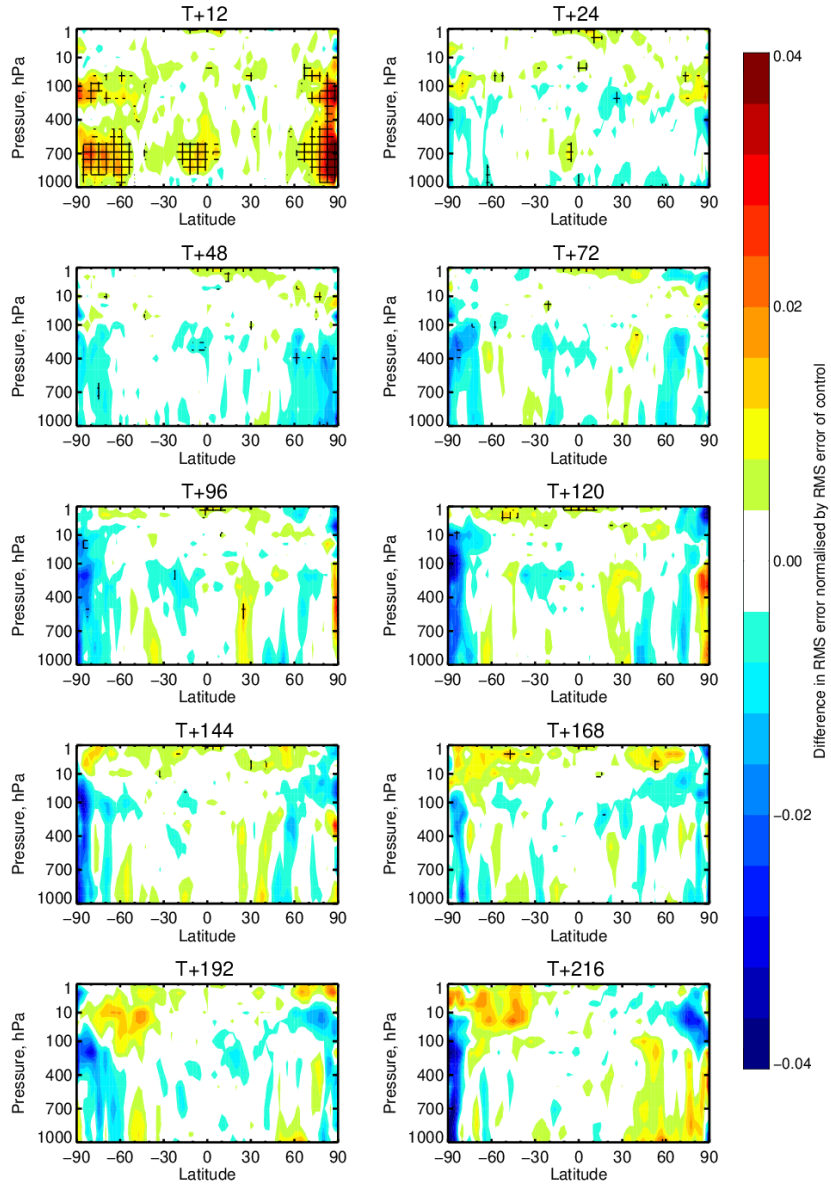


Figure 59. Zonal average normalised change in the RMS (root mean square) error of wind vector from assimilating only Mie-cloudy for the period 2 August 2019 to 31 December 2019. Negative values (blue) indicate a reduction in error from assimilating Aeolus and red values an increase in error. Verified against operational analyses. Cross-hatching indicating 95% confidence.

#### 4.3.4.4 Improving Mie-cloudy impact via the inclusion of representativeness error in the assigned observation error

The Mie-cloudy data impact can be improved significantly by accounting for representativeness error in the assigned observation error. With the help of “Desroziers diagnostics” and by the expectation for the standard deviation of O-B as a function of the assigned observation error it was found that a more realistic assigned observation error could be obtained by scaling the L2Bp estimated error (1-sigma) by 1.25 and quadratically adding this to a constant representativeness error of 2 m/s. Figure 60 compares the impact of using the revised observation error formulation versus the previous scaling of L2Bp estimated error by 1.75, with zero representativeness error. This is verified with ATMS microwave radiances. The impact on the tropospheric humidity channels (18-22) is improved most when representativeness error is considered. There is also improvement for the tropospheric temperature channels (6-9) and for the highest stratospheric temperature channels (14 and 15). This is only the first attempt at improving the assigned observation error in this way and it is expected that refinements will provide further improvements.

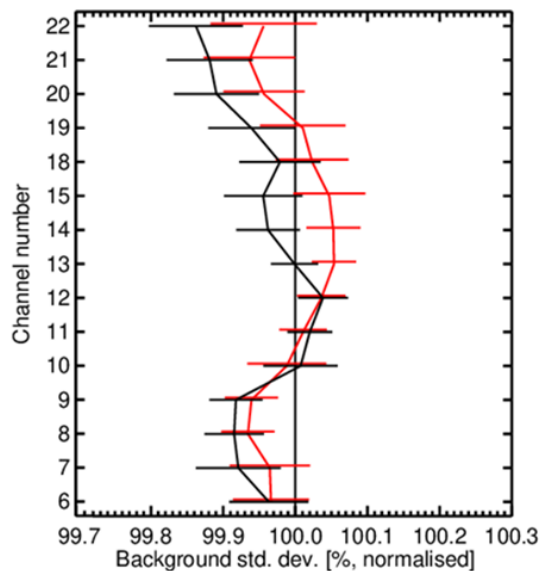


Figure 60. Change in standard deviation of O-B departures relative to global ATMS microwave radiances resulting from assimilating Aeolus HLOS wind observations, normalised so that the control is 100%. The red line is with Mie-cloudy only using the original assigned error model and the black line is with the new error model including representativeness error. Values below 100% show an improved fit from assimilating Aeolus and above 100% show a degraded fit. For the period 2 August 2019 to 31 December 2019

An improvement in forecast impact when assimilating Mie-cloudy winds with the improved assigned observation error model is shown in Figure 61, this should be compared to the impact from the original error model as shown in Figure 59; there is a lot more blue (positive impact) with the refined error model.

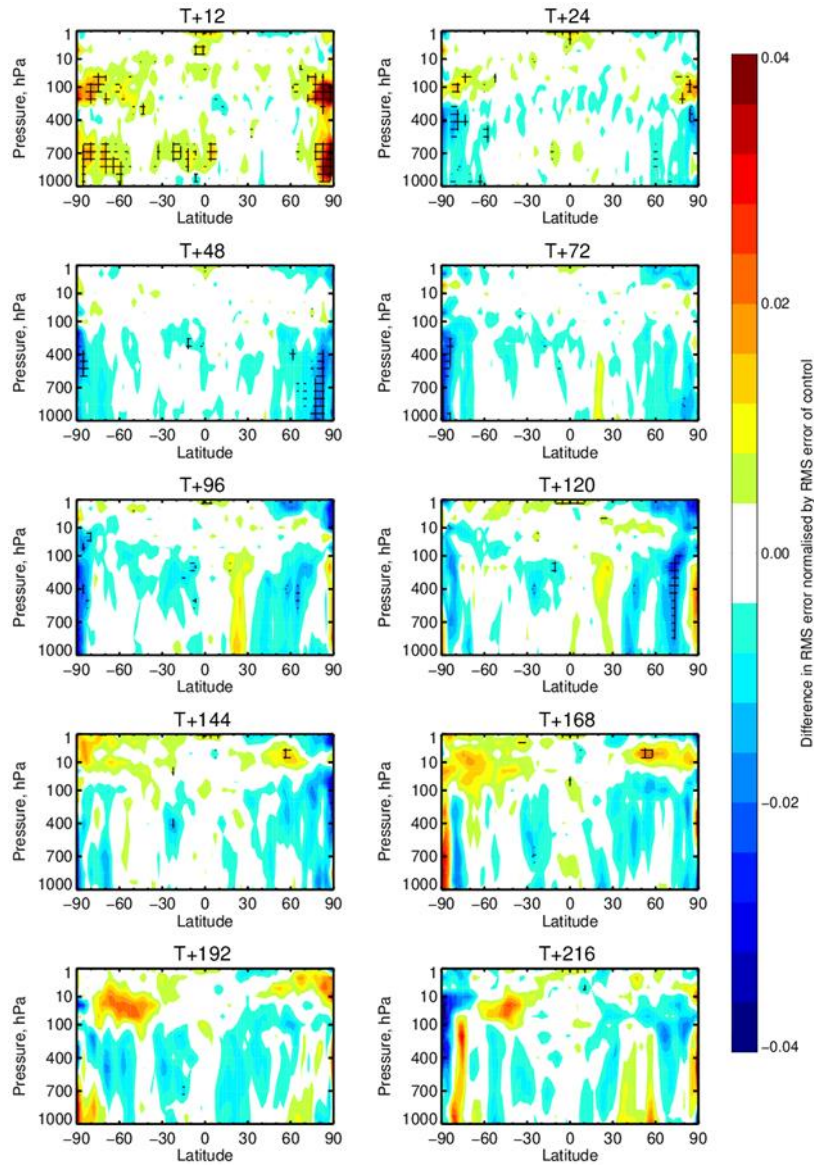


Figure 61. Zonal average normalised change in the RMS (root mean square) error of wind vector from assimilating only Mie-cloudy with an improved assigned error model for the period 2 August 2019 to 31 December 2019. Negative values (blue) indicate a reduction in error from assimilating Aeolus and red values an increase in error. Verified against operational analyses. Cross-hatching indicating 95% confidence.

#### 4.3.5 FSOI results from ECMWF operations

Section 2.5 gives a description of the forecast sensitivity observation impact (FSOI) method. The results here are produced from ECMWF’s operational data assimilation FSOI results for the period 9-22 January 2020. When evaluating full impact of a large observation subset, FSOI does not require as long a period as OSEs to reach a robust result, since it is a short-range forecast verification method using a global verification metric in observation space. The so-called “relative FSOI” used to present the results here is the percentage of the total FSOI (i.e. reduction in global dry energy norm error) split into various subsets of observations. On the other hand, the absolute FSOI is expressed in units of  $10^{-5}$  J/kg.

In Figure 62 the relative FSOI is partitioned into a long list of instrument types and in Figure 63 it is partitioned into larger observation groups using the naming conventions employed by ECMWF. Figure 62 shows that Aeolus L2B winds are rather important, coming fifth out of around eighty instruments (providing about 3.8% of the total forecast improvement). In terms of space-based instruments, only EUMETSAT's MetOp B and C's IASI (Infrared Atmospheric Sounding Interferometer) radiances and the United States' NPP (National Polar-orbiting Partnership) ATMS (Advanced Technology Microwave Sounder) radiances have larger short-range forecast impact. These are operational instruments which have been developed and exploited in operational NWP for a long time, so it is impressive to see that Aeolus is nearly as important. The largest impact comes from WIGOS (WMO Integrated Global Observing System) AMDAR (Aircraft Meteorological Data Relay), which are in situ commercial aircraft observations of wind, temperature and humidity. There is a large sample of aircraft observations assimilated and they provide very accurate observations at an important altitude (cruise level, often in the polar jet stream) for weather forecasting; but their impact is not evenly distributed across the globe.

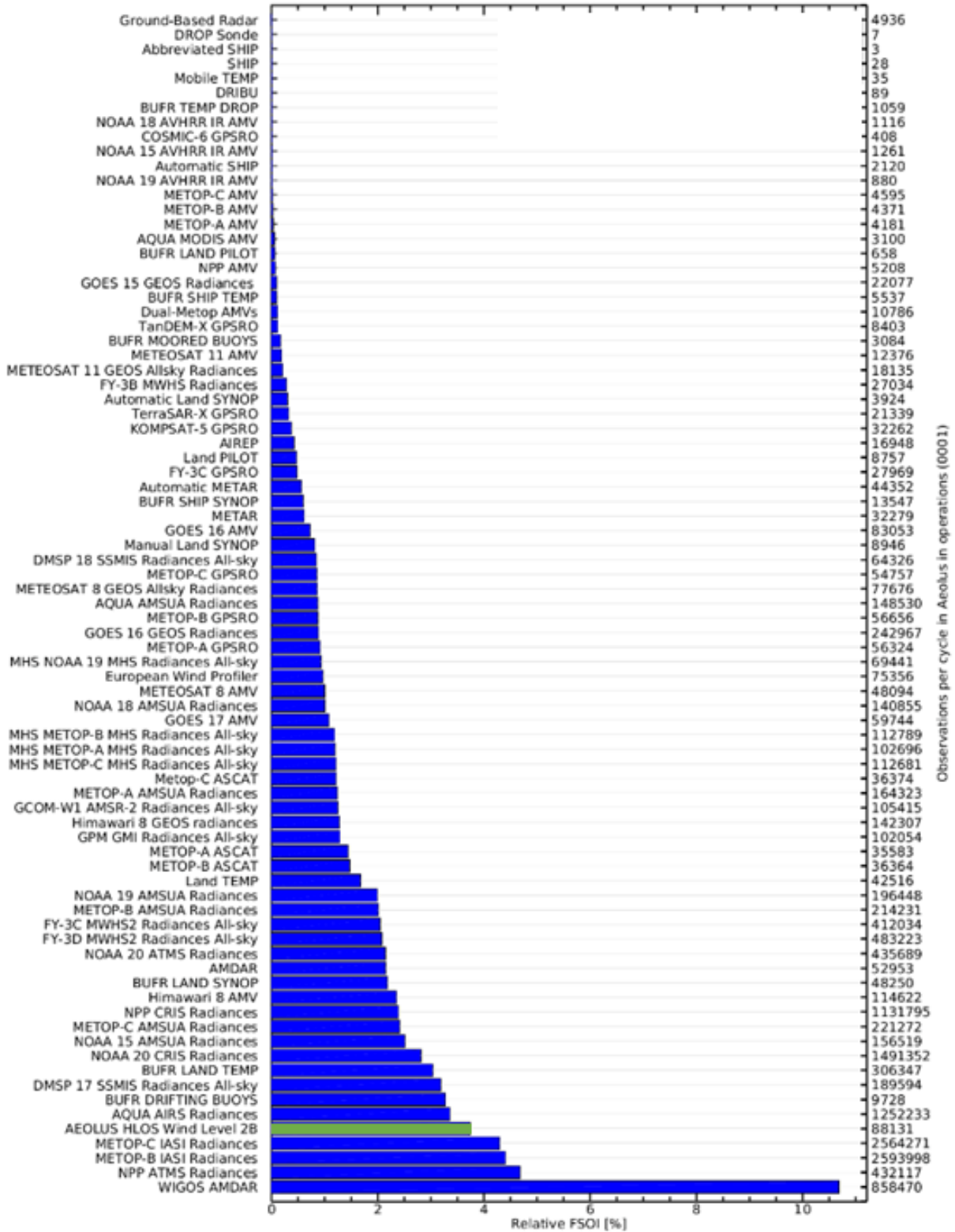


Figure 62. Relative FSOI (%) from ECMWF’s operational system, partitioned by instrument types, averaged over the period 9 January 2020 to 22 January 2020. Aeolus is listed as “AEOLUS HLOS Wind Level 2B”, with the green bar. The number of observations used on average per 12 hour period is shown on the right hand side.

When relative FSOI is partitioned into larger observation groups, as in Figure 63, then Aeolus, being the only contributor to the “Wind lidar” group still does reasonably well being similar in impact to GPSRO for this particular period. One should note that the availability of observations in the global observing system is changing all the time, so this may not be representative for a different period. Many of these observation groups, such as microwave water vapour (WV) (which has the largest impact) are made up from many satellites.

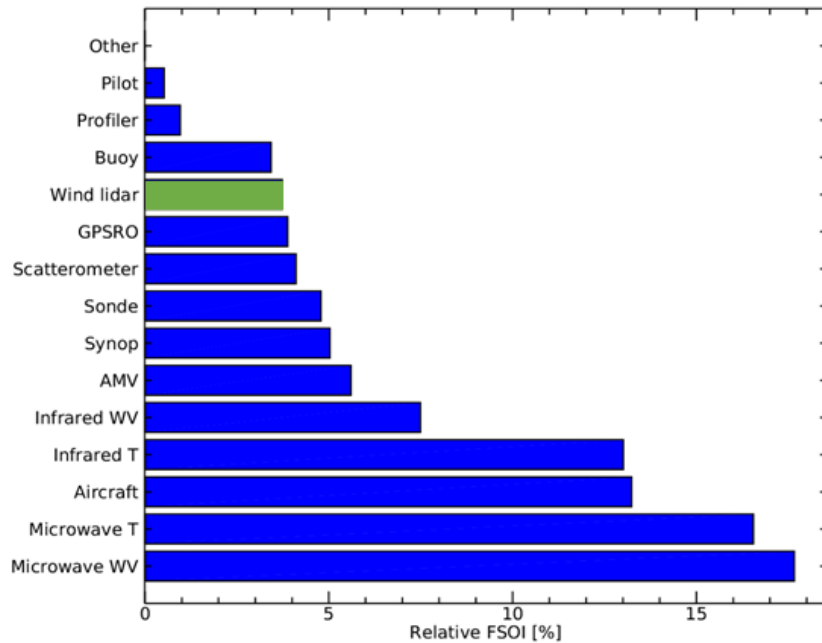


Figure 63. Relative FSOI (%) from ECMWF’s operational system, partitioned by observation groups, averaged over the period 9/1/2020 to 22/1/2020. Aeolus is the only member of the “Wind lidar” group, with a green bar.

Figure 64 and Figure 65 show zonal average plots of the absolute FSOI scores (in units of  $10^{-5}$  J/kg) for Rayleigh-clear and Mie-cloudy HLOS winds respectively (only for ascending orbits). This is for the period 19/1/20 to 8/2/20. The Rayleigh winds have the largest impact in the tropics, peaking at around 150 hPa (~14 km). The altitude of peak tropical impact agrees with the short-range forecast fit to radiosonde winds and GPSRO from assimilating Aeolus, as shown in the various OSEs. Elsewhere the impact is more of a small positive effect. The Mie-cloudy impact looks to be more variable with patches of larger negative impact and patches of larger positive impact but being positive impact overall. Optimisation of the assigned Mie observation error may improve this; see Section 4.3.4.4.

Figure 66 and Figure 67 show maps of the mean absolute FSOI from Rayleigh-clear and Mie-cloudy observations geolocated in the 0-400 hPa range respectively, for the period 13/1/19 to 7/2/19. The Rayleigh short-range forecast impact peaks in the tropics around Africa and the East Pacific; in agreement with the areas where Aeolus changes the wind most (see Section 4.3.2). For Mie, as in the zonal average plot, the impact looks more variable, but with patches of larger magnitude than the Rayleigh, which must reflect the greater weight given to the observations due to the smaller observation errors. The biggest positive impact of the Mie tends to be over ocean areas.

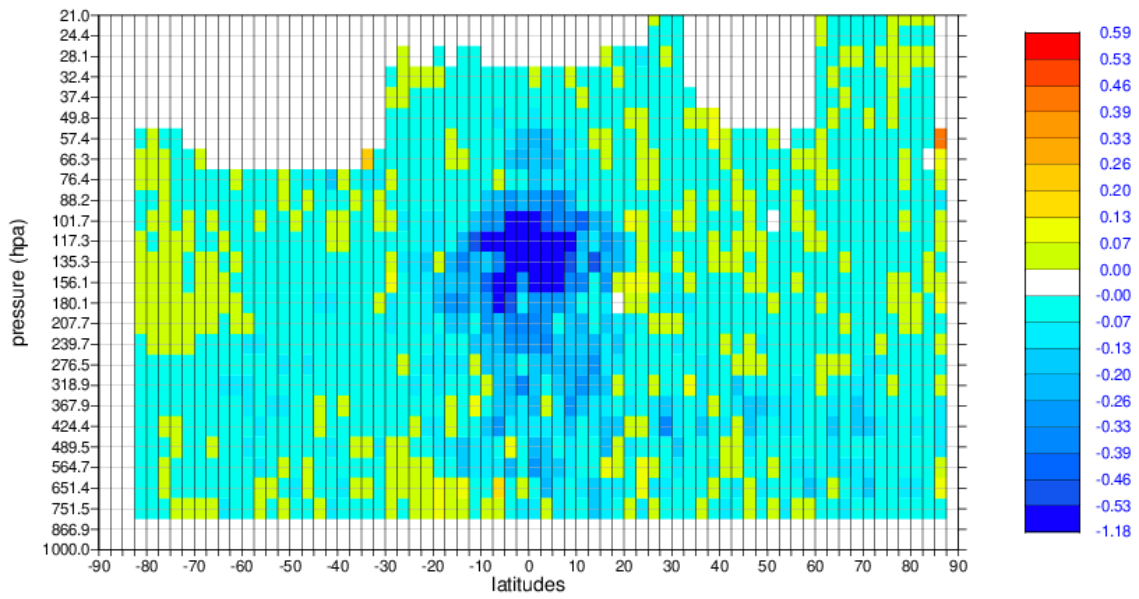


Figure 64. Zonal average plot of the Level-2B Rayleigh-clear (ascending orbits only) FSOI ( $10^{-5}$  J/kg) for the period 19 January 2020 until 8 February 2020. Blue colours are an improvement.

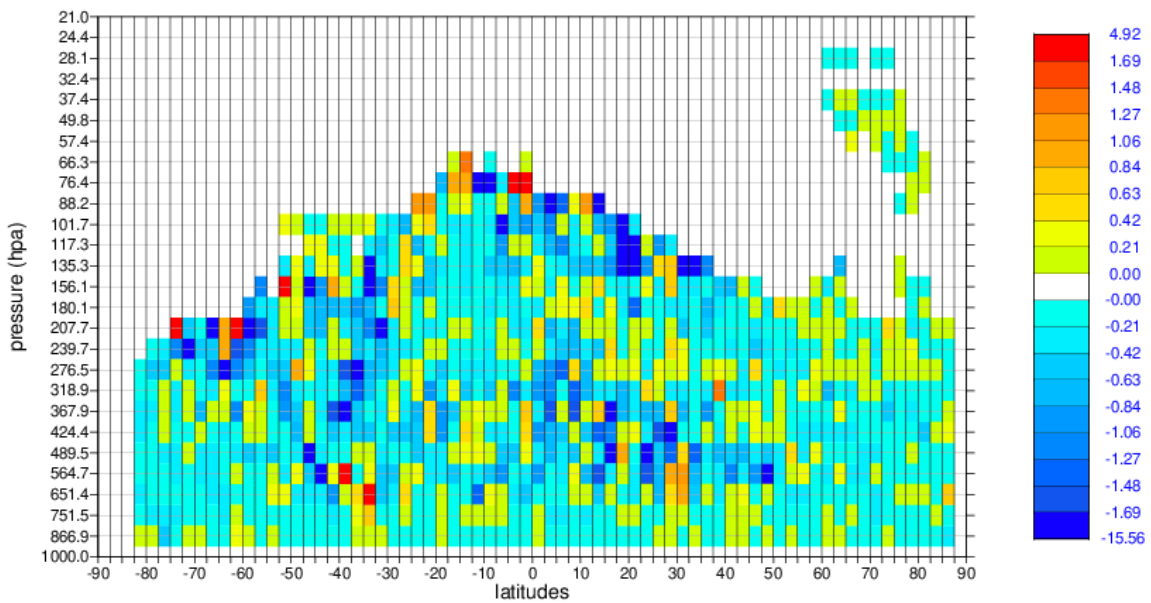


Figure 65. Zonal average plot of the Level-2B Mie-cloudy (ascending orbits only) FSOI ( $10^{-5}$  J/kg) for the period 19 January 2020 until 8 February 2020. Blue colours are an improvement.

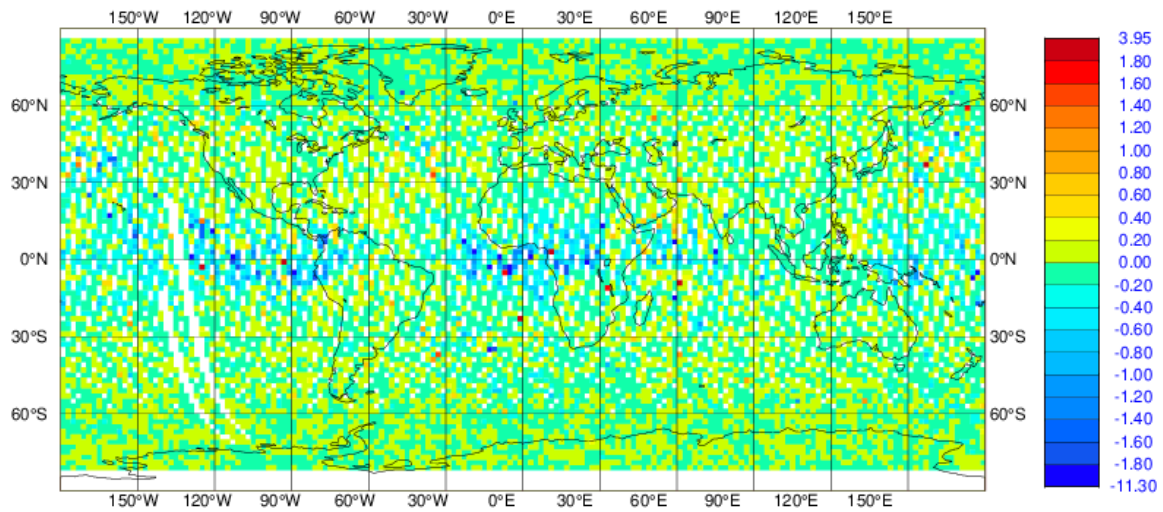


Figure 66. Map of the 0-400 hPa pressure range Rayleigh-clear (ascending orbits only) FSOI ( $10^{-5}$  J/kg) for the period 13 January 2020 until 7 February 2020. Blue colours are an improvement.

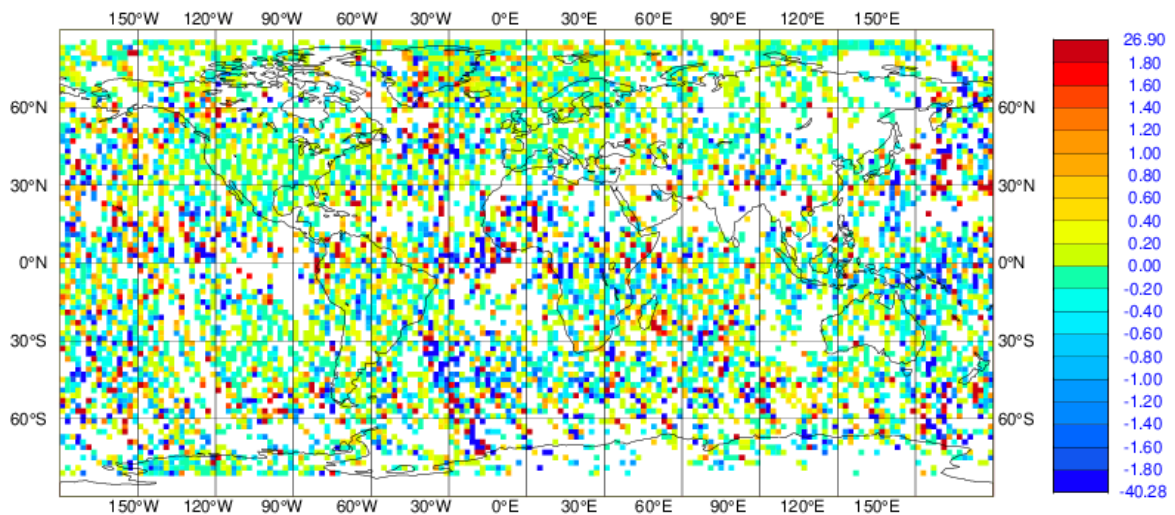


Figure 67. Map of the 0-400 hPa pressure range Mie-cloudy (ascending orbits only) FSOI ( $10^{-5}$  J/kg) for the period 13 January 2020 until 7 February 2020. Blue colours are an improvement.

For Aeolus the FSOI per observation is high compared to other satellite data, coming second only to scatterometer ocean surface wind data, see Figure 68 (various types of in situ data have more impact per observation, such as dropsondes and ground based observations). This indicates the values of wind profile observations from space.

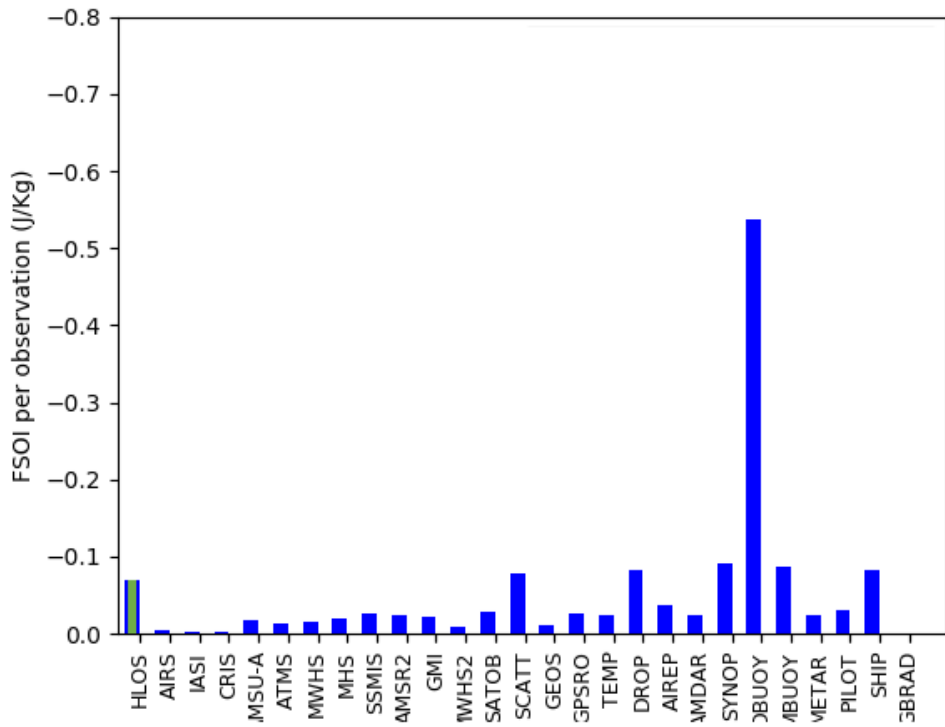


Figure 68. Absolute FSOI per observation for the period 10 January 2020 to 31 January 2020. Aeolus is labelled as “HLOS”, with green bar.

## 5 Discussion

ESA's Aeolus mission requirements document (Ingmann and Straume, 2016) states a required precision of 2.5 m/s in the free troposphere and biases less than 0.7 m/s. These requirements assumed specific horizontal averaging scales, vertical range-bin thicknesses and time-scales for the metrics, making it non-trivial to compare to real Aeolus noise data. Although varying through the mission so far (and requiring some assumptions on the magnitude of ECMWF model errors), a precision of approximately 4-5 m/s and 3 m/s is estimated for the L2B Rayleigh-clear and Mie-cloudy HLOS winds respectively (see Section 3.1.4). These precisions are considerably worse than the mission requirements, therefore we conclude that they are not being met so far. The global average short-range forecast errors are thought to be around 1.8 m/s in HLOS wind space (although can reach much larger values in local conditions), so we are in a regime for the Rayleigh where the instrument noise dominates in the data assimilation, in comparison to e.g. representativeness error. The L2B Mie-cloudy random error estimates are closer to the mission requirements than the Rayleigh-clear in the free troposphere due to strong backscatter from ice and water clouds meaning the random errors are limited by other effects. However, random errors for winds from aerosol backscatter are strongly depending on the instrument signal levels. The Mie winds have larger representativeness errors than the Rayleigh due to the scattering often coming from small-scale cloud features.

The main reason for not yet achieving the mission requirements is the lower than expected atmospheric signal levels, as confirmed by DLR's investigations for the Rayleigh channel (personal communication). It has been shown that the atmospheric path Rayleigh signal is around 2.7 times lower than expected for the FM-A laser, which when considering only shot-noise effects would make the Rayleigh wind random errors about 64% larger than otherwise. For early FM-B this factor is less, but still more than a factor 2. Such a loss of signal would lead to 2.5 m/s (the required precision) times 1.64 = 4.1 m/s which is in rough agreement with our precision estimate based on background departure values. With lower signal the unavoidable solar background noise becomes a much more dominant term for the Rayleigh winds, therefore making the seasonal variation in errors larger.

The cause of the lower than expected signal levels is still being investigated. For both FM-A and FM-B the atmospheric signal levels have dropped at rather high rates (recent DLR results). For FM-B a 30% drop of atmospheric signal was seen between late June 2019 and early January 2020, whereas the laser energy dropped by only 13%. This is thought to be related to signal losses due to laser pointing drifting and possible clipping within the instrument, however this is still unclear. Lower signal levels also degrade the quality of the calibrations due to lower quality ground returns, making the systematic error mission requirements more difficult to achieve.

Despite the higher than expected Rayleigh random errors, we have shown that Aeolus still gives a very useful positive impact in global NWP; even for the late FM-A period with largest random errors. It is thought that the continuous nature of the lidar curtain leads to some redundancy of wind information, hence larger random errors are probably not as damaging as they could be if the profiles were all very well separated in space and time (a benefit of continuous rather than burst mode); also, Horányi et al. (2015b) showed that HLOS wind random error increases are not as damaging to NWP impact as much as perhaps expected. The positive impact is surely assisted by the fact that the global observing system is still significantly lacking in global wind profiles.

The global average bias (accuracy) of Aeolus HLOS winds has been observed to have significant drifts with time (for periods longer than a few days) due to instrumental drifts and the difficulty in obtaining high quality weekly calibrations for automated updates which would compensate for such instrument drifts. Global average Rayleigh biases have varied from being close to zero in some periods, to be several m/s HLOS in others due to the drifts. For example, for FM-B the global Rayleigh bias has been drifting in the negative direction at a very high rate of around 3 m/s per month. The Mie global average bias drifted during the FM-A period, but is, in contrast to the Rayleigh, relatively stable for FM-B.

Very large Rayleigh HLOS wind biases that vary within the orbit were discovered. An important result of our study has been to identify that wind biases are highly correlated with variations in the temperature gradients across the telescope's primary (M1) mirror; see Section 3.2.1. The Mie biases have some residual dependence on orbit phase angle, but it is unclear at present what is causing this. The Mie channel sensitivity to M1 mirror temperature gradients appears to be around a factor ten less than the Rayleigh channel.

The telescope temperature dependent bias correction is part of the L2Bp v3.30 delivered on 31 January 2020. This is using a new auxiliary file (AUX\_TEL\_12) to provide linear regression coefficients between telescope temperatures and HLOS wind bias; the processor then applies the correction coefficients using the housekeeping temperatures. This version was implemented operationally on 20 April 2020.

Neither the Mie-cloudy nor Rayleigh-clear winds have so far in the mission met the mission requirements on accuracy (systematic errors). There is the potential to meet the requirements for systematic errors of both channels as our knowledge of their causes and hence correction strategies can be developed; for example, the telescope temperature dependent bias correction is resulted in very significant reduction in wind speed biases. This bias correction scheme is also taking care of longer-term global offset biases.

It was demonstrated with the ECMWF system by Horányi et al. (2015b) that using real HLOS winds (derived pre-launch from conventional wind observations) with artificial biases that were a large fraction of the standard deviation of observation error causes a considerable reduction in positive impact, and with large enough bias an overall negative impact can result. Therefore, it is very important to deal with biases in the data assimilation of Aeolus (if not already corrected in L2B products).

To try to avoid the negative impact of bias, we initially chose to limit the CP FM-A OSE period to 40 days when the global average bias looked reasonably stable with time (and could be easily corrected as a constant offset). However, in hindsight, as shown in Section 3.2.1, biases did exist in that period, varying with orbit phase angle (M1 temperature dependent) and wind speed (imperfect calibration files). The CP OSE was run beyond mid-October 2018 and the results confirmed our expectations (results not shown), in that the medium range forecast impact gradually reduced as the experiment period was extended beyond 16 October 2018. This is thought to be due to the general increase in global average bias and due to the increasing number of hot pixels causing biased winds for the associated range-bins. Many of the issues of the early FM-A period will be resolved in a future reprocessed dataset. It would be interesting to see how much the NWP impact can improve by using the reprocessed dataset.

For the late FM-A period OSEs it was demonstrated that a bias correction scheme for the HLOS winds, using the ECMWF model as reference, significantly boosted the impact. The bias correction uses mean O-B statistics over the past week as a function of the satellite's argument of latitude. This

bias correction strategy was also used and further refined for the early FM-B period experiments. The solution that gave greatest impact for the Rayleigh channel for early FM-B also included the longitude dimension to the bias correction look-up table. The longitudinal aspect was needed for the Rayleigh channel to account for the clear variations in Rayleigh bias with longitude that were being observed with FM-B O-B statistics. Very recent results (not shown) has confirmed that the L2Bp v3.30 AUX\_TEL\_12 telescope mirror temperature based bias correction is doing a significantly better job for these scene dependent biases. NWP impact studies using this improved bias correction method has just started. The expectation is that the NWP impact will increase.

A surprise from the CP Aeolus OSE was that the impact in the tropics was rather small and that the SH impact was stronger. The tropics was expected to be where Aeolus winds would provide the largest impact, due dynamical arguments suggesting the importance of wind versus mass information due to the large tropical Rossby radius of deformation. This was also the expectation given the results using real in situ wind observations (Horányi et al. (2015a)). However, this limited tropical impact is now thought to have been due to an uncorrected orbital phase dependent biases in the observations for the CP OSE, because with argument of latitude dependent bias correction in the late FM-A and FM-B periods we started to see significantly positive impact in the tropical forecasts. For the CP OSE in the tropics the Rayleigh winds in the descending orbit phase had a bias of around 1-2 m/s, whereas the bias in the ascending phase was small, as shown in Figure 16a. This increased the strength of the on average easterly tropical winds, as indicated in Figure 29. The O-B bias was increased relative to tropical radiosonde zonal winds in the focus period (not shown).

Another potential contributor to the lower tropical impact during the CP, is suggested by the poorer fit to AMSU-A lower stratospheric temperature information channels in the tropics. We expected that winds would have most impact in the tropical upper-troposphere/lower-stratosphere (UTLS), an area which typically has large vertical wind shear. However, it seems likely that the 2 km thick in the UTLS during the CP, were not representative given that they are assimilated as point winds, which may have created dubious analysis increments. Ways to mitigate this include: improving the observation operator to a vertically averaging one, blacklist range-bins deemed too thick, or selecting thinner range-bins in NWP sensitive areas (more favourable UTLS 1 km thick range-bin settings became the default on 26 February 2019). The negative impact verified by AMSU-A was particularly due to Rayleigh winds, as confirmed in Figure 30, perhaps because of the large sample of 2 km thick Rayleigh winds from the mostly clear air of the UTLS. More recent OSEs, run during periods with more suitable range-bin settings for NWP have not seen the negative impact against AMSU-A for the Rayleigh channel, which supports this hypothesis.

All the Aeolus OSEs to date have shown improvements in the fit of the short-range forecasts to other observations sensitive to wind, temperature and humidity. This is considered as a very reliable demonstration that Aeolus is improving the analysis and forecasts. The improvements in fit to humidity sensitive observations is because improved winds lead to more accurate advection of humidity. This is the reverse effect to that described for the All-sky radiance assimilation results (Geer et al., 2018), in which the assimilation of humidity and cloud sensitive observations during the 4D-Var window leads to the model incrementing the wind field at the start of the window, such that the humidity is advected better to improve the fit to humidity sensitive observations.

It is found that the impact of Rayleigh-clear winds is significantly larger than Mie-cloudy winds in OSEs. It is thought that the massively superior coverage of the atmosphere with Rayleigh-clear winds

is the reason for this, despite its higher noise levels. The Mie-cloudy winds impact is small but positive overall in OSEs. The FSOI statistics show that the Mie-cloudy winds impact can be very large via this short-range forecast metric. The impact of Mie-cloudy on its own does show some degradations in short-range forecast fit to stratospheric temperatures. However, recent efforts to improve Mie assimilation, particularly the observation error modelling is showing promise.

The impact of Aeolus from short-range to medium-range as verified against analyses (i.e. the typical OSE metric) are showing some consistent patterns for the different periods of the mission so far. Some of the consistent patterns include the following: Systematic changes in the tropical zonal winds that persist throughout the forecasts range which is mostly due to the Rayleigh winds. The random changes in the wind field due to Aeolus are on average largest in the tropical convective zones and SH storm track regions. Positive impact has been demonstrated on the forecasts of vector wind, temperature and humidity (and hence geopotential height) for the SH and tropics, peaking in the upper troposphere, particularly for the late FM-A and early FM-B periods.

The short-range forecast impact is also confirmed to be good from the FSOI results of Section 4.3.5. Aeolus data perform well based on the FSOI metric, when considering the small number of observations available and assimilated and the fact it is sampling the earth via only one satellite. The impact per observation is confirmed to be high, compared to other observing systems.

The relative impact of Aeolus on the short-range forecast (versus observations) can be qualitatively compared to OSE denial experiments from recent years at ECMWF (Bormann et al., 2019). Aeolus' approximate 1% improvement in short-range forecast wind fit is similar in magnitude to that determined for GPSRO, infrared radiances and AMVs, which can be considered a good result for Aeolus since it only provides less than 1% of the observations assimilated.

Some of the changes in the processing chain which are believed to be the main reasons for improved NWP impact of Aeolus so far during the mission are:

- The bias correction of Rayleigh winds using the telescope's M1 temperatures information.
- Increasing the number of Mie winds via reducing the grouping length-scale. This has been shown to lead to only a modest increase in random error, yet to increase the number of Mie observation by a factor 2-3. Currently the maximum Mie grouping length is set to 14 km.
- A correction of the hot-pixel dark current offsets, updated every 6 hours, in the L1B processing step, which massively reduced biases and avoids having to discard specific range-bins.
- Better classification of Rayleigh measurement-bins into clear and cloudy, so fewer are erroneously classified as cloudy and hence signal is wasted for the Rayleigh-clear winds. This was done via using the L1B measurement refined Mie SNR for classification.
- An improved use of Mie backscatter signal on the Rayleigh channel, should allow for better quality Rayleigh-cloudy winds and hence more observations (we have not yet tested the impact of Rayleigh-cloudy winds).
- More favourable vertical sampling (range-bin settings), selected for maximum NWP impact.
- More accurate Rayleigh observation error estimates for the polar summer

Some improvements of NWP impact from Aeolus processing chain changes are expected soon:

- Potentially improved Rayleigh classification using the Mie refined SNR and/or the Optical Properties Code.

- Optimisation of the L2B processor settings more generally.
- Better calibration for Rayleigh-cloudy wind retrievals

Potential larger Aeolus NWP impact via improvement on the data assimilation method:

- Better observation error modelling e.g. to consider a more physically based representativeness error formulation for Mie-cloudy winds.
- Improvements in observation operator, in order to reduce representativeness error by vertical averaging of model winds to match Aeolus range-bin resolution.
- Assessment of spatial thinning near the Poles, due to potential oversampling.
- Use of Rayleigh-cloudy HLOS winds

## 6 Conclusions

Aeolus, the first Doppler wind lidar in space, produces wind observations of a high enough quality to improve weather forecasts. This was demonstrated via statistics comparing Aeolus Level-2B (L2B) HLOS winds to the ECMWF model equivalents and by running OSEs (Observing System Experiments) and FSOI (forecast sensitivity observation impact) assessments that showed positive impact on global NWP forecasts from the data assimilation of Aeolus. The estimated precision of Aeolus L2B HLOS winds is approximately 4-5 m/s for the Rayleigh-clear winds and ~3 m/s for the Mie-cloudy winds. The data has enough information content to improve the ECMWF forecasts despite having higher noise levels and larger biases than expected from pre-launch expectations.

However, this positive impact relied on a bias correction using the ECMWF NWP short-range model forecast as a reference. The biases during the mission have been shown to vary in a very complex way, so they have taken longer to investigate and hence potentially correct than expected pre-launch. This apply for both the ground processing chain and in the NWP data assimilation system. The investigative process to improve the data quality is continuing as there are still several unexplained quality issues that we are aware of today.

NWP impact experiments (OSEs) show a positive impact for Aeolus in all three periods tested so far; the early FM-A Commissioning Phase, late FM-A data and early FM-B data. The impact is found to be greatest for the early FM-B period, when the signal levels were highest. Positive impact was shown by the improved short-range forecast departure fits relative to many reliable in situ and satellite observation types. The improvements in short-range forecasts are seen for observations sensitive to wind, temperature and humidity. The largest impact is found in the tropical upper troposphere.

Rayleigh winds provide most of the positive impact as shown via OSEs, presumably due their much greater spatial coverage than Mie winds, despite being noisier observations, but recent results show that the impact of the Mie winds can be improved via better modelling of the assigned observation errors in data assimilation. Based on the FSOI (24-hour forecast impact) metric, the Mie-cloudy winds gives a larger impact than the Rayleigh-clear winds for the period where 14 km averaging is used for the Mie-cloudy data. This is not in line with the OSE impact studies.

The impact of Aeolus is significantly improved when using a bias correction scheme (as tested for the late FM-A and early FM-B periods), to try to account for the variation of HLOS wind bias with

argument of latitude (orbit phase angle) and geodetic longitude. This is particularly the case for the Rayleigh-clear data).

As part of the bias investigations we identified (in September 2019) a strong linear correlation between the M1 telescope temperatures and the HLOS wind biases, as described in Section 3.2.1. This led us to propose a bias correction method that use linear regression coefficients computed daily from NRT-available telemetry housekeeping temperatures to estimate HLOS bias corrections. Further investigations in collaboration with DLR revealed that this method was working very well. The L2B processor was updated on 31 January 2020 and implemented operationally on 20 April 2020. Due to the significant Aeolus wind product bias reduction, the data has been released to the public on 12 May 2020. NWP impact studies using the new improved bias correction method has been initiated at ECMWF. It is expected that the improved bias correction will increase the impact of Rayleigh winds.

A limitation of the OSE during the Commissioning Phase was the short time period. The late FM-A and FM-B periods were much longer experiments allowing for greater statistical significance. When reprocessed datasets eventually become available providing consistent data, it will be possible to more reliably compare Aeolus impact in different seasons.

There is an increase in random errors for the Rayleigh winds (by about 25%) in the mid-troposphere during the first six months of FM-B data. This is expected to lead to a reduced NWP impact of Aeolus relative to what has been shown for the earlier FM-B period.

Aeolus' impact on short-range forecasts (via OSE metrics) is found to be of a similar magnitude to some other important satellite observing systems used at ECMWF in recent years (e.g. GPSRO, infrared radiances and AMVs based on the results of Bormann et al. 2019) which is an encouraging result; especially because, being one instrument on one satellite, it accounts for less than 1% of the observations assimilated. Given the evidence that Aeolus is providing a useful contribution to the global observing system it was decided to switch Aeolus on in operational data assimilation at ECMWF on 9 January 2020. The FSOI results that are available since Aeolus went operational are corroborating Aeolus' positive impact on short-range forecasts seen with other metrics; the impact per observation is particularly high compared to other satellite data sources (second after scatterometer ocean surface winds). Aeolus' overall FSOI is similar in magnitude to that of scatterometer data, radiosondes, AMVs and GPSRO for the January 2020 period (however the amount of GPSRO data assimilated and hence FSOI has increased substantially since then, with the arrival of COSMIC-2 data).

## Acknowledgements

This research is funded by the European Space Agency (ESA) in the framework of the activities of the Aeolus Data Innovation and Science Cluster (DISC) consortium. The presented work includes preliminary data (not fully calibrated/validated and not yet publicly released) of the Aeolus mission that is part of the European Space Agency (ESA) Earth Explorer Programme.

Thanks to the many experts from the DISC and from ESA (particularly Oliver Reitebuch (DLR), Thomas Kanitz (ESA), Fabian Weiler (DLR), Thomas Flament (Météo-France), Jos de Kloe (KNMI) and Dorit Huber (DoRIT)) which provided a fruitful forum for discussion during the Aeolus mission so far. Thanks to Mohamed Dahoui (ECMWF) for advice and support on observation monitoring.

## References

- Abdalla, S, L. Isaksen, Peter A. E. M. Janssen, Nils Wedi, Effective spectral resolution of ECMWF atmospheric forecast models, 2013, ECMWF Newsletter, Newsletter Feature Article, ECMWF
- Andersson, E., Hollingsworth, A., Kelly, G., Lönnberg, P., Pailleux, J. and Zhang, Z. (1991) Global observing system experiments on operational statistical retrievals of satellite sounding data. *Monthly Weather Review*, 119, 1851– 1864.
- Baker, WE, Atlas, RM, Cardinali, C, Clement, A, Emmitt, GD, Gentry, BM, Hardesty, RM, Källén, E, Kavaya, MJ, Langland, R, Ma, Z, Masutani, M, McCarty, W, Pierce, RB, Pu, Z, Riishøjgaard, LP, Ryan, J, Tucker, S, Weissmann, M, Yoe, JG. 2014. Lidar-measured wind profiles: the missing link in the global observing system. *Bulletin of the American Meteorological Society* 95: 4: 543– 564
- Bormann, N., H. Lawrence and J. Farnan, 2019: Global observing system experiments in the ECMWF assimilation system, ECMWF Technical Memorandum, 839
- Cardinali, C., 2009: Monitoring the observation impact on the short-range forecast. *Q. J. R. Meteorol. Soc.* 135: 239-250.
- Desroziers, G., Berre, L., Chapnik, B. and P. Poli, 2005: Diagnostics of observation, background and analysis-error statistics in observation space. *Q. J. R. Meteorol. Soc.*, 131, 3385-3396.
- ECMWF, 2018: IFS Documentation CY45R1. Available from ECMWF: <https://www.ecmwf.int/en/forecasts/documentation-and-support/changes-ecmwf-model/ifs-documentation>
- ESA, 2008: “ADM-Aeolus Science Report”, SP-1311,'ADM-Aeolus', April 2008, ISBN 978-92-9221-404-3, ISSN 0379-6566, 130 pp, available at: <https://earth.esa.int/documents/10174/1590943/AEOL002.pdf>
- ESA, 2019: “The Living Planet Programme”, available at: [https://www.esa.int/Our\\_Activities/Observing\\_the\\_Earth/The\\_Living\\_Planet\\_Programme](https://www.esa.int/Our_Activities/Observing_the_Earth/The_Living_Planet_Programme)
- Frost, C. and S. Thompson (2000). "Correcting for regression dilution bias: comparison of methods for a single predictor variable." *Journal of the Royal Statistical Society Series A* 163: 173–190.

- Geer, A. J., K. Lonitz, P. Weston, M. Kazumori, K. Okamoto, Y. Zhu, E. H. Liu, A. Collard, W. Bell, S. Migliorini, P. Chambon, N. Fourrié, M-J Kim, C. Köpken-Watts, C. Schraff, 2018: All-sky satellite data assimilation at operational weather forecasting centres. *Q. J. R. Meteorol. Soc.*, 144, 1191-1217. <https://doi.org/10.1002/qj.3202>
- Hollingsworth, A., D.B. Shaw, P. Lönnberg, L. Illari, K. Arpe, and A.J. Simmons, 1986: Monitoring of Observation and Analysis Quality by a Data Assimilation System. *Mon. Wea. Rev.*, 114, 861–879, [https://doi.org/10.1175/1520-0493\(1986\)114](https://doi.org/10.1175/1520-0493(1986)114)
- Horányi, A., Cardinali, C., Rennie, M. and Isaksen, L. (2015a) The assimilation of horizontal line-of-sight wind information into the ECMWF data assimilation and forecasting system. Part I: the assessment of wind impact. *Quarterly Journal of the Royal Meteorological Society*, 141, 1223–1232. <https://doi.org/10.1002/qj.2430>
- Horányi, A., Cardinali, C., Rennie, M. and Isaksen, L. (2015b) The assimilation of horizontal line-of-sight wind information into the ECMWF data assimilation and forecasting system. Part II: The impact of degraded wind observations. *Quarterly Journal of the Royal Meteorological Society*, 141, 1233–1243. <https://doi.org/10.1002/qj.2551>
- Illingworth, A. J., Battaglia, A., Bradford, J., Forsythe, M., Joe, P., Kollias, P., Lean, K., Lori, M., Mahfouf, J.-F., Mello, S., Midthassel, R., Munro, Y., Nicol, J., Potthast, R., Rennie, M., Stein, T. H. M., Tanelli, S., Tridon, F., Walden, C. J. and Wolde, M. (2018) WIVERN: A new satellite concept to provide global in-cloud winds, precipitation and cloud properties. *Bulletin of the American Meteorological Society*, 99 (8). pp. 1669-1687. ISSN 1520-0477
- Ingmann, P., and A.G. Straume, 2016: ADM-Aeolus Mission Requirements Document, November 2016, AE-RP-ESA-SY-001, available at: [https://earth.esa.int/pi/esa?type=file&table=aotarget&cmd=image&alias=Aeolus\\_MRD](https://earth.esa.int/pi/esa?type=file&table=aotarget&cmd=image&alias=Aeolus_MRD)
- Isaksen, L., Bonavita, M, Buizza, R, Fisher, M, Haseler, J, Leutbecher, M and L. Raynaud, 2010: Ensemble of data assimilations at ECMWF. ECMWF Technical Memorandum 646. Available from ECMWF <https://www.ecmwf.int/en/elibrary>
- Janiskova M. and C. Cardinali, 2016: On the Impact of the Diabatic Component in the Forecast Sensitivity Observation Impact Diagnostics, ECMWF Tech. Memo., 786, 18pp
- Järvinen, H., Andersson, E. and F. Bouttier, 1999: Variational assimilation of time sequences of surface observations with serially correlated errors. *Tellus A*, 51, Issue 4, 469-488.
- Langland, RH and NL Baker, 2004: Estimation of observation impact using the NRL atmospheric variational data assimilation adjoint system. *Tellus A*, 56, Issue3, 189-201.
- Lu, Q, W. Bell, P. Bauer, N. Bormann, and C. Peubey. Characterizing the FY-3A microwave temperature sounder using the ECMWF model. *J. Atmos. Oceanic Technol.*, 28:1373–1389, 2011a.
- Ma, Z, Riishøjgaard, LP, Masutani, M, Woollen, JS, Emmitt, GD. 2015. Impact of different satellite wind Lidar telescope configurations on NCEP GFS forecast skill in observing system simulation experiments. *Journal of Atmospheric and Oceanic Technology* 32: 3: 478–495
- Malardel, S, Wedi, N, Deconinck, W, Diamantakis, M, Kuehnlein, C, Mozdzyński, G, Hamrud, M, Smolarkiewicz, P, A new grid for the IFS, 2016, ECMWF Newsletter 146, <https://www.ecmwf.int/node/17262>

- Marseille, GJ, Stoffelen, A, Barkmeijer, J. 2008. Impact assessment of prospective space-borne Doppler wind lidar observation scenarios. *Tellus A* 60: 234– 248
- Podglajen, A., Hertzog, A., Plougonven, R. and N. Žagar, 2014: Assessment of the accuracy of (re)analyses in the equatorial lower stratosphere. *J.Geoph.Res.*, 119, Issue19, 11,166-11,188. <https://doi.org/10.1002/2014JD021849>
- Rennie, M., 2016, Advanced monitoring of Aeolus winds, ESA Technical Note 16, AE-TN-ECMWF-GS-16, v1.3, available from:  
<https://confluence.ecmwf.int/display/AEOL/L2B+team+technical+reports+and+relevant+papers>
- Rennie, M., de Kloe, J., Marseille, GJ., 2019, Aeolus Level-2B Algorithm Theoretical Basis Document, version 3.2, ESA reference: AE-TN-ECMWF-L2BP-0023, available from:  
<https://confluence.ecmwf.int/display/AEOL/L2B+processor+documentation+and+datasets>
- Ruppert, D. (2010). *Statistics and Data Analysis for Financial Engineering*. Springer. p. 118. ISBN 9781441977878. Retrieved 2015-08-27
- Stoffelen, A., 1999: A Simple Method for Calibration of a Scatterometer over the Ocean. *J. Atmos. Oceanic Technol.*, 16, 275–282, [https://doi.org/10.1175/1520-0426\(1999\)016](https://doi.org/10.1175/1520-0426(1999)016)
- Stoffelen, A, Marseille, GJ, Bouttier, F, Vasiljevic, D, de Haan, S, Cardinali, C. 2006. ADM-Aeolus Doppler wind lidar observing system simulation experiment. *Quarterly Journal of the Royal Meteorological Society* 132: 1927– 1947, <https://doi.org/10.1256/qj.05.83>
- Tan, DGH, Andersson, E, Fisher, M, Isaksen, L. 2007. Observing-system impact assessment using a data assimilation ensemble technique: application to the ADM-Aeolus wind profiling mission. *Quarterly Journal of the Royal Meteorological Society* 133: 381– 390, <https://doi.org/10.1002/qj.43>
- Tan, DGH, Andersson, E, De Kloe, J, Marseille, GJ, Stoffelen, A, Poli, P, Denneulin, ML, Dabas, A, Huber, D, Reitebuch, O, Flamant, P, Le Rille, O, Nett, H. 2008. The ADM-Aeolus wind retrieval algorithms. *Tellus A* 60: 2: 191– 205, <https://doi.org/10.1111/j.1600-0870.2007.00285.x>.
- Weissmann, M., and C. Cardinali, 2007: Impact of airborne Doppler lidar observations on ECMWF forecasts. *Quart. J. Roy. Meteor. Soc.*, 133, 107–116.
- WMO, 2018: “Rolling Review of Requirements and Statements of Guidance”, available at <http://www.wmo.int/pages/prog/www/OSY/GOS-RRR.html>

## Appendix

### Acronyms

4D-Var	Four-dimensional variational data assimilation
ACCD	Accumulation charge coupled device
ALADIN	Atmospheric LAsEr Doppler Instrument
AMDAR	Aircraft Meteorological DAta Relay
AMSR-2	Advanced Microwave Scanning Radiometer 2
AMSU-A	Advanced Microwave Sounding Unit-A
AMV	Atmospheric Motion Vector
AOCS	Attitude and Orbital Control Systems
ASCAT	Advanced SCATterometer
ATBD	Algorithm Theoretical Baseline Document
ATMS	Advanced Technology Microwave Sounder
BRC	Basic Repeat Cycle
BUFR	Binary Universal Form for the Representation of meteorological data
CAL/VAL	Calibration and Validation
CP	Commissioning Phase
CrIS	Cross-track Infrared Sounder
CSR	Corrected Spectral Registration
DEM	Digital Elevation Model

DISC	Data Innovation Science Cluster
DLR	Deutsches Zentrum für Luft- und Raumfahrt (German Aerospace Center)
DS	Defence and Space
DUDE	Down Under Dark Experiment
DWL	Doppler Wind Lidar
ECMWF	European Centre for Medium-range Weather Forecasts
EDA	Ensemble of Data Assimilations
EE	Earth Explorer
EGM96	Earth Gravitational Model 96
ESA	European Space Agency
EUMETSAT	European Organisation for the Exploitation of Meteorological Satellites
FM	Flight model
FSOI	Forecast Sensitivity Observation Impact
FY3B	Feng-Yun - 3B satellite
GOS	Global Observing System
GPSRO	Global Positioning System radio occultation
HBE	Harmonic Bias Estimator
HLOS	Horizontal line-of-sight
IASI	Infrared Atmospheric Sounding Interferometer

IFS	Integrated Forecasting System (at ECMWF)
IRC	Instrument Response Calibration
ISR	Instrument Spectral Registration
KNMI	Koninklijk Nederlands Meteorologisch Instituut (The Royal Netherlands Meteorological Institute)
L1B	Level 1B
L1Bp	Level 1B processor
L2B	Level 2B
L2Bp	Level 2B processor
L2/Met PF	Level 2 Meteorological processing facility
L2C	Level 2C
LOS	Line-of-sight
MAD	Median absolute deviation
MDA	MacDonald, Dettwiler and Associates
MetOp	Series of EUMETSAT polar orbiting satellites
MHS	Microwave Humidity Sounder
MRC	Mie Response Calibration
NH	Northern Hemisphere
NPP	National Polar-orbiting Partnership
NRT	Near real-time

NWP	Numerical Weather Prediction
OSE	Observing System Experiment
O-A	Observation minus analysis
O-B	Observation minus background
ODB	Observational DataBase (used by ECMWF)
PDGS	Payload Data Ground Segment
QC	Quality control
RALT	Radar altimeter
RBC	Rayleigh-Brillouin Correction
RBS	Range bin settings
RD	Research department (at ECMWF)
RMS	Root mean square
RMSE	RMS error
RRC	Rayleigh Response Calibration
SH	Southern Hemisphere
SNR	Signal to noise ratio
TN	Technical Note
UTLS	upper-troposphere/lower-stratosphere
UV	Ultra-violet

WIGOS	WMO Integrated Global Observing System
WMO	World Meteorological Organisation
ZWC	Zero Wind Correction